universität wien

DISSERTATION

A genome wide RNAi Screen in *D. melanogaster* for the Identification of Genes involved in Border Cell Migration

angestrebter akademischer Grad

Doktor der Naturwissenschaften (Dr.rer.nat.)

Verfasserin :	**Dipl. Ing. Hannah Neumeier**
Matrikel-Nummer:	9840036
Dissertationsgebiet:	A 091 490 (Molekulare Biologie)
Betreuer:	Prof. J. Victor Small

Wien, am 28. August 2008

Acknowledgements

I want to thank my family and Martin for supporting me in my education.

I would like to thank **Georg Dietzl**, **Frank Schnorrer** and **Carlos Ribeiro** for teaching me the basics in Drosophila genetics in the very beginning. In addition I enjoyed that Georg is always in the mood for doing some “fun on the side”.

I would like to thank **Sheetal Bhalerao** for her constant constructive criticism and mental support in the lab and during shopping tours.

I would like to thank **Stefanie Benesch** who is a wonderful friend and colleague for her enthusiasm and expertise.

I would like to thank **Constance Richter** for her advice and funny conversations during fly pushing back to back.

I want to thank all the people involved in an RNAi screen:
(Georg Dietzl, Frank Schnorrer, Carlos Ribeiro, Mattias Alenius, Africa Couto, Martin Häsemeyer, Laszlo Tirian, Jennifer Mummery, Constance Richter, Ralph Neumüller) - for discussions about the latest hot candidate hits and sharing times of routine-dilated hours.

I want to thank **Peter Duchek** for his support and scientific advice

I want to thank **Pawel Pasierbek** for never getting tired or angry during help at the microscope.

I want to thank **Tibor Kulcsar** and **Hannes Tkladetz** for excellent help with graphics.

I want to thank **David Kummerer** from the workshop for making extra-wishes superfast and for showing me how to cut a winding.

I want to say thank you to **Vic Small** and **Barry Dickson** who offered me to work on such a state of the art technique project.
I want to thank **Vic Small** for undergoing such an adventurous project.

Table of contents

Summary

The transition of a cell from a sessile to a migratory state is a feature shared by normal cells during development and abnormal cells during metastasis. Much interest thus centers on the profile of gene expression required for programmed and uncontrolled cell migration. Border cells in the fruit fly *Drosophila melanogaster* undergo invasive and programmed cluster migration during oogenesis and therefore represent an attractive model system for the analysis of cell migration in vivo. The goal of this thesis was to identify novel genes required for cell migration in order to better understand migration processes. A comprehensive knowledge of genes crucial for migration could potentially lead to the assignment of drug targets to specifically block deleterious migration such as occurs in metastasis.

In this thesis, I show that RNAi can be employed to study border cell migration. The RNAi effect is specific and strong enough to phenocopy mutant genes already known to be required for border cell migration. These background RNAi studies encouraged me to perform a systematic genome wide RNAi based analysis of border cell migration using the transgenic RNAi collection generated by the group of B. Dickson. The RNAi screen enabled me to identify 52 novel genes, which were previously not implicated in border cell migration.

Here, I present the realization and description of the first genome wide RNAi screen for genes involved in migration using *D. melanogaster* border cell migration during oogenesis as a model system. Furthermore, I present the initiated characterization of one of the genes identified in the screen, designated as *wanderlust*. *Wanderlust* belongs to the neuroligin familiy of proteins thought to be restricted in expression to neuronal cells, but now identified as a regulator of border cell migration.

Zusammenfassung

Im Verlauf von normalen Entwicklungsprozessen sowie während abnormer Metastasenausbildung weisen Zellen eine bemerkenswerte Umstellung von "unbeweglich" auf "beweglich" auf. Grosses Interesse gilt daher der Erforschung des Expressionsprofils notwendiger Gene während der Zellwanderung selbst. Die Oogenese von der Fruchtfliege *Drosophila melanogaster* weist programmierte invasive Zellwanderung von sogenannten "Border Cells" auf. Diese spezialisierten Zellen führen einen Übergang von endothelial (stationär) zu mesenchymal (beweglich) durch und wandern zwischen anderen Zellen durch die gesamte Eikammer. Border cell Wanderung ist ein interessantes Modellsystem für in vivo Zellmigration, da viele Parallelen zu sowohl normaler wie auch abnormer Zellmigration vorhanden sind. In Vorversuchen zeige ich, dass durch die RNAi knock down Technik "Border cell" spezifische Gene ausgeschaltet werden können und bereits publizierte Phänotypen reproduziert und phänokopiert werden können. Ich habe die einzigarte RNAi Fliegenbibliothek, (von der Gruppe von Dr. B. Dickson hergestellt) genutzt, um nach Genen zu suchen, die für Zellbewegung speziell während Border Cell Wanderung nötig sind.
Zum ersten Mal in *Drosophila* Genetik war es möglich, einen systematischen genomweiten RNA interference (RNAi) Screen für Border Cell Wanderung durchzuführen. Im Zuge dieses Screens habe ich 52 neue Gene identifiziert, die bisher noch nicht mit Border Cell Wanderung in Verbindung gebracht worden sind. In der vorliegenden Dissertation präsentiere ich die Realisierung und Durchführung eines genomweiten RNAi Screens, der Border Cell Wanderung während *Drosophila* Oogenese als Modellsystem verwendet. Darüberhinaus stelle ich ein neu identifiziertes Gen CG34139 vor, das bisher noch nicht charakterisiert wurde und benenne es *wanderlust*. *Wanderlust* ist ein Vertreter der Neuroligine und reguliert Border Cell Wanderung.

1 Introduction

1.1 Aim of the project

From the first cell divisions to maintenance of multi cellular organisms it is essential for cells to be motile. Developmental processes exhibit programmed migration events such as gastrulation, organogenesis, tubular structure formation, wound healing, nerve outgrowth or immune defense. All these processes and many more depend on the action of migratory cells. Invasive and migratory cells dictate cancer metastasis formation leading to severe organ malfunction and even death. Cell migration is a central event during development and disease. Understanding how the process cell migration works may help to manipulate wanted or unwanted cell migration in the future.

The aim of this PhD was to perform a genome wide RNA interference (RNAi) screen in the fruit fly *Drosophila melanogaster* for the identification and characterization of novel genes involved in border cell migration using state of the art genetic and biochemistry techniques. Furthermore, one identified gene should be analyzed in detail for its function during border cell migration.

For the first time, it is possible to perform systematic functional genetic screens in *Drosophila.* The availability of a genome wide transgenic fly collection of an inducible gene knock down system enabled me to screen for genes involved in cell migration in vivo. I performed a genome wide RNAi screen for genes required specifically during border cell migration in the fruit fly *Drosophila melanogaster*. Dissecting how the process of border cell migration works will help us to understand other migratory/invasive processes.

1.2 Model system

1.2.1 The fruit fly *Drosophila melanogaster*

The fruit fly *Drosophila melanogaster* has been used as model system ever since Thomas Hunt Morgan started breeding it in 1910. He searched for a small, cheap and fast breeding animal model, properties he found in the fruit fly. Fortunately for fruit fly geneticists, it turned out that the fruit fly is indeed an ideal model organism: in addition to Morgan's requirements for a model organism, the fruit fly has a small genome and only a few, namely four, chromosomes. *Drosophila* development from the egg to the fertile adult fly takes 10 days (at 25°C) and is divided into four developmental phases: embryo, larva, pupa and adult. Embryogenesis occurs surprisingly fast and is completed after only 1 day (figure 1.1A). The larval stage takes 4 days and in this period, the larva is mainly a feeding and growing organism, interrupted by two molting events (figure 1.1B). The larval stage is followed by pupariation for 4 days, in which the animal undergoes dramatic metamorphoses events: the worm-like larva develops into a six legged, winged, complex adult fly (figure 1.1C). One day after eclosion from the pupal case, the adult fly is fertile for reproduction and the cycle can start again. Females (figure 1.1D left fly) and males (figure 1.1D right fly) are phenotypically discriminated by several features: the male genital apparatus is easily recognized by the dark brown protruding genital arch, whereas the female fly exhibits no visible external genitalia. Male flies exclusively exhibit so-called sex combs, black comb-like hairs, on the first leg pair. The lower part of the back of male flies shows stronger pigmentation than females, the darker pigmentation gave rise to the latin name "melanogaster – black bellied". However under different environmental conditions pigmentation differs and is not a bona fide sex discrimination feature. Most of the times, females are a bit larger in size, but size differences between sexes vary as well, especially during malnutrition phases.

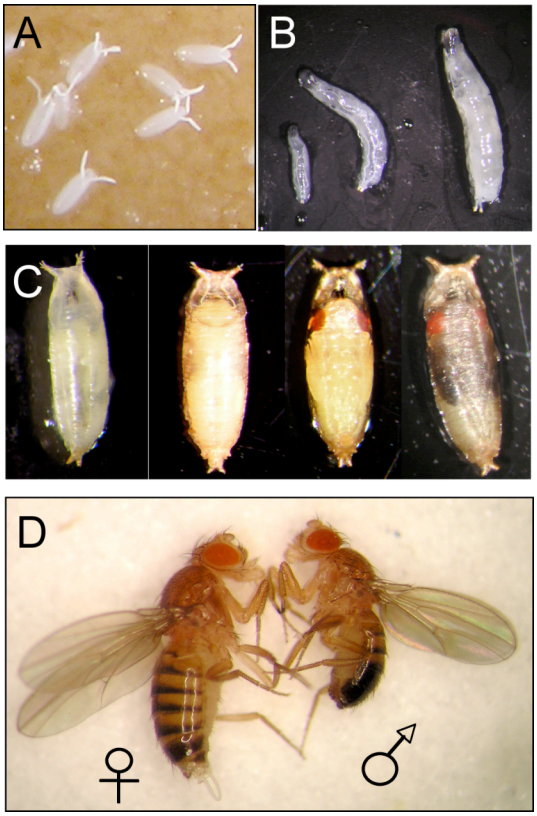

Figure 1.1: Development of D. melanogaster. A) Embryo, **B)** first, second and third larval stage, **C)** prepupa, pupa, pupa with developed red eyes, pupa with developed wings (black patches), **D)** female and male adult fly

1.2.2 Modes of cell migration

Cell migration is an important feature of higher eukaryotes. The ability to move enables cells to create new environments (embryogenesis) and to react to environmental changes and injury (e.g. macrophages migrate to inflammation sites).

Cells exhibit different modes of migrations: they are able to migrate as single cells (leukocytes, in vitro cell culture), in groups (mammary gland formation, precursor cells of the zebrafish lateral line organ, *Drosophila* border cells) or as entire sheets (Martin and Wood 2002).

Single cell migration

Every cell type displays different shape and rigidity properties, resulting from the inner structure of the cytoskeleton, which is composed of a filamentous actin network, a microtubule network and intermediate filaments.

Cell migration is driven by the actin rich protrusion of the so-called lamellipodium (leading edge) in the front of a cell, mediated by polymerization of monomeric actin into actin filaments. At the same time, the cell needs to form new attachment sites to the substratum at specific foci mediated by so-called focal adhesions. Tension to retract the cell rear is built up through contractile stress fibers connected to focal adhesions. As a consequence of moving forward, the moving cell has to detach from the substratum in the rear by dissolving of focal adhesions and pulling the rest of the cell forward.

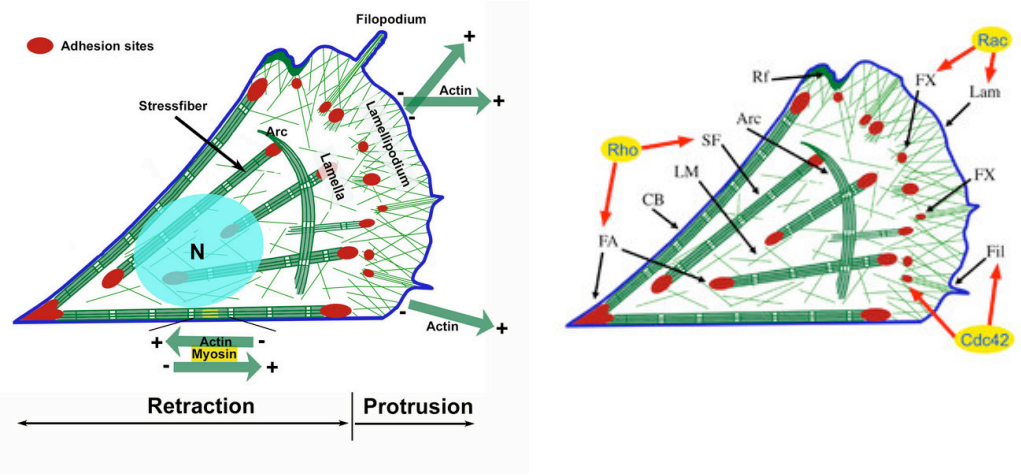

Figure 1.2: Schematic of a moving cell. left) moving cell with actin cytoskeleton components. **Right)** Rho GTPase family members Rho, Rac and Cdc42 and their influence on different cytoskeletal structures: FA – focal adhesion, Rf – ruffle, SF – stress fiber, Fil – filopodium, FX – focal complex, Lam – lamellipodium, LM – lamella meshwork, CB – cortical bundle, schematics taken from J.V. Small (http://cellix.imba.oeaw.ac.at/)

The moving cell is polarized in front and back, visible by the presence of a flat protrusion, the lamellipodium in the front of the cell. The lamellipodium is characterized by its criss-cross arranged actin filaments, nowhere else in the cell are actin filaments arranged in such a fashion (figure1.2). It was shown that the action of different small GTPase Rho family members is required in different functional areas of the cell to promote coordinated migration. Rac is required in the front to signal the production of the lamellipodium, whereas active Cdc42 induces formation of filopodia, Rho is active in the cell body and induces stress fiber bundles. Rac, and Cdc42 are required for focal complex formation, which are precursors of focal adhesions that mature through the subsequent of activation of Rho (Mackay and Hall 1998; Rottner, Hall et al. 1999)(figure 1.2).

Modes of collective cell migration

Migration of multiple cells requires close contact and coordination between the cells in order to perform directed migration. Collective cell migration is found in many different phases of embryogenesis and development. Fish possess an organ to sense movement and vibrations in their environment in order to orient in the water, avoid collisions and locate prey or enemies, the *so-called* lateral line. The lateral line spans the entire length of the animal. Development of the lateral line was studied in the zebrafish embryo (*Danio rerio*) and was shown to result from the collective migration of a cohort of over 100 cells migrating towards the chemokine SDF1a (stromal cell derived factor 1a). On the way towards the posterior part of the embryo, cells from the primordium cluster are left behind on a linear track, making the lateral line (figure 1.3). Live imaging studies revealed highly dynamic cellular activity of front cells. Recently, two independent SDF1a receptors were identified as required for proper lateral line primordium migration, each of the receptors acting at different locations in the migrating group of cells, namely Cxcr4b (chemokine C-X-C motif receptor 4b) acting in the leading edge and Cxcr7 (chemokine C-X-C motif receptor 7) acting in the trailing edge of the migrating primordium (Valentin, Haas et al. 2007).

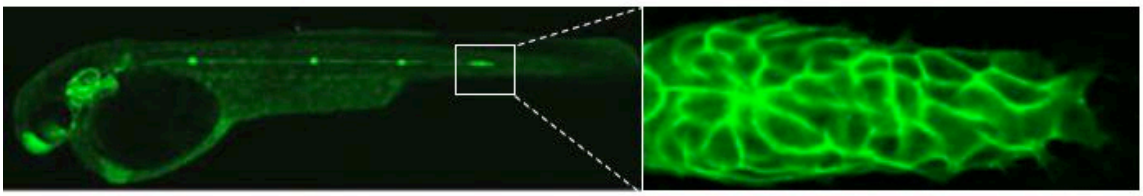

Figure 1.3: Zebrafish lateral line precursor migration, a zebrafish embryo expressing ClaudinB::GFP in the developing lateral line, close-up of the front most cell group, images taken from Darren Gilmour

Another example for collective cell migration serves mammary duct formation in the adult mouse. Mammary duct formation was recently described as collective cell migration without

the use of cellular extensions or protrusion (Ewald, Brenot et al. 2008). The observation of migration without cellular protrusions is very contradictory to the paradigm that migrating cells need protrusions for migration. However, it remains to be further clarified, if protrusions are not present, or not visible yet with the techniques used for this study, or if other forces such as collective pushing mediate necessary forces to advance (figure 1.4).

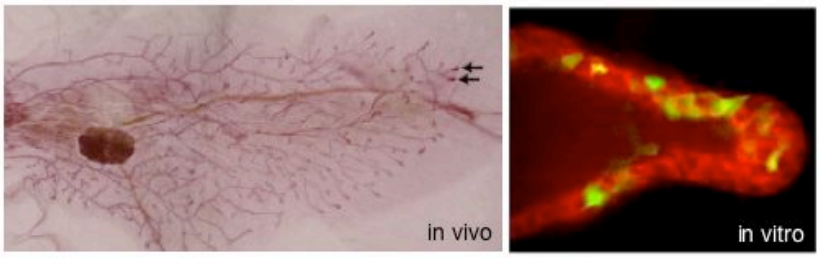

Figure 1.4: Mouse mammary duct formation: a fully developed mouse mammary gland with terminal end buds (arrows), confocal image of an in vitro developing terminal end bud labeled with cell tracker dye (red) and Sca1-GFP mosaic knock in cells (green), images taken from (Ewald, Brenot et al. 2008)

Epithelial sheet migration is found e.g. in *Drosophila* during the so-called embryonic phase "dorsal closure" starting at 11 hours after fertilization. In this last major morphogenetic phase of embryogenesis, two opposing epithelial sheets of the epidermis approach each other in order to completely close and seal the embryo in a zippering fashion (Martin and Wood 2002) (figure 1.5). Dorsal closure is a very prominent and important hallmark in embryogenesis; defective dorsal closure results in a dead embryo with a hole in the cuticle.

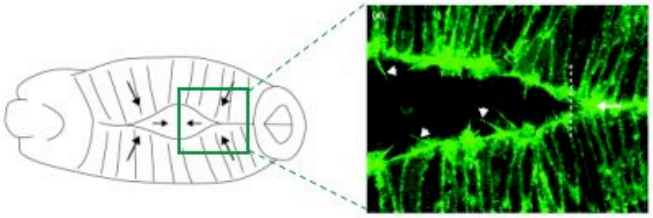

Figure 1.5: *Drosophila* embryonic dorsal closure: schematic and confocal image showing edges of the approaching epithelial sheets expressing GFP-actin, adapted from (Martin and Wood 2002)

Drosophila border cell migration during oogenesis exhibits fewer cells in the migrating unit compared to the examples discussed above, namely 6 – 10 cells per cluster. Border cell migration is an attractive and genetically pliable system for studying invasion and cell migration, it will be discussed in detail in the following section (1.2.3).

1.2.3 Border cell migration

Border cell migration is a cluster migration process and an important hallmark of *Drosophila* oogenesis during stage 9 out of 14 defined developmental oogenesis stages (S1 – 14) (King 1970). Border cell migration is a directed migration of 6 – 10 epithelial derived cells. Successful border cell migration is required for the formation of a functional micropyle, a canal apparatus made of extracellular material (chorion), through which sperm enters and fertilizes the egg (Montell, Rorth et al. 1992). Severe defects in border cell migration result in sterile females due to a malformed micropylar apparatus lacking a pore, therefore blocking sperm entry.

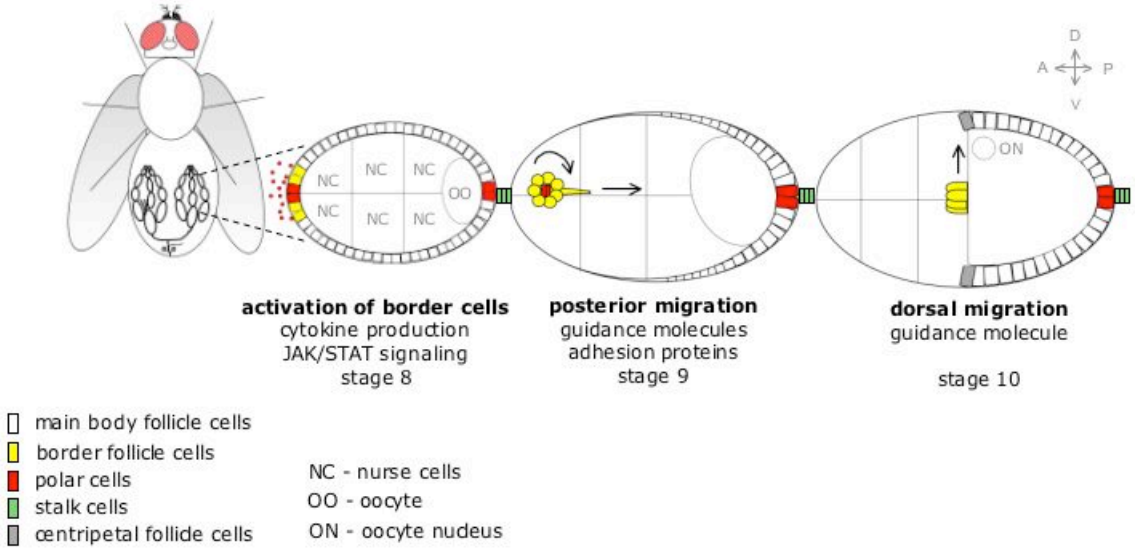

Figure 1.6: Schematic overview from stage 8 to stage 10 of oogenesis. The female reproductive organ – the ovary, with its ovarioles and selected egg chamber stages 8-10, relevant for border cell migration, are shown. Activation, posterior migration, arrival of border cells at oocyte and dorsal migration of border cells is depicted. Anterior is to the left, dorsal is up.

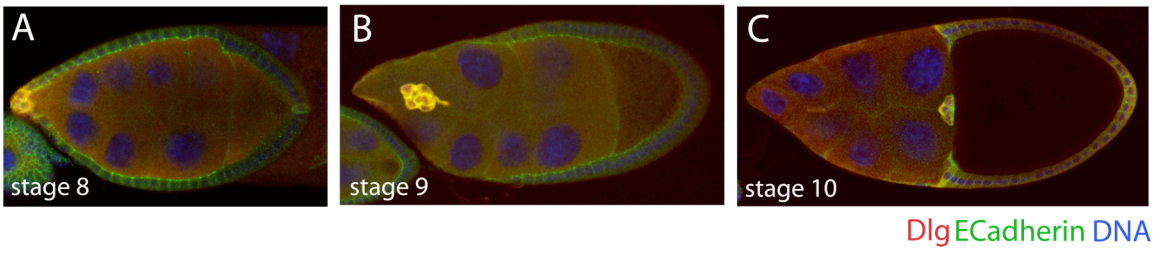

Figure 1.7: Overview of border cell migration. Wild type egg chambers of stages 8 - 10 are shown, stained for Discs large (Dlg, red), E-cadherin (green) and DNA (blue), anterior is to the left. **A)** Polar cells round up late in a stage 8 egg chamber and activate neighboring follicle cells to become border cells. **B)** Border cells migrate towards the oocyte showing a long cellular protrusion in a stage 9 egg chamber. **C)** stage 10: the border cell cluster has arrived at the oocyte

The female reproductive organ, the ovary - consists of multiple connected (10 – 15) strings, the so-called ovarioles. The ovarioles harbor stem cells and egg chambers of different stages. A typical egg chamber consists of two cell types: germline derived inner cells and a monolayer of hundreds of soma derived follicle cells. The germline-derived cells are generated in the germarium, the anteriormost tip of each ovariole, containing the stem cells. After 4 rounds of cell division of a stem cell, 16 interconnected cells are produced. One of these 16 germline-derived cells becomes the oocyte, whereas the other 15 cells become so-called nurse cells, which will generate enormous amounts of mRNA for the growing oocyte. The germline-derived cells are covered by an epithelium of follicle cells generated by division of somatic stem cells. This follicular epithelium combines properties of both a primary and secondary epithelium due to the presence of a zonula aderens, resulting from, among others the expression of Crumbs (Crb) (Tepass, Theres et al. 1990). Follicle cells secrete the egg shell (chorion), provide patterning signals to the oocyte (figure 1.8) and transport yolk protein to the oocyte starting at mid-oogenesis.

Follicle cells can be subdivided into main body follicle cells (the majority of follicle cells), stretched cells, border cells, posterior terminal cells, centripetal follicle cells, a polar cell pair at each tip of the egg chamber and stalk cells, which connect neighboring egg chambers (figure 1.6). Until the end of stage 8 of oogenesis, follicle cells are uniformely distributed in a monolayer covering the entire egg chamber (figure 1.6, 1.7 stage 8). A subset of follicle cells at each tip of the egg chamber, two specialized cell pairs, *so-called* polar cells start to secrete the cytokine unpaired (upd, also called outstretched/os by polar cells). Binding of unpaired to its receptor domeless (dome) induces dome receptor clustering, phosphorylation by hopscotch, finally triggering JAK/STAT localization to the nucleus and upregulation of border cell specific genes. In this manner, follicle cells surrounding the polar cells are activated and become border cells.

The first gene identified required for border cell migration was *slbo* (*slow border cells*), a basic leucine zipper transcription factor identified in a p-element loss of function screen (Montell, Rorth et al. 1992). Strong alleles of *slbo* dramatically impaired border cell migration and caused the females to be sterile. Some years later it was shown that slbo is a downstream target of JAK/STAT signaling (Montell and Silver 2001).

Graded JAK/STAT signaling was shown to induce different follicle fates relative to their distance from the poles (= source of the ligand unpaired) into border, stretched, centripetal and main body follicle cells. Combined action of graded JAK/STAT signaling and Gurken/EGFR signaling induces posterior follicle cell fate and suppresses border cell formation in posterior polar cells (Xi, McGregor et al. 2003) (see figure 1.8).

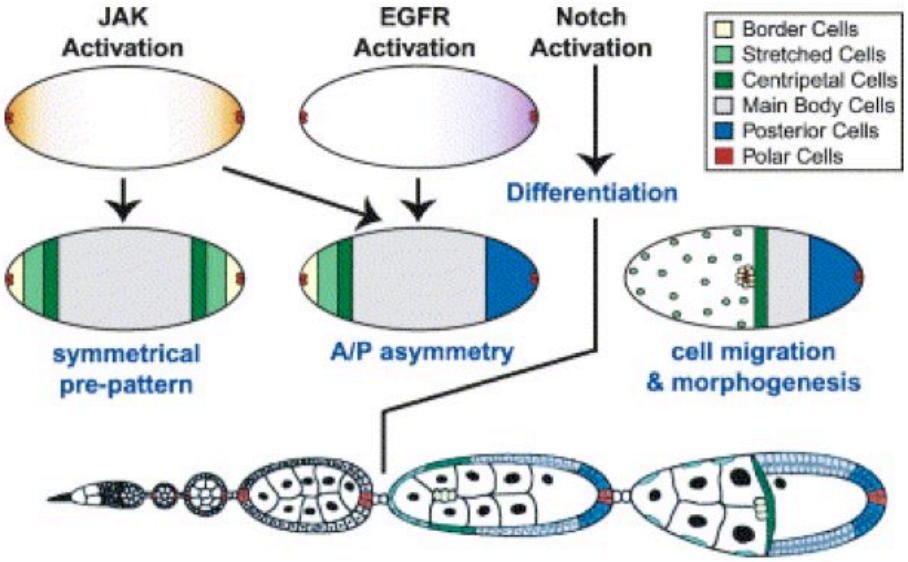

Figure 1.8: Notch activity, graded JAK/STAT activity and Gurken/EGFR activation creates anterior and posterior follicle cell fates, model taken from (Xi, McGregor et al. 2003)

In addition, other signals are known to be involved in border cell migration such as steroid hormone ecdysone signaling, requiring ecdysone receptor (EcR) and taiman (tai) as receptor coactivator for properly timed border cell migration (Bai, Uehara et al. 2000). Once activated, border cells migrate towards a source of chemoattractants established as EGF and PVF1 (PDGF- and VEGF-related factor 1), sensed by their receptors EGFR (Epidermal growth factor receptor, also called Torpedo) and PVR (PDGF- and VEGF-receptor related), respectively on the surface of migrating border cells (Duchek and Rorth 2001; Duchek, Somogyi et al. 2001). Just prior to delamination, a so-called long cellular extension protrudes from the border cells, “exploring” the environment in the direction of movement (Fulga and Rorth 2002).

At stage 9, border cells become migratory and invasive but retain some epithelial properties, the transition to mesenchymal is not complete. For example, E-Cadherin junctions between border cells and polar cells remain epithelial, whereas the interface between border cells and nurse cells appears mesenchymal by reduced E-Cadherin levels (Niewiadomska, Godt et al. 1999).

Recently, it was shown that the planar polarity pathway is involved in border cell migration (Bastock and Strutt 2007). The planar cell polarity (PCP) pathway is required for the proper polarity establishment in neighboring cells in non-migratory cells such as in the formation of bristles. Main players in the planar cell polarity pathway are the transmembrane receptor Frizzled (fz), another transmembrane protein Strabismus (Stb) and the cytoplasmic proteins

Dishevelled (Dsh) and Prickle (Pck). Bastock and Strutt showed that egg chambers mutant for planar cell polarity players delay border cell migration, thus not completely blocking but making it less efficient but the cluster eventually reaches the oocyte. Pcp mutant border cells exhibited significantly less actin rich protrusions compared to wild type, suggesting that the planar cell polarity pathway induces abnormal cytoskeleton dynamics.

Live imaging studies of border cell migration

So far, border cell migration was studied in fixed egg chambers showing snapshots of the migration process. Recently, a protocol was developed which allowed the culture of egg chambers for some hours facilitating the study of border cell migration by live imaging. It became clear that cluster cells are highly dynamic during migration; border cells constantly change position within the cluster, which was an unexpected and interesting finding. All border cells, except for the non-migratory polar cells, exhibit this surprising shuffling property during migration. The reason why border cells exhibit such variable positioning within the cluster is not known. Recently, it was postulated that the migration phase could be subdivided into 2 phases: in phase 1 the cluster is rather stretched and migrates fast, cluster cells do not show extensive shuffling activity. However in phase 2 the cluster starts to “tumble” with extensive cellular rearrangements, but moves significantly slower than in phase 1. It was shown that the two molecules ELMO and myoblast city (mbc) are responsible for the tumbling activity of the border cell cluster in phase 1 (Bianco, Poukkula et al. 2007).

After a migration time of about 4 – 6 hours of squeezing through nurse cells, the border cell cluster reaches its primary target, the oocyte. This position of the border cells at stage 10A “at the border” between nurse cells and oocyte gave rise to the name “border cell cluster”. In concert with border cell migration during stage 9, the monolayered follicle layer becomes active and moves over the entire egg chamber towards the oocyte until the majority of follicle cells cover the oocyte and a very few leftover cells (stretch cells) cover the nurse cells. Follicle cells covering the oocyte establish a so-called single layered columnar epithelium, whereby cell heights are at least twice their width.

The posterior directed migration of border cells is followed by a dorsal migration (during stage 10B) towards the oocyte nucleus mediated by EGF and EGFR. At the same time, centripetal follicle cells (= follicle cells at the edge of oocyte, neighboring stretch cells) start to invaginate between nurse cells and oocyte from all sides and form a confluent layer together with the border cells around the oocyte.

All these cellular rearrangements of border cells and follicle cells during stage 9 and stage 10 serve to convert the epithelium-covered egg chamber into an epithelium-covered oocyte. It is essential for border cells to stay together, since they can perform their later task of

building a functional micropyle only as a cluster. If they would move over the entire egg chamber as the other follicle cells do, they would end up as stretch cells, losing contact with each other and they would never contact the oocyte. The only option they have is to stay together and migrate through the egg chamber between the nurse cells as a cluster.

Downstream targets of slbo

Slbo is a CCAAT enhancer binding protein (C/EBP) transcription factor required for border cell identity and migration. *Drosophila slbo* exhibits an entire protein family as human homolog, namely the C/EBP trancription factor family encoded by six genes (C/EBPα, β, γ, δ, ε, ζ). C/EBPs were shown to function in complexes with foxo1, Smad proteins or chromatin modifiers thus regulating a multitude of genes with CCAAT consensus promotors (Nerlov 2008). C/EBP members were even found to be involved as nuclear constraints of long-term synaptic plasticity and memory in mice, however the exact downstream targets are not yet identified (Chen, Muzzio et al. 2003).

Little is known about *Drosophila* slbo downstream targets. So far, the transcription factor jing, the homophilic cell-cell adhesion protein E-Cadherin (shotgun), and MyosinVI (jaguar), focal adhesion kinase (Fak) were identified as downstream targets of slbo (Niewiadomska, Godt et al. 1999; Bai, Uehara et al. 2000; Liu and Montell 2001; Montell 2001; Geisbrecht and Montell 2002). The presence of the cell-cell adhesion molecule E-Cadherin is required in both border cells and nurse cells for proper border cell migration. In E-Cadherin mutants affecting either nurse cells or border cells, a severe block in border cell migration is induced, demonstrating that the homophilic adhesion property of E-Cadherin is absolutely required for border cell migration (Oda, Uemura et al. 1997). In contrast to metastasized cancers, border cells retain expression of E-Cadherin throughout migration and even upregulate the level of E-Cadherin between border cells, probably because border cells need to stay together as group, which is achieved by stable cell-cell contacts. While the loss of E-Cadherin is normally a hallmark of invasiveness and migration in mammalian systems, *Drosophila* border cells even enhance adhesion within the cluster, and E-Cadherin is required on both cell types, nurse and border cells to accomplish migration. An explanation for this phenomenon could be that different cell types react differently to increased levels of E-Cadherin. Human ovarian cancer cells exhibit, like border cells, increased levels of E-Cadherin required for migration (Ong, Maines Bandiera et al. 2000). Migratory border cells have to rapidly establish and dissolve adhesion complexes between border cells and nurse cells. The *slbo* downstream target focal adhesion kinase (FAK) was shown to be elevated in border cells and FAK is proposed to promote rapid turnover of focal adhesions (Bai, Uehara et al. 2000).

Approaches to study border cell migration

Hitherto, border cell migration was studied using genetics approaches such as p-element "loss of function" screens (Montell, Rorth et al. 1992; Liu and Montell 1999) overexpression or suppressor screens using successfully revealing major players in this process (Rorth, Szabo et al. 1998; Mathieu, Sung et al. 2007). Recently, two groups independently performed expression profiles of migrating border cells and identified genes up/downregulated during migration and putative downstream targets dependent on slbo. Unfortunately, the results of these two projects showed very little overlap, indicating the limitation of these approaches (Borghese, Fletcher et al. 2006; Wang, Bo et al. 2006). Further experiments will be required to show if these screens have uncovered genes important for border cell migration.

1.2.4 Apical-basal polarity and cell-cell junctions in epithelial cells

Due to the nature and possible function of one of the genes uncovered in my border cell migration screen, I will briefly review what is known about cell-cell junctions and polarity determinants in *Drosophila*. All cells are polarized, meaning that cells distinguish between front/back, top/bottom or inside/outside. Cells can be polarized in many different ways, depending on the view, relative to the outside or to itself. Within a cell, entire organelles such as the Golgi apparatus, or the protein composition on the membrane or in the cytosol, even mRNA can be unequally distributed. Subcompartment polarizations including asymmetric protein distributions are necessary for processes such as establishment of anterior-posterior axis, asymmetric cell division and migration. The *Drosophila* oocyte exhibits anterior-posterior pre-patterning in the oocyte to establish front and back of the future embryo. Gurken/Torpedo signaling (corresponding to the mammalian EGFR signaling) to somatic follicle cells surrounding the oocyte establishes the anterior-posterior axis. After the anterior-posterior axis is established in the follicle cells, *bicoid* and *oskar* mRNA are transported via microtubules through the ring canals into the oocyte. Bicoid mRNA is deposited at the anterior cortex, whereas oskar mRNA and Staufen protein are transported by kinesin towards the plus ends of microtubules to the posterior pole of the oocyte, thus pre-determining the body axis of the embryo (Riechmann and Ephrussi 2001). Epithelial cells exhibit an apicobasal polarization. The basal side of epithelial cells underlies the basement membrane per definition, whereas the apical side contacts the germline

(figure 1.9). In the follicular epithelium of the ovary, apical faces towards the oocyte and the nurse cells, whereas basal faces surrounding muscle sheets. In the follicular epithelium of the ovary, polarization of follicle cells is initiated by contact to the basement membrane, where a basal membrane is established, distinct from the rest of the plasma membrane. In a second step, the follicular epithelium is fully polarized by contact of follicle cells to the germline cells.

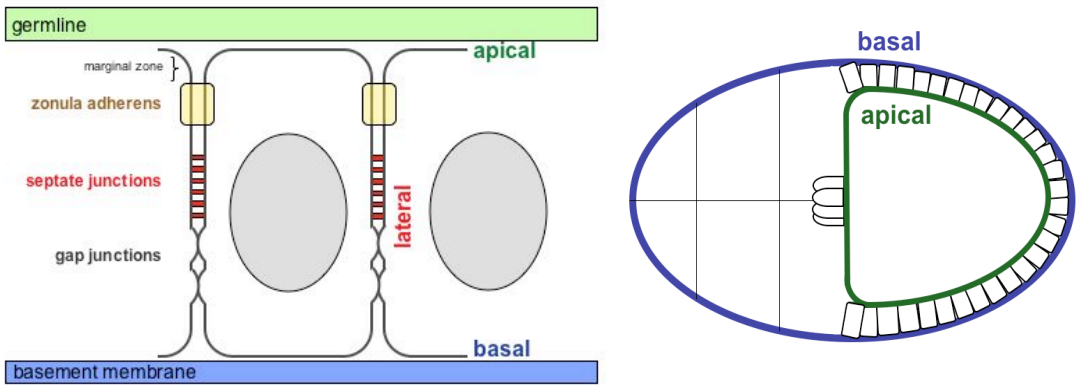

Figure 1.9: Structure and polarity of an epithelium. Left) Schematic drawing of a follicular epithelium consisting of an apical side facing the germline cells, a marginal zone above the zonula adherens, a basal side contacting the basement membrane and lateral zones with a zonula adherens (adherens junctions), septate junctions in a ladder-like structure and gap junctions. **Right)** apical-basal polarity of a stage 10 egg chamber

Proteins of the Par (partition defective) complex were some of the first identified proteins necessary for anterior-posterior axis formation in *C. elegans* after fertilization. The Par proteins consist of six proteins (Par1 – Par6) and are evolutionary conserved. Proper Par protein function requires atypical protein kinase C (aPKC) interacting with the Par3 and Par6 as the aPKC-Par complex. The Par-aPKC system exhibits three serine/threonine kinases (aPKC, Par-1, Par-4), two PDZ domain containing scaffold proteins (Par-3, Par6), 14-3-3 family member (Par-5), and one RING finger protein (Par-2), however the *Drosophila* and mammalian homolog of Par-2 is not yet identified.

In *Drosophila* epithelial follicle cells aPKC, Par-3 (bazooka) and Par-6 are found on the apical side, whereas Par-1 is located basolateral. Phosphorylation of Par-3 by Par-1 induces local destabilization of the aPKC-Par complex and restricts the aPKC-Par complex to the apical side. Par-5 and Par-4 do not show asymmetric localization in the follicular epithelium (Suzuki and Ohno 2006). During border cell migration aPKC, Par-3 and Par-6 remain asymmetrically localized, perpendicular to the direction of migration, indicating that par protein polarity is maintained within the cluster. In addition, Par-3 and Par-6 were shown to be required for border cell migration (Pinheiro and Montell 2004).

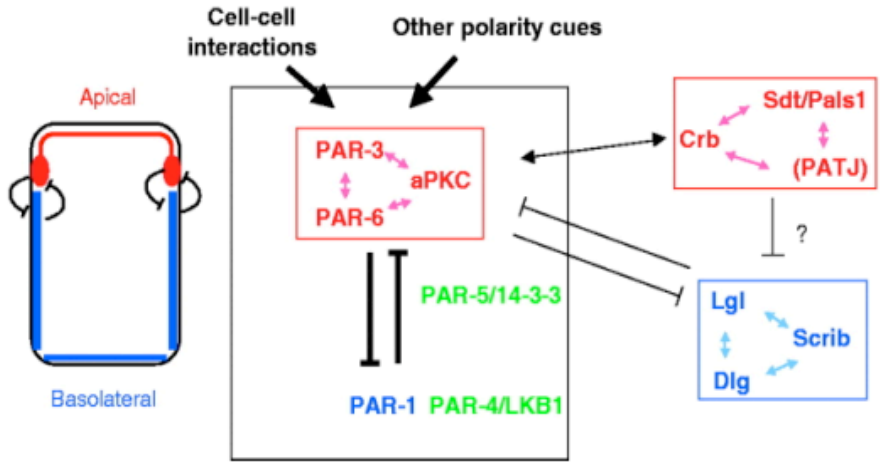

Figure 1.10: Overview of the polarization of an epithelium in *Drosophila* and interactions of the aPKC-Par comlex, the Crb complex and the Scrib complex, schematic taken from (Suzuki and Ohno 2006)

Studies in the fruit fly revealed two more protein complexes, the Crb (Crumbs) complex and the Scrib (Scribble) complex, both required for regulation of polarization. The Crb complex consists of Paj (Pals associated tight junction protein, a multi PDZ domain protein), Sdt (Stardust, a MAGUK protein) and the transmembrane protein Crumbs itself, localizing to the marginal zone (apical in epithelia). Apical localization of the aPKC-Par complex not only depends on Par-1 lateral exclusion but also on Crb-comlex mediated apical recruitment (Suzuki and Ohno 2006).

The Scrib complex consists of Lgl (lethal giant larvae, a myosin II binding protein with WD40 domains), Dlg (Disc large, a MAGUK protein) and Scrib (a LAP protein), localizing to basolateral membranes. Scrib complex proteins are components of septate junctions, which are ladder-like junctions corresponding to tight junctions in vertebrates. Both Lgl and Dlg were identified as being tumor suppressors in *Drosophila*, upon mutation, for example Dlg mutant follicular epithelia develop invasive tumors (De Lorenzo, Mechler et al. 1999).

All three complexes, PAR, Scrib and Crb, were shown to interact with each other, by restricting basolateral membrane domains and in positioning adherens junctions (Cereijido, Contreras et al. 2008).

1.3 Reverse genetics

“Understanding how organisms work” is the key question in the life sciences driving research for several different reasons: curiosity of mankind, desire to explain processes, the hope to cure diseases and development of new technologies. The discovery of genes as

the carriers of heritable information launched an entire era of genetics trying to “read” and understand genes in any living organism. Until now, a lot of genes are uncharacterized, independently of the organism. The classic approach to study gene function is mutagenizing the genome with chemicals, ionizing radiation or transposable elements followed by identifying the mutated gene responsible for a visible phenotype, called forward genetics. Researchers try to correlate phenotypes and underlying mutations of single genes in order to find those genes responsible for specific processes. High throughput sequencing projects of many organisms have generated valuable data sets of genomic sequences from microbes, viruses, plants, worms, insects and mammals and are still ongoing. These data sets serve as platform for multiple research disciplines such as species evolution or genetics. These days, researchers assign functions to genes, called reverse genetics.
In 2000, the first genome draft of *D. melanogaster* was published and with this the era of *Drosophila* reverse genetics was initiated (Adams, Celniker et al. 2000). Genes, whose presence was so far unknown, could be studied for their function. Gene function can be studied by mutation, deletion, over-expression, or silencing of the respective gene. Especially silencing of genes using RNA interference became a popular tool to study gene function promising even therapeutic applications in animal models (Neeta Shrivastava 2008).

1.3.1 RNA interference

RNA interference (RNAi) is the silencing of a gene product at the level of mRNA, thus the protein product fails to be made and the loss of function phenotype of this gene can studied. RNAi was first observed as an unexpected byproduct of an over-expression experiment in petunia plants. Instead of over-expression of a red pigmentation enzyme resulting in intense red flowers, some plants had colorless flowers indicating that both the transgene and the endogenous gene did not produce protein products (Napoli, Lemieux et al. 1990). This phenomenon was initially called post-transcriptional gene silencing (PTGS) but the mechanism behind it was not clear. Andrew Fire and Craig Mello discovered in the nematode worm, that injected double stranded RNA was the molecular species causing gene silencing (Fire, Xu et al. 1998) and coined this phenomenon “RNA interference”.

Double stranded RNA in a cell is recognized as foreign and unwanted. For example, some RNA viruses contain their genome as double stranded RNA (e.g. rotaviruses), which will be transcribed to DNA with a RNA dependent polymerase in the host cell and therefore poses

a potential danger to the cell. The RNase type III Dicer recognizes and cleaves double stranded RNA into small interfering RNA (siRNA) fragments of 21 – 23 nucleotides in length. SiRNAs are loaded onto the protein complex RISC (RNA induced silencing complex), which enables strand separation and pairing with complementary endogenous mRNA. One strand (= guide strand) of the siRNA is incorporated into RISC by binding to argonaute, the catalytically active RNase, but is not degraded. However, the other strand (= passenger strand) is cleaved by argonaute and therefore destroyed. In consequence, the guide strand on the RISC aligns with complementary mRNA and cleavage of mRNA occurs at sites of alignment. In general, the RNAi pathway is used as host defense mechanism against virus infections or as a regulator of gene expression using endogenously transcribed non-coding micro RNAs (miRNAs). Introduction of exogenous dsRNA enables controlled cleavage of target mRNA, which is exploited not only in basic research but is also being developed for therapeutic applications such as in the treatment of cancer, neurodegenerative diseases and infections to silence identified key molecules. For example, liposomal based delivery of siRNAs to silence the tyrosine kinase receptor EphA2, which is over-expressed in ovarian cancers, resulted in a 50% reduction of tumor size within 4 weeks of treatment (Landen, Chavez-Reyes et al. 2005). The challenge for therapeutic approaches is the successful delivery of dsRNA species into the target tissue or cells. Naked siRNA is extremely unstable, it needs to be stabilized for example by packaging into liposomes or delivery molecules (e.g. cholesterol, transferrin, antibodies), or it is locally applied e.g. by injection directly into the tissue such as eye, lung or central nervous system.

1.3.2 RNA interference in *Drosophila*

The RNAi machinery is being exploited for induction of gene silencing not only in *Drosophila* but as well of course in *C. elegans*, plants, mice, in various mammalian cell culture systems and recently in primary neuronal *Drosophila* cells (Sepp, Hong et al. 2008) In the course of my PhD, RNA mediated knock down was achieved by the use of the binary yeast Gal4/UAS system (Brand and Perrimon 1993) and the expression of an inverted repeat construct. In general, a tissue-, cell-, or stage specific promotor-Gal4 fusion transgene drives expression of an inverted repeat construct under the control of UAS (upstream activating sequence) (figure 1.11). Gene knock down is achieved only in the tissue where Gal4 is active; the rest of the organism is unaffected. Genes are knocked down at the level of mRNA, through mRNA degradation and protein translation does not take place. Using this UAS/Gal4

system, developmentally required genes can be studied in later stages of development for different functions, which would be otherwise not possible due to death of the organism and other more technically demanding methods have to be applied.

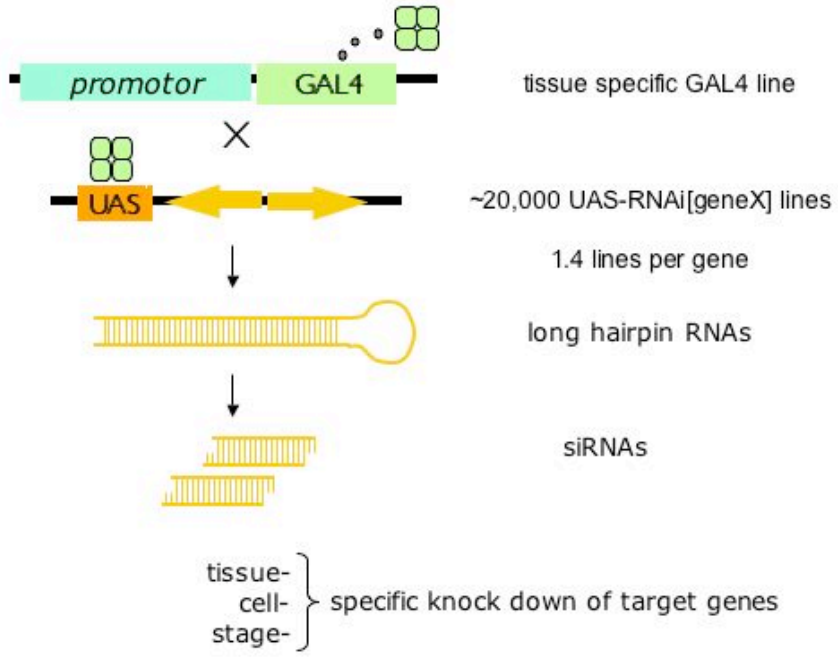

Figure 1.11: Induction of RNAi using the binary UAS/Gal4 system. Tissue specific expression of the trancription factor Gal4 induces transcription and formation of a long hairpin structure, which will be cleaved into short interfering RNAis, inducing endogenous degradation of complementary mRNA and knock down.

Dietzl et al. 2007 constructed and generated a collection of transgenic flies each containing an inverted repeat construct under UAS control for the targeted silencing of almost every gene in *Drosophila*. Every transgenic RNAi stock harbors an inverted repeat of 300 – 400 bp length under the control of UAS inserted somewhere in the genome. The RNAi transgene remains silent throughout maintenance of the stock. Only if the RNAi construct is combined with a promotor-Gal4 fusion by a crossing experiment, all progeny will induce RNAi mediated knock down corresponding to the expression pattern of the Gal4 inducer. In brief, Gal4 binds to the UAS element upstream of the inverted repeat and initiates transcription. mRNA of the inverted repeat assembles itself into a secondary hairpin structure. Double stranded RNA is recognized and induces the enzyme dicer to cleave the entire hairpin into 21 nucleotide pieces. These 21mers are incorporated into the RISC complex, binding corresponding endogenous full length mRNA. Double stranded RNA is not tolerated by the cellular machinery and is degraded. In consequence, both the endogenous and inverted repeat hairpin are degraded and result in suppression of the gene product. The availability of the unique *Drosophila* RNAi library in Vienna formed the basis of the border cell migration screen undertaken during my thesis work.

2 Results

2.1 Genome wide systematic RNAi screen

2.1.1 Setup of the RNAi screen

RNAi has become a convenient and powerful method to investigate gene function in a large number of systems and organisms ranging from cell culture to *C. elegans*, *Drosophila* and mice. With RNAi technology, it became possible to induce gene knock down in a tissue, cell or stage specific manner in contrast to studying whole body mutants. Inducible gene knock down facilitates the functional analysis of developmentally required genes, which was, until now, not possible due to death of the mutant animal. In 2006, Andrew Fire and Craig Mello received the Nobel Prize in Physiology for the discovery of the molecular species of RNA mediated gene silencing in *C. elegans* (Fire, Xu et al. 1998). Their work laid the foundations for the discovery of an entirely new RNA degradation and regulation machinery as well as RNA mediated silencing itself.

In this thesis I describe a genome wide RNAi screen utilizing border cell migration as migration system. For performance of an RNAi screen, one needs five things in general: an appropriate model system, a collection of transgenic RNAi fruit flies, a strong and selective inducer fly strain, at least one positive control and process optimization.

Model system*: Drosophila* border cell migration is ideal as a model system for studying cell migration in vivo: it is a programmed migration event representing both normal and pathological migration events. Border cell migration is a well-studied and attractive migration process as a model for invasive cell migration. In addition, as any other *Drosophila* model system, border cell migration offers the advantage of being genetically modified with state of the art genetic tools.

Transgenic RNAi fly stocks: I could make use of the unique genome wide collection of transgenic RNAi fly stocks generated by the group of B. Dickson (Dietzl, Chen et al. 2007), maintained and organized by the Vienna Drosophila Research Center (VDRC).

Selective inducer: For selected expression of the RNAi inducing hairpins I used the border cell specific promotor-Gal4 fusion “slbo-Gal4” to selectively knock down genes in a tissue specific manner (Rorth, Szabo et al. 1998). Slbo-Gal4 is expressed in posterior and anterior

border cells starting from late stage 8 onwards, as well as in centripetal follicle cells from stage 10 (figure 2.1). However, slbo-Gal4 expression is excluded from polar cells, the non-migratory pair of cells in the middle of the cluster. I recombined a reporter gene UAS-CD8GFP (mouse antigen CD8 fused to GFP, membrane targeted) to slbo-Gal4, which enabled me to visualize cells expressing both the RNAi construct and reporter gene.

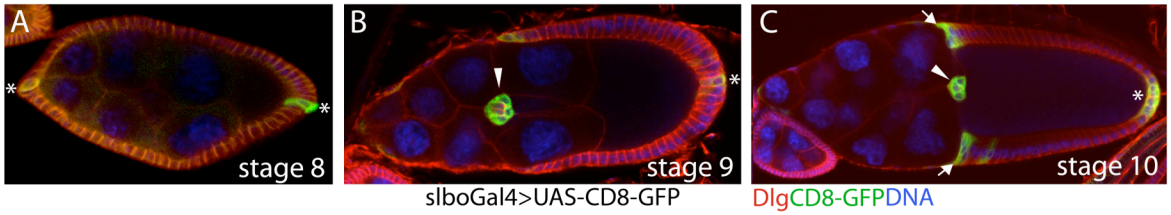

Figure 2.1: Expression pattern of the inducer line slbo-Gal4. Egg chambers of different stages expressing CD8-GFP under the control of slbo-Gal4, stained for Dlg (red), DNA (blue), CD8-GFP (green), arrowhead marks border cell cluster, asterisks marks polar cells, arrows mark centripetal follicle cells. **A)** stage 8 egg chamber, **B)** stage 9 egg chamber, **C)** stage 10 egg chamber

Slbo-Gal4 is expressed starting from late stage 8 egg chambers in anterior polar cells (figure 2.1A). During stage 9, slbo-Gal4 labels border cells (arrowhead) excluding anterior polar cells, but is active in posterior polar cells (figure 2.1B). Stage 10 egg chambers show slbo-Gal4 activity in border cells, centripetal follicle cells and posterior polar cells and neighboring follicle cells (figure 2.1C). The level of expression increases over time, visible if GFP intensities of panels A and B of figure 2.1 are compared

Positive controls: At the time I started the screen, 24 genes were known to be required for border cell migration (Naora and Montell 2005), of which I expected 22 genes to be able to see a phenotype. I tested as many genes as were available from the library (the collection was in the process of being generated and grew successively) and I could successfully knock down and phenocopy the known mutant phenotypes with RNAi of the five genes slbo (Montell, Rorth et al. 1992), domeless (Ghiglione, Devergne et al. 2002), shotgun (Oda, Uemura et al. 1997), Mrtf/mal-d (Somogyi and Rorth 2004) and taiman (Bai, Uehara et al. 2000) (Figure 2.2). All of these RNAi constructs showed a high phenotype penetrance, meaning a lot of egg chambers with defective border cell migration could be reproducibly observed in each RNAi experiment. In addition, all my positive controls gave rise to sterile females, indicating that RNAi knock down affects all egg chambers produced by the females.

Knock down of slbo itself yielded a high percentage of egg chambers with a border cell cluster stuck at the anterior tip of the egg chamber (52% of all egg chambers examined) (figure 2.2B-B'). Shotgun RNAi results in non-migrating or non-invasive border cell clusters

(observed in 69% of egg chambers)(figure 2.2C-C'). Non-invasive shotgun RNAi clusters typically stuck eccentrically on the surface of nurse cells, whereas normally the cluster is located in the center of the egg chamber along its anterior-posterior axis. Domeless RNAi induced dramatic defects on the border cell cluster shape and integrity (figure 2.2D-D') or completely blocked border cell migration (52%). Shape defects are characterized by a stretched border cell cluster, as if some cells are left behind on the way towards the oocyte. The quantification method used throughout the thesis for scoring migration defects, was not suitable for shape defects spanning large distances in the egg chamber, therefore I scored any domeless-type shape defect according to the midmost position of cells within the stretched cluster. Taiman RNAi egg chambers showed a dramatic block in border cell migration, 79% of all scored egg chambers completely lacked migration (figure2.2E). Mal-d RNAi egg chambers exhibited as all the other positive controls a large fraction of blocked border cell migration (88%) (figure 2.2F). RNAi mal-d egg chambers resemble weaker alleles of *Mal-d* mutant egg chambers. A strong allele of *mal-d* mutant lacking the first exon exhibits so-called cytoblasts, detached protrusions of the border cell cluster without nuclei, along the way of migration in front of the arrested border cell cluster, (Somogyi and Rorth 2004). I could not observe cytoblasts in mal-d RNAi egg chambers, which might be due to the fact that RNAi did not completely knock down mal-d protein resembling a weak allele of *mal-d* with some leftover function.

It has to be mentioned that all RNAi lines inducing any penetrant defect, result in mixed and variable phenotypes of border cell migration according to the accomplished migration distance. For this reason, the border cell cluster position is measured by stage 10 relative to its final position at the oocyte (figure 2.2G).

The quantification scheme was organized in a way that the migration distance was divided in five zones ranging from complete migration, ¾ of the distance, ½ of the distance, ¼ of the distance and no migration (0). Quantifications of all positive controls are depicted in figure 2.2H.

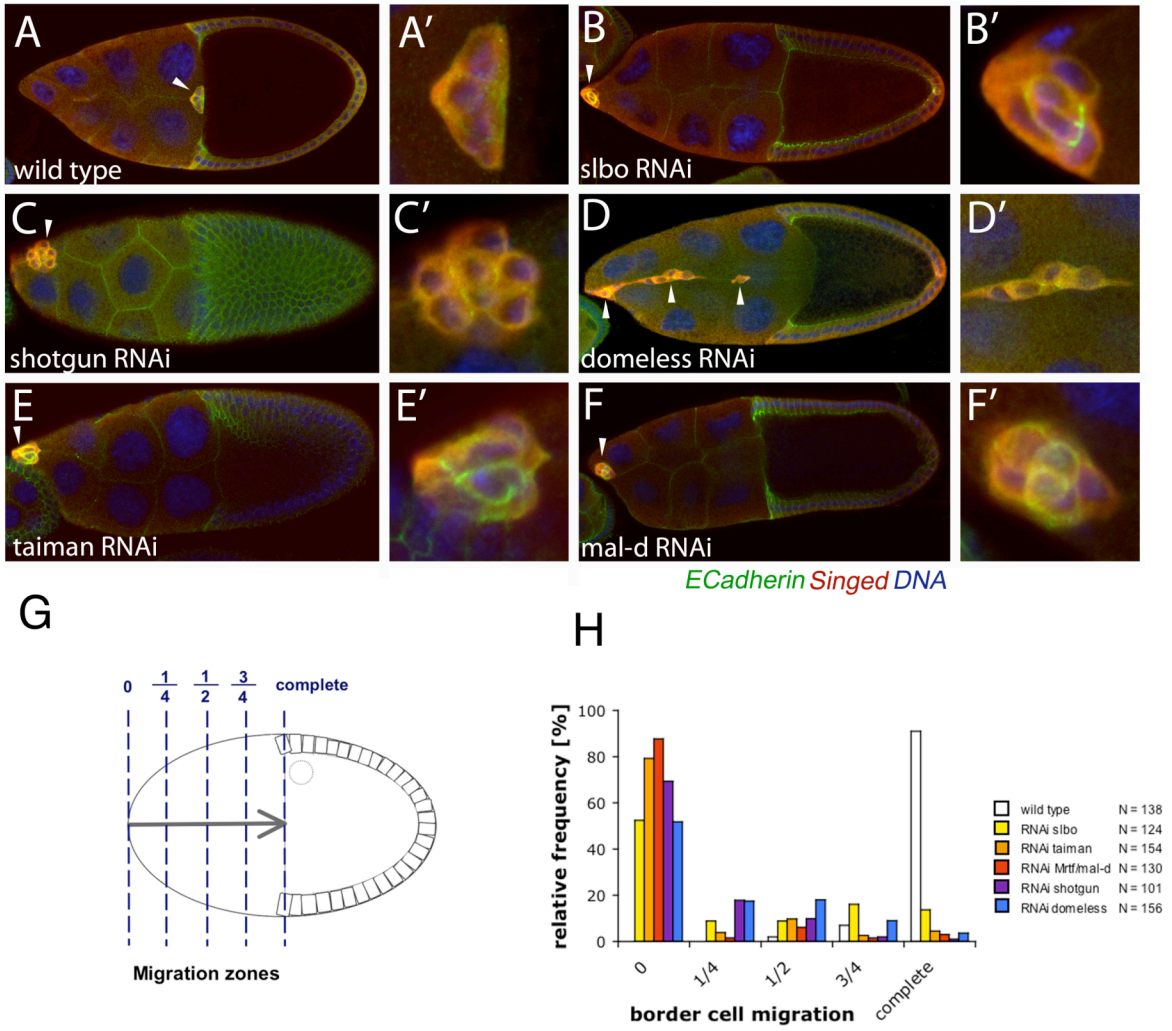

Figure 2.2: RNAi mediated knock down of positive controls blocks border cell migration. Stage 10 slbo-Gal4 egg chambers expressing UAS-RNAi[X] were stained for E-Cadherin (green), Singed (red) and DNA (blue). Arrowheads indicate border cell clusters, zoom-in of border cell clusters in (‘). **A-A’)** wild type egg chamber, **B-B’)** slbo-RNAi, **C-C’)** shotgun-RNAi, **D-D’)** domeless-RNAi, **E-E’)** taiman-RNAi, **F-F’)** mal-d-RNAi, **G)** quantification system of border cell migration defects showing five zones of migration relative to the entire distance to the oocyte, **H)** Border cell migration quantification of positive controls

Process optimization:

Documentation: The VDRC uses bar code assisted databases for maintaining, organization and ordering of fly stocks generated by Georg Dietzl and Christian Schusterreiter. The same barcode system is used for data collection and organization of screening data in order to ensure unbiased and blind screening as much as possible and to reduce formal errors to a minimum.

Fly crosses: Large-scale amounts of crosses between virgin females of the inducer line with males of the RNAi library require an enormous number and regular supply of virgin

females. Manual sorting and collection of virgin females is extremely time consuming. Therefore, I combined the inducer fly stock to a fly line exhibiting an apoptosis-inducing gene under a heat shock promoter (heat shock-hid, hs-hid) inserted on the Y chromosome (Y hs-hid). All flies (males) carrying the transgene will express the gene called hid (head involution defective) upon heat shock and will die due to massive induced apoptosis. Females of this fly stock never carry the inducible transgene and can develop normally after the heat shock until adulthood without being fertilized since all males are dead. Using the Y hs-hid transgene and a timed heat shock during larval development, large amounts of unfertilized females (= virgins) can be easily generated. In order to keep the Yhs-hid stock alive for normal breeding, the temperature should never exceed 25°C. The Yhs-hid transgenic fly stock was designed and generated by Georg Dietzl for the use of large scale producation of virgin females and was used by almost all current RNAi screeners. More technical related optimizations are described in the section material and methods.

2.1.2 Procedure of the RNAi screen

Figure 2.3 shows the screening workflow of the genome wide RNAi border cell migration screen. In the screening phase, between 400 and 800 individual crosses with males of the library were set up simultaneously. The number of initiated crosses depended on external parameters such as available manpower in the fly facility or screening persons, condition, health and availability of fly stocks in the library, resulting in fluctuating screening throughputs. The screening procedure was performed in a continuous mode, every week crosses were set up, whereas progeny flies from previous weeks were processed and analyzed. Fly crosses were kept at 25°C until adulthood. 14 days after set up of the cross, F1 progeny flies were collected for testing. Per RNAi knock down genotype, 5 females with the correct genotype (inducer + RNAi transgenes) together with 3 males of any genotype were sorted and fattened with additional yeast for 1 day to increase egg chamber production. In addition, flies for testing were kept at 27°C during this day to enhance expression of the hairpin construct. On the next day, 3 well-fed females per genotype (they show a swollen abdomen) were CO_2 anesthetized and their ovaries dissected. The ovaries were fixed, washed, mounted on glass slides and labeled with the corresponding barcode tag.

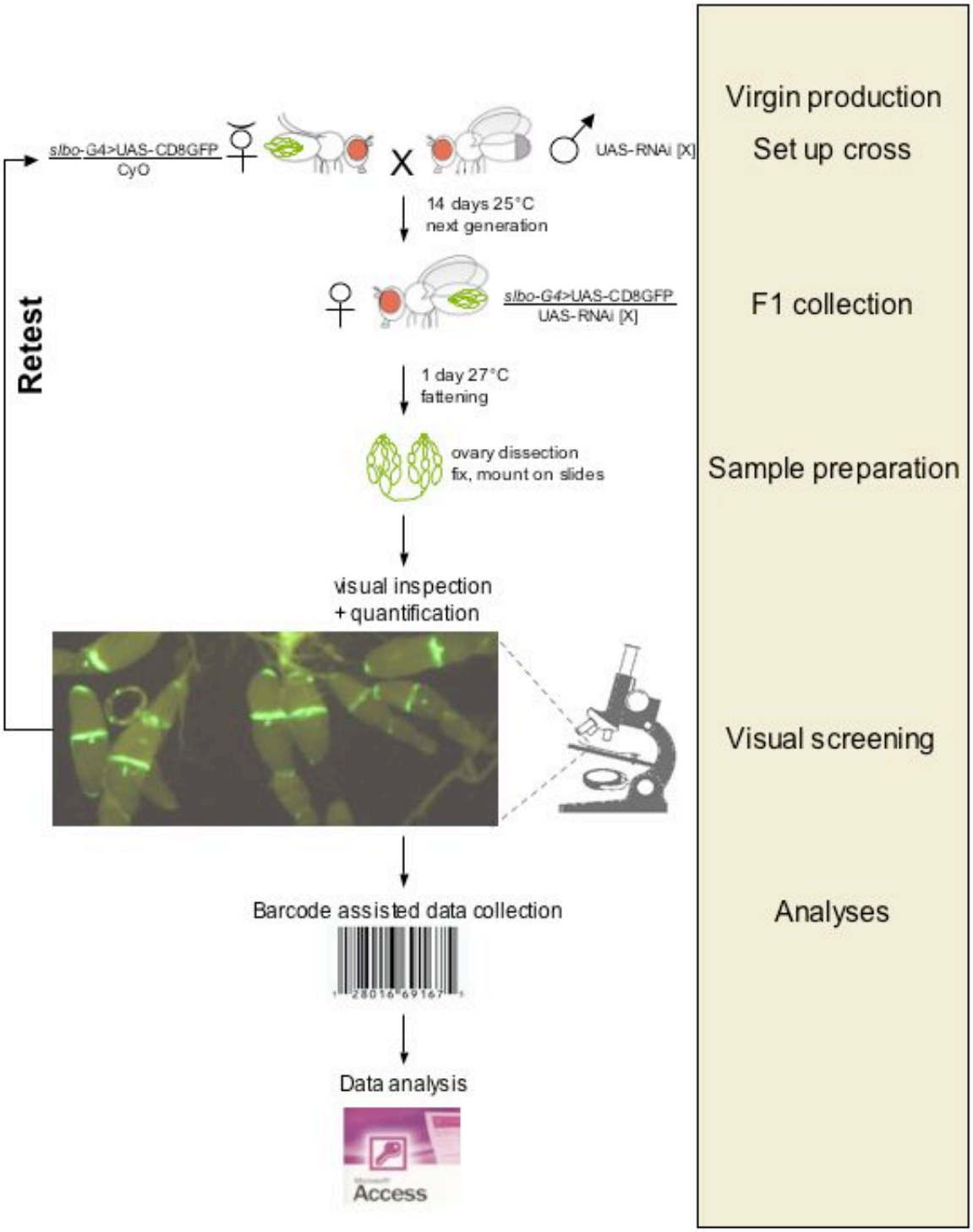

Figure 2.3: **Workflow of the genome wide RNAi screen.** The screening procedure is divided into virgin production, set up of the fly cross, F1 progeny collection, sample preparation, visual screening and analyses. The screen was performed in batches of 400 – 800 RNAi lines/week.

2.1.3 Scoring system and classification of phenotypes

Visual inspection of each genotype was performed using a Leica fluorescence microscope and 5x objective. All stage 10 egg chambers per sample were screened for the criterion: "Has the border cell cluster arrived at the oocyte by stage 10?" In the first instance during inspection of a sample, stage 10 egg chambers were scored subjectively for the absence of any phenotype. A score "no abnormality detected (NAD) was assigned to egg chambers showing wild type features. Samples showing very few, mild or drastic defects in border cell migration were quantified according to a scoring scheme from 0 to 10 (table 2.1) and classification of phenotypes (figure 2.4) (delayed migration, no migration, wild type and other).

% egg chambers with defective cluster migration	Screening Score
0 - 5%	0
6 - 15%	1
16 - 25%	2
26 - 35%	3
36 - 45%	4
46 - 55%	5
56 - 65%	6
66 - 75%	7
76 - 85%	8
86 - 95%	9
96 - 100%	10

Table 2.1: Scoring rating for the proportion of egg chambers with defective cluster migration

Scores 0 to 10 describe how many egg chambers show any defects of the border cell cluster migration. A score of 10 means, all egg chambers show defective border cell cluster migration and the RNAi phenotype is extremely penetrant. A high screening score is therefore desirable. Table 2.1 shows the decoding key for the screening scores. It has to be mentioned that screening scores 0 and 10 exhibit a 5 % penetrance difference to the next classes (1 and 9) whereas all other scores exhibit a 10 % difference to the next class. I decided to make these two extreme classes tighter because on the one side a score of 0 is not interesting and on the other side I know score 10 means an exceptional strong phenotype, thereby increasing the value of this score. The phenotype classification I used during the screen is a simplified version of the classification commonly used in the border cell field, where the egg chamber is divided into five different zones of possible cluster position.

Figure 2.4: Expression pattern of slbo-Gal4 at stage 10 and observed phenotype classes. Schematic drawings of the most abundant observed phenotypes during the screen (wild type, delayed and no migration). Delayed migration was the most prominent class, whereas the position of the border cell cluster relative to the oocyte was not further specified in this system.

In the pilot-screening phase, I tested positive controls and a random set of genes in order to test throughput capacities and to see which phenotypes can be obtained. From the positive control set I saw that I could phenocopy even border cell cluster shape regulators such as domeless and I hoped to identify more of genes responsible for shape integrity. Unfortunately, the majority of genes identified showed the classes delayed migration or no migration phenotype defects. At the same time, the positive controls and novel identified genes exhibited a mixture of phenotype classes. It is known that RNAi mediated knock down results in variable phenotypes within an experiment. For the border cell system I cannot judge if the introduction of RNAi increases phenotype variability. Even null mutant analyses using border cell migration exhibit significant variations in phenotype strength (Somogyi and Rorth 2004).

2.1.4 Screening strategies

2.1.4.1 Female sterility

The initial strategy was to use sterility/fertility as screening readout, since a complete lack of border cell migration results in sterile females. Indeed, I observed sterile females in all the positive control RNAi experiments. I wanted to make use of this observation as an indirect readout for border cell migration. The assay is very quick since “yes or no” offspring are immediately visible. Females would be allowed to lay eggs, which would develop into larvae with wild type, but not with sterile females. The assay would simply be a check for the presence or absence of offspring (larvae). Unfortunately, it turned out that not all sterile females showed defects in border cell migration. Moreover, some fertile females showed

mild but significant border cell migration defects and these candidates would have been missed by screening for sterility as primary readout. As consequence, I decided to use a different albeit much more labor-intensive readout for border cell migration.

2.1.4.2 Visual inspection

I chose the relative position of the border cell cluster at stage 10 as a visual and direct screening readout for border cell migration. Every egg chamber was judged for successfully completion or defective border cell migration and the overall shape of the border cell cluster. The border cell cluster was visualized under the fluorescence microscope by excitation of a membrane tethered GFP marker (CD8-GFP) under the control of slbo-Gal4. Visual inspection is a reliable assay but the sample preparation and the screening effort are very time-consuming compared to simply looking for sterile females. Nevertheless, I decided to perform a genome wide screen using large-scale ovary dissection and visual screening to identify genes involved in border cell migration.

2.1.5 Screening results

2.1.5.1 Screening hit rate

In August 2005, I started the genome wide RNAi screen for border cell migration using the sterility assay as screening readout. As already described, I realized that sterility is not a bona fide readout for defective border cell migration, so I changed the screening procedure to a dissection and visual inspection based screening in November 2005. I retested putative hits along the way in order to be as unbiased as possible. I stopped screening in September 2007 with an "end of screen party". Taken together, the pilot phase and screening phase took about 2.5 years.

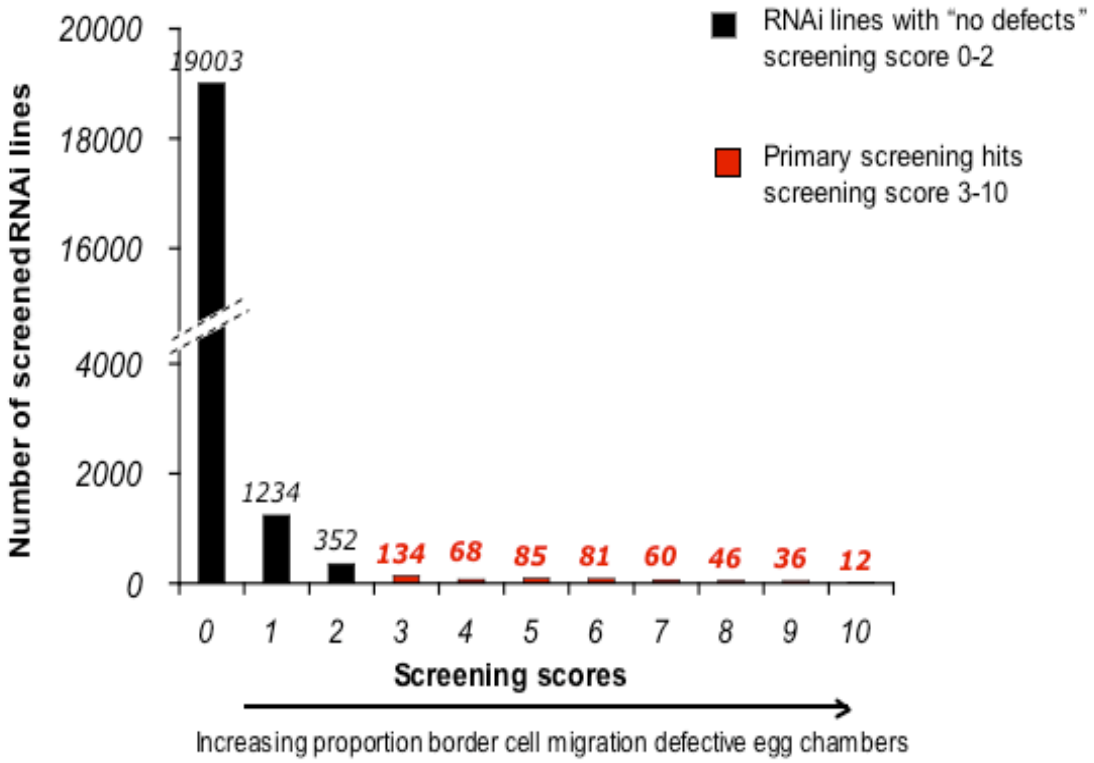

Figure 2.5: Screening score distribution of all screened lines. Absolute frequency distribution of the number of screened lines in each screening score class. The cutoff for potential hits was assigned to 3, black bars represent RNAi lines which gave no significant defects (screening score 0-2), red bars represent primary screening hits (screening score 3-10).

Figure 2.5 shows the frequency distribution of all screened RNAi lines versus the penetrance of the RNAi effect in the RNAi border cell migration screen. In total, 21111 fly lines were screened (including retests), represented by 19582 independent transformants and 12169 genes, covering 87% of the *Drosophila melanogaster* genome. Currently, the VDRC collection covers 88% of the fly genome.

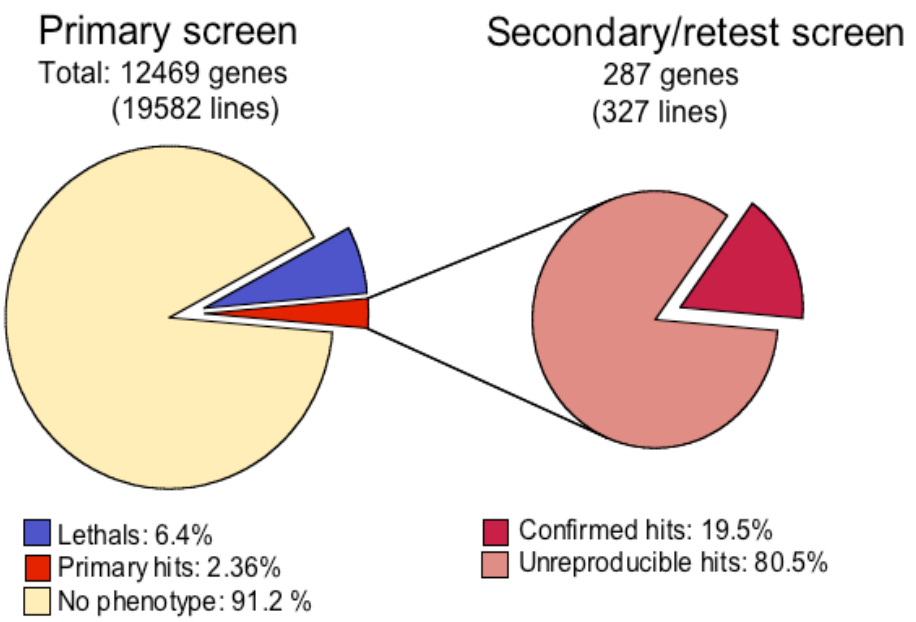

Figure 2.6: Statistics of the primary screen and retest screen, percentages are calculated from all screened genes

Figure 2.6 shows a pie chart of the number of lines picked up in the primary screens (327 lines or 287 genes) corresponding to a primary hit rate of 2.36 % which reduced to a final hit rate of 0.46 %, corresponding to 57 genes after retesting at least once (=minimum). The question arising is, why not all lines picked up in the primary screen could be verified with repeating, and why are there more lines than genes picked up? It is known that the site of insertion in the genome influences the strength of expression of the hairpin independently of the inducer strength, giving rise to different hairpin expression levels within different transformants of the same construct. Another possibility is, that insertion of the RNAi construct into a regulatory element induces nearby genes to be misregulated and to interfere with the model system independently of the RNAi knock down. Therefore, the VDRC collection exhibits for some genes 2 transformants of the same RNAi construct. Ideally, a hit is represented by two independent insertion transformants, showing reproducible strong phenotypes with both lines after RNAi induction. However, reality rather shows that for some hits, the second line does not show a phenotype. In these cases it is unclear if the phenotype is dependent on the insertion site or the RNAi itself. These genes could then classify as hits and need further investigation.

2.1.5.2 Lethality rate

During the RNAi screen I observed that RNAi induction using slbo-Gal4 sometimes resulted in dead pupae. Of all lines tested, 1026 lines (778 genes) resulted in dead flies during a late pupal stage, resulting in an overall line lethality rate of 5.2 % (6.4 % of all genes tested). Lethality was subjectively scored by roughly estimating the percentage of dead pupae (black bodies in pupal case) in the range of 0 (0% lethals) to 10 (100% lethals). However, I defined a lethal gene if the lethality score was greater or equal to 5. The observation of lethality is explained by ectopic expression of the inducer line in a different tissue at this pupal stage of development (probably in neurons, but not further characterized). It happens very often that transcription factor promotor-Gal4 fusions exhibit more than one tissue of expression. The observation of lethality was therefore not unusual. In the set of the so-called “lethal genes”, mostly house keeping genes such as ribosome subunits, transcription and translation machinery components were found (figure 2.7). Before I started to screen, I expected to pick up a lot of housekeeping genes since cell viability is crucial for cell migration. It turned out that a lot of house keeping genes are lethal in my screening set up and therefore the number of unspecific hits decreased dramatically. Likewise, less time was spent analyzing RNAi phenotypes induced by unspecific effects. A complete list of lethal genes after knock down can be found in the appendix.

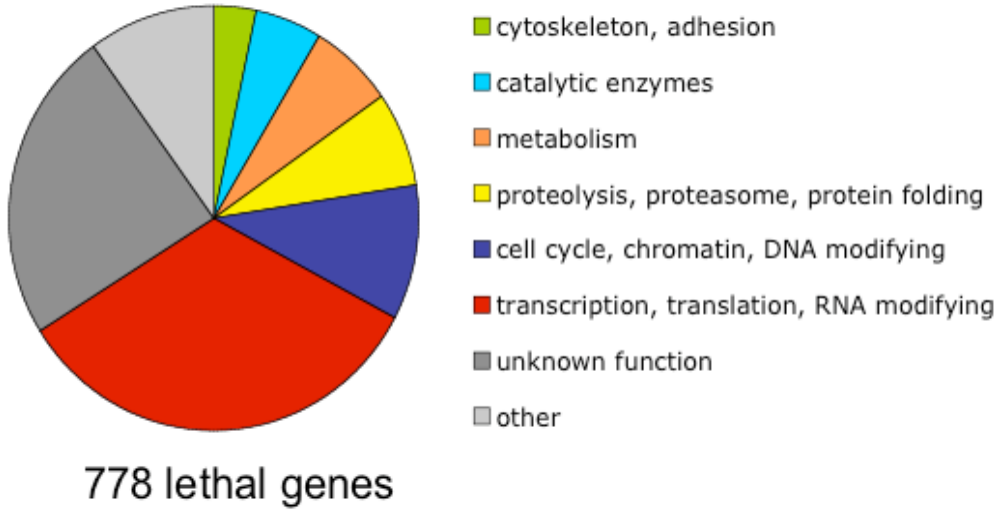

Figure 2.7: Pie chart of lethal genes sorted by their function, 778 genes were scored as lethal with a lethality score of ≥ 5

The majority of lethal genes were in the functional class involved in transcription, translation and RNA modifying proteins (33.4%), followed by the class with unknown function (24%). Proteins involved in cell cycle, mitosis, chromatin architecture or DNA modifying enzymes represented another predominant class (10%) of lethal genes. Overall, these genes are

required for maintenance and proper cell metabolism and silencing of these genes interferes with cell viability.

2.1.5.3 Hits are enriched for low s19 scores and multiple CAN repeats

Researchers in the RNAi field, performing small scale RNAi experiments and large-scale screens, realized the necessity to exclude, or at least predict, possible unspecific off-target effects resulting from the technique itself. Some screening setups tend to repeatedly knock down unrelated molecules in addition to the protein of interest. These false positive target molecules tend to exhibit poly-glutamine (poly Q) rich stretches encoded by CAN repeats. For example, β-catenin is mainly targeted in wnt signaling screens due to its multiple ankyrin repeats (Kulkarni, Booker et al. 2006). Unspecific co-knock down increases the false positive hit rate dramatically and increases time necessary to identify true positives.
Georg Dietzl introduced a parameter to estimate the specificity of knock down by an in silico analysis of all RNAi constructs (Dietzl, Chen et al. 2007). The so-called s19 score estimates how many possibly cleaved 19 mer nucleotides of the entire RNAi construct complement the gene of interest or other genes (=off-target). The ratio of on-targets and off-targets results in the s19 score, with 1 being the optimal “on-score” corresponding to 100% specificity for the target gene. Dietzl, Chen et al. suggested the assignment of off-target ranking for a s19 score below 0.8, however it remains to be tested how well these in silico predictions reflect reality.
I subjected all my hits to the s19 analysis and established that 82 % of all border cell migration hits exhibit an s19 score below 0.8 indicating that the possibility of off-targets is relatively high and very few RNAi constructs seem to be specific. It seems as if this screening set up for border cell migration is especially prone to off-target hits (see Figure 2.8). For the analysis of all these genes I sorted all hits for the s19 score in order to prioritize for specific knock down. Surprisingly, my positive controls were scattered over the entire range of s19 score, indicating that even genes with low s19 scores can be relevant hits (see Figure 2.8). In order to confirm whether all hits are indeed required for border cell migration, each one has to be analyzed in detail with mutants and localization studies.

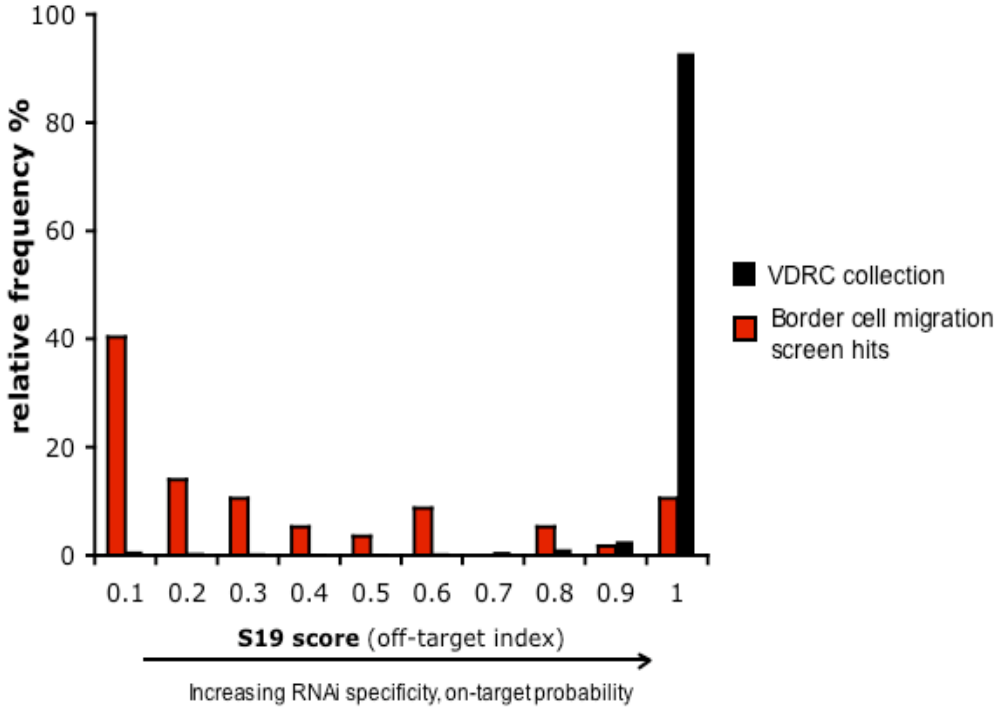

Figure 2.8: Border cell migration hits are enriched for low S19 scores compared to the entire VDRC collection. Relative frequency distribution of the s19 score calculated for the inverted repeats from the entire VDRC collection (black) and border cell migration screen hits (grey). The majority of the VDRC collection exhibits a very good s19 score of between 1 and 0.9 (95.4%), by that means the majority of constructs do not show any indication of off-target probability. Hits of the border cell migration screen are enriched in constructs of an s19 score of about 0.1 and the entire distribution is left-shifted towards lower s19 scores.

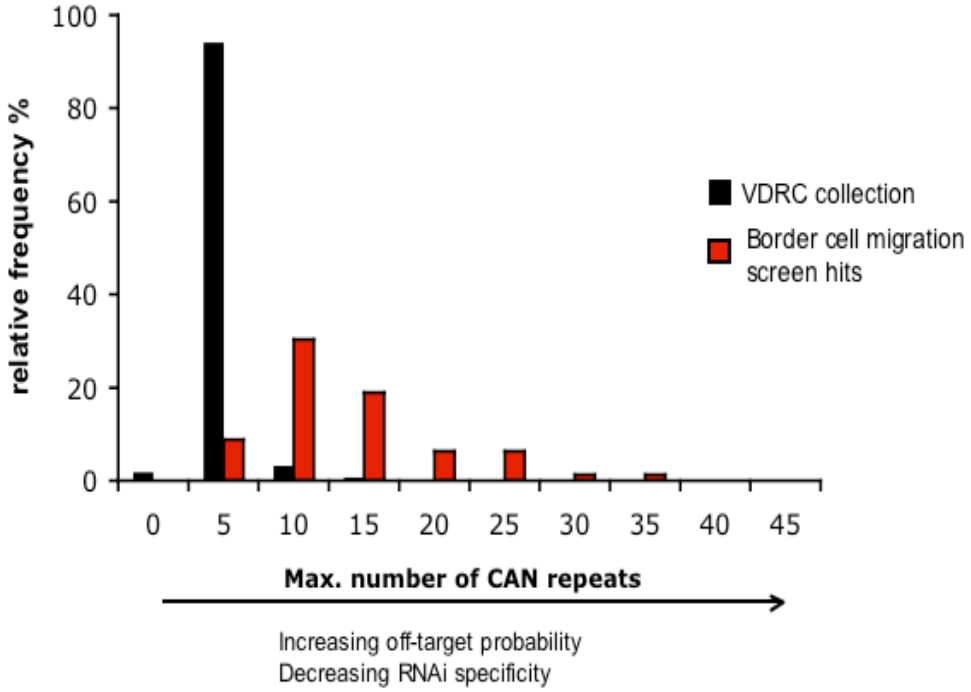

Figure 2.9: Border cell migration hits are enriched for 10-15 CAN repeats compared to the entire VDRC collection. Relative frequency distribution of maximum number of CAN repeats within the inverted repeats of the VDRC collection (black) and border cell migration screen hits (grey).

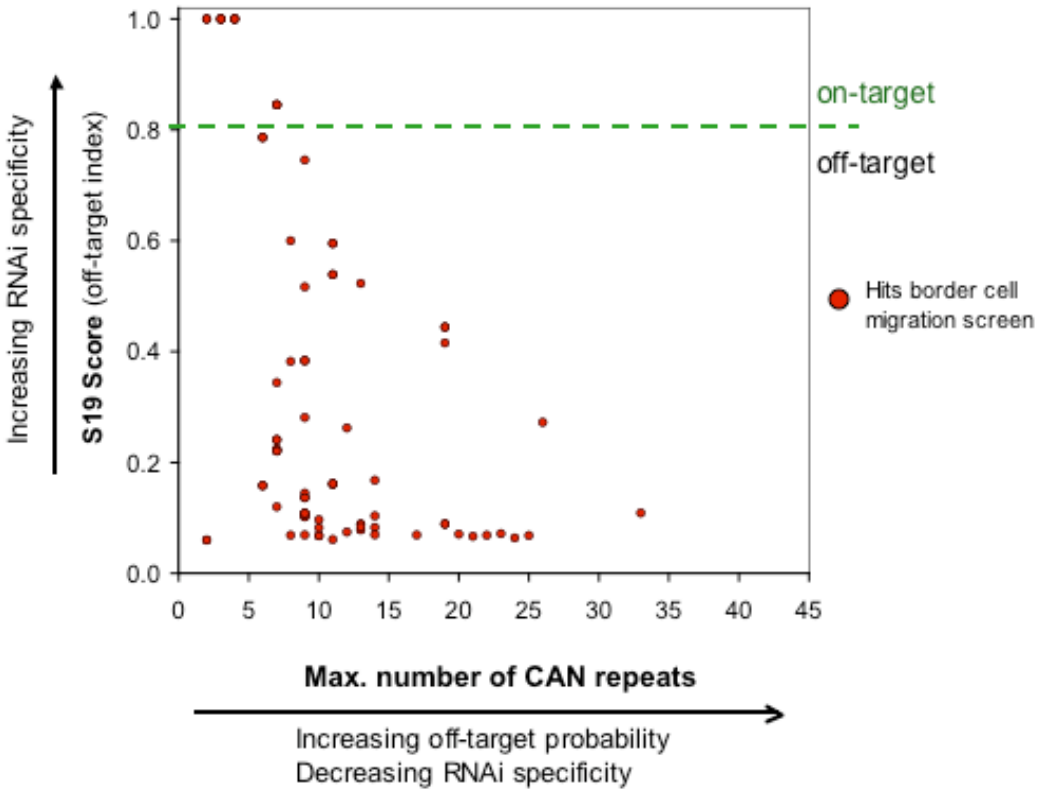

Figure 2.10: **Relationship between s19 and maximum number of CAN repeats of border cell migration hits.** Scatterplot of s19 scores versus maximum number of CAN repeats from border cell migration hits.

Figure 2.9 shows compares the frequency distribution of the maximum number of CAN repeats within the cloned hairpin of the VDRC collection and the border cell migration hits, indicating that hits are enriched for maximum number of CAN repeats of 10 -15. I wanted to know if the CAN repeat correlates with the s19 score, meaning that the increased CAN repeats are the reason for the low s19 score? Therefore, the s19 score versus the maximum number of CAN repeats of all border cell migration hits were plotted, shown in figure 2.10, suggesting that the majority of data points do not show a correlation between s19 and CAN repeat number, only very few low s19 scores can be explained by a high number of CAN repeats.

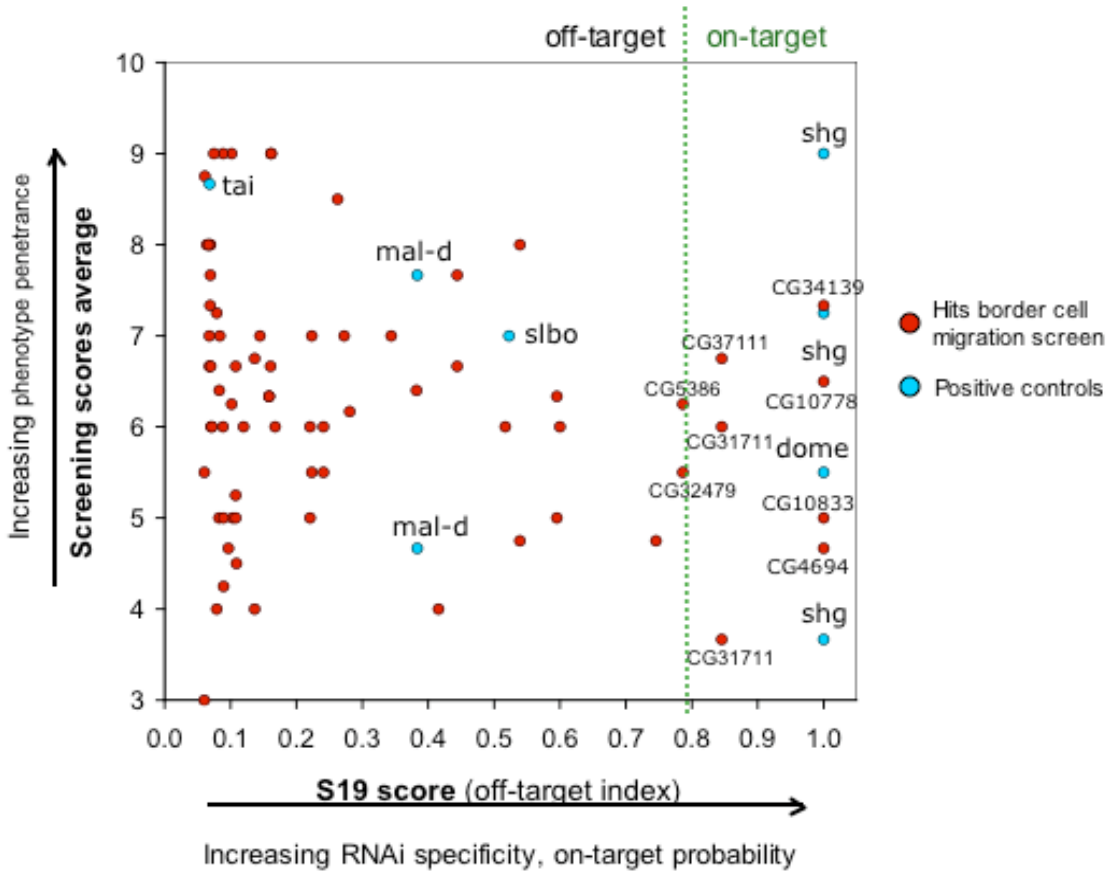

Figure 2.11: Screening score versus s19 distribution of positive controls among border cell migration hits. Scatterplot of average screening scores versus s19 score from border cell migration hits, red dots indicate novel identified genes, blue dots indicate positive controls

Figure 2.11 compares the migration defects (average of screening scores) with the s19 score of the RNAi constructs from border cell screen hits. It becomes evident that there is no relationship between screening score and s19 score. In addition, positive controls (red dots) are scattered over the entire range of the s19 score. However all these relationship analysis are of descriptive nature and need to be reevaluated with detailed individual characterization for confirmation. In summary, the s19 score is a guide, but by no mean, a reliable measure of false positives.

2.1.5.4 Hits are enriched for transcription factors

Initially, this screen was performed in order to find novel regulators of the cytoskeleton. (Rogers, Wiedemann et al. 2003) performed a small scale RNAi screen, they tested about 90 genes implicated in lamella formation in *Drosophila* S2 cells using siRNA and identified a small set to be required in this in vitro system, such as Arp2/3, SCAR, capping protein,

cofilin or profilin. In an analogous way, we wanted to identify novel regulators for an in vivo migration system. After the first weeks of testing positive controls and prescreening, it became evident that the classes of genes that can be picked up by this assay were neither components of the cytoskeleton nor already known regulators such as Rho, Rac or MyosinVI (*jaguar*). On the contrary, rather transcription factors and miscellaneous genes of unknown function were found. The time window of RNAi expression and individual protein half-life can explain this observation. The longer RNAi is expressed developmentally prior to the screening assay, the more time is available to turn over and degrade already made proteins. If proteins of interest exhibit a long protein half-life, it will take longer in order to reduce protein amounts and observe the knock down effect. In contrast, proteins with a fast turnover will be knocked down earlier and the effect is earlier detectable. In the case for the border cell migration screen, slbo-Gal4 determines the time of RNAi expression. Slbo-Gal4 is expressed only shortly in the range of hours (stage 8) prior to migration of the cluster and the time point of the assay (stage 10). In this RNAi screening set up, genes with a short protein half-life or those turned on during the stages of interest can be picked up, which is on the one hand advantageous since the switch between non-migratory and migratory has to happen fast. Cytoskeleton components and regulators need longer RNAi expression windows in the range of days to be depleted (personal communications from screening colleagues). The final list of hits confirms these preliminary observations, namely the biggest class of genes are transcription factors, followed by genes without annotated protein domain structures. Figure 2.12 shows the complete list of genes reproducibly picked up in the border cell migration screen.

CG number		Gene name	Screening score average	max.no CAN repeats	S19	Function
CG3722	*	*shotgun*	9.0	4	1.0	cell-cell adhesion
CG34139	*		7.3	3	1.0	neuroligin
CG14226	*	*domeless*	5.5	3	1.0	receptor
CG4694	*	*hermaphrodite*	4.7	3	1.0	transcription factor
CG10778	*		6.5	2	1.0	prenyltransferase
CG31711	*		3.7	7	0.8	phosphorylation
CG5386	*		6.3	6	0.8	-
CG32479	*		5.5	6	0.8	deubiquitination
CG15690	*		4.8	9	0.7	-
CG15494	*		6.0	8	0.6	-
CG13287	*		6.3	11	0.6	transcription factor
CG15781	*		8.0	11	0.5	transcription factor
CG4354	*	*slbo*	7.0	13	0.5	transcription factor
CG32334	*		6.0	9	0.5	-
CG7552			7.7	19	0.4	-
CG13235			4.0	19	0.4	-
CG32296	*	*Mrtf/mal-d*	7.7	9	0.4	transcription factor
CG7317		*CG34401*	6.4	8	0.4	transcription factor
CG12218		*mei-p26*	7.0	7	0.3	germ cell development
CG17077		*pointed*	6.2	9	0.3	transcription factor
CG14560		*ms-opa*	7.0	26	0.3	-
CG15765			8.5	12	0.3	-
CG30123			6.0	7	0.2	sulfotransferase
CG16777			7.0	7	0.2	-
CG1130		*scratch*	6.0	7	0.2	transcription factor
CG15455			6.0	14	0.2	-
CG14180			9.0	11	0.2	-
CG7803		*zeste*	6.7	11	0.2	transcription factor
CG11245			6.3	6	0.2	-
CG32771			7.0	9	0.1	-
CG32132			6.8	9	0.1	-
CG14264			6.0	7	0.1	-
CG6026			4.5	33	0.1	-
CG10883			6.7	9	0.1	-
CG2829		*tlk*	5.0	14	0.1	phosphorylation
CG5905		*Neprilysin1*	9.0	9	0.1	metalloprotease
CG18024		*SoxNeuro*	4.7	10	0.1	transcription factor
CG11505			5.0	19	0.1	-
CG3143		*foxo*	9.0	13	0.1	transcription factor
CG14459			7.0	13	0.1	-
CG4070		*Tis11*	6.4	14	0.1	-
CG2368		*pipsqueak*	5.0	10	0.1	transcription factor
CG32045		*furry*	7.3	13	0.1	transcription factor
CG30126			9.0	12	0.1	-
CG12223		*Dsp1*	6.0	23	0.1	transcript, corepressor
CG6191			6.0	20	0.1	-
CG18599			6.7	14	0.1	-
CG11873			7.7	9	0.1	-
CG32606			8.0	17	0.1	-
CG31847			7.3	8	0.1	-
CG13109	*	*taiman*	8.7	22	0.1	coactivator
CG32778			6.7	25	0.1	-
CG32049			8.0	10	0.1	-
CG13260			8.0	21	0.1	-
CG15470			8.0	24	0.1	-
CG31761		*bruno-2*	8.8	11	0.1	mRNA binding
CG3851		*odd skipped*	5.5	2	0.1	morphogenesis

Figure 2.12: Border cell migration hits sorted by s19 score. Hits are shown with their CG number, gene name if present, the average screening score, the maximum number of CAN repeats, the s19 score of corresponding inverted repeats, and the annotated putative function. Red asterisks indicate positive controls, green asterisks mark highly specific and interesting genes, yellow asterisks mark genes of medium specificity and interest.

2.2 Characterization of CG34139 (wanderlust)

2.2.1 RNAi phenotype

CG34139 was identified as a modulator of border cell migration using RNAi mediated knock down in a systematic genome wide RNAi screen. *CG34139* is so far uncharacterized and I designate this gene as "wanderlust" abbreviated as "wadl", due to its role in migration. The phenotype of *wanderlust*-T2 (transformant 2) RNAi is extremely strong and was reproducible in all retesting experiments. In *wanderlust*-T2 RNAi samples, the majority of border cell clusters (49 %) did not move away from the anterior tip of the egg chamber until stage 10 (figure 2.13B). In total, 83 % of all egg chambers showed a defective phenotype ranging from no migration until ¾ completed migration, only very few egg chambers successfully completed migration to the oocyte (17 %) (figure 2.13D).

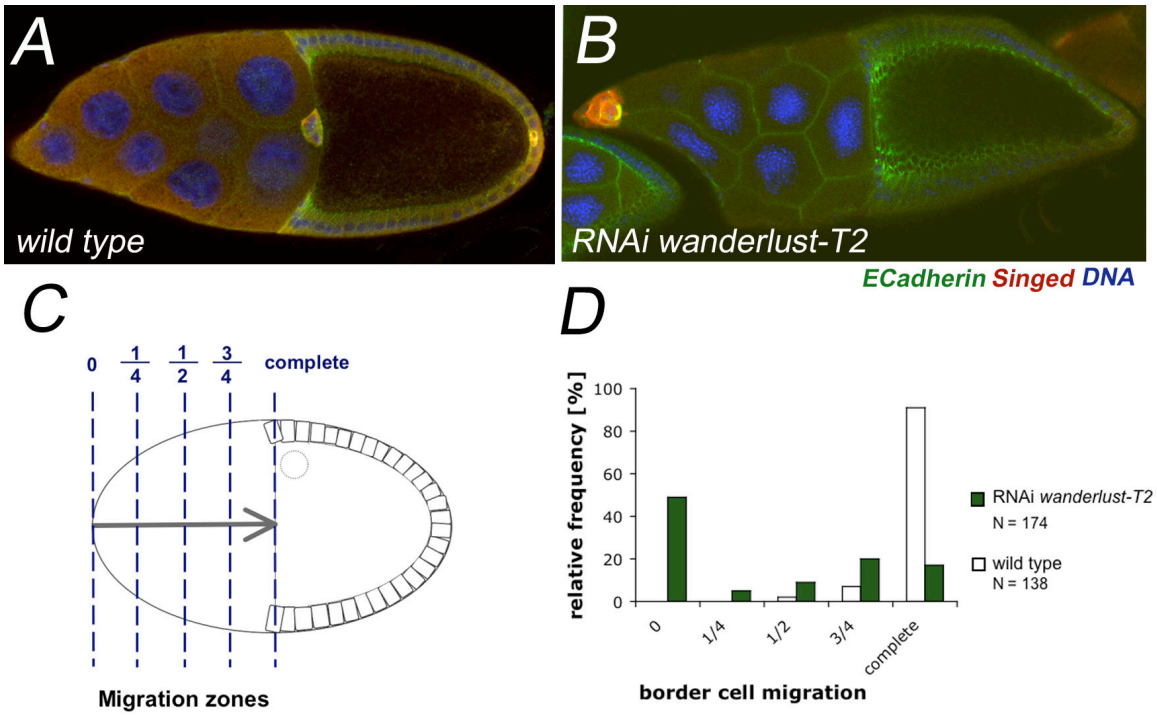

Figure 2.13: *Wanderlust-T2* RNAi induces a block in border cell migration. Stage 10 egg chambers were stained for ECadherin (green), Singed (red) and DNA (blue). RNAi was induced by slbo-Gal4. **A)** wild type, **B)** *wanderlust-T2* RNAi, **C)** quantification of wild type and *wanderlust-T2* RNAi samples

The large-scale visual inspection, using CD8-GFP as marker during the screen, was followed by a more detailed description of obtained phenotypes. Figure 2.13B shows a *wanderlust-T2* RNAi stage 10 egg chamber induced with slbo-Gal4 and stained for Singed (Sn), a marker for the border cell cluster and E-Cadherin, staining cell-cell contacts. The border cell cluster has formed properly but it did not migrate towards the oocyte. In wild type egg chambers the border cell cluster typically arrived at the oocyte by stage 10 (figure 2.13A). A second transformant line (designated as RNAi *wanderlust-T1*) is available for wanderlust, however upon knock down it results in a much milder phenotype than compared to the *wanderlust-T2* line picked up in the screen.
Immunofluorescence pictures of egg chambers and its border cell clusters only show a snapshot of border cell migration and does not unveil underlying cellular dynamics during the migration process. Live imaging of the border cell cluster both under wild type and RNAi knock down conditions was therefore performed (see below).

Until recently, researchers failed to find conditions to maintain egg chambers in vitro to image border cell migration. In 2007, three independent publications claimed to have developed a method for cultivation of egg chambers in order to study border cell migration (Bianco, Poukkula et al. 2007; Prasad and Montell 2007; Tekotte, Tollervey et al. 2007). 2 out of these 3 publications used among other ingredients, bovine insulin as a key reagent. However, (Tekotte, Tollervey et al. 2007) cultivated egg chamber in halocarbon oil without additives resulting equally long cultivation periods for imaging.

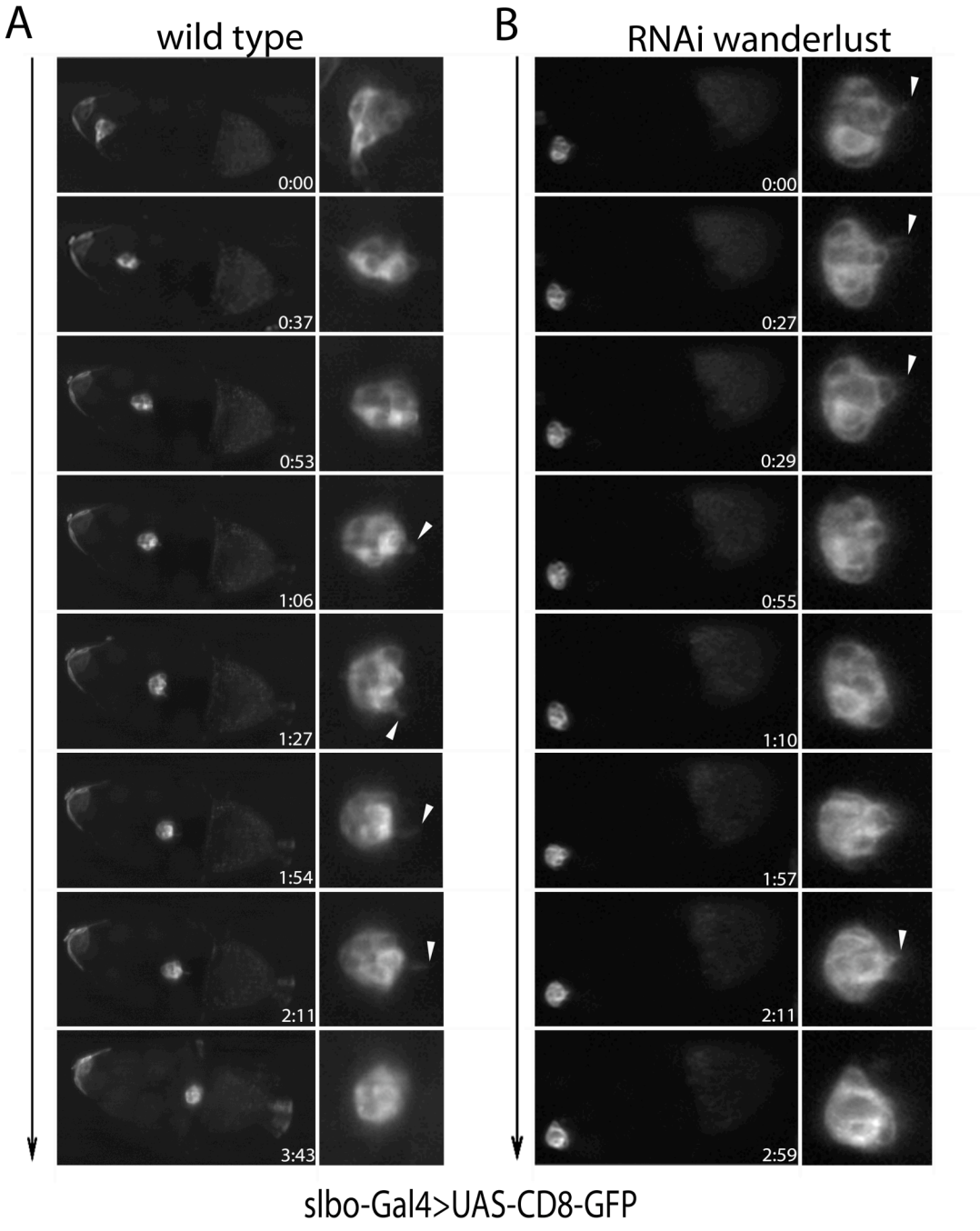

Figure 2.14: Live imaging of A) wild type and B) *wanderlust-T2* RNAi egg chambers. Slbo-Gal4>UAS-CD8-GFP expressing egg chambers are imaged over multiple hours, zoom-in of border cell cluster is shown for each time point, arrowheads mark protrusions. *Wanderlust-T2* RNAi egg chambers exhibit internal shuffling activity and produce cellular protrusions (arrowheads) though cluster migration is blocked. Elapsed time is given in hours:minutes.

I established in vitro cultivation of egg chambers according to Prasad and Montell 2007 with slight modifications and it worked the very first time. Nevertheless, the cultivation is not extremely robust and the efficiency of successful border cell migration under wild type

conditions is extremely variable from experiment to experiment probably due to damage of the egg chambers during dissection and isolation.

As described (Bianco, Poukkula et al. 2007; Prasad and Montell 2007), I could observe the cluster moving in a unique way, meaning the cells showed a very dynamic behavior within the cluster while migrating as a whole. Border cells constantly exchanged positions relative to each other (see wild type movie). This observation of cells constantly shuffling around and changing position relative to each other was very surprising and intriguing. Is this shuffling necessary for migration or is it an artifact of cultivation using insulin as additive? Do other cluster migration processes migrate similarly? These questions are not answered here but long-term experiments using this cultivation technique will tell. Here, I show stills from a movie for both wild type and *wanderlust-T2* RNAi egg chambers depicted in figure 2.14. RNAi *wanderlust-T2* border cells exhibit cellular activity, the cells change positions relative to each other and they generate cellular protrusions, it seems as if they want to separate but cannot, or they do not know where to go because they lost directionality or polarity. During imaging, the oocyte develops normally, judged by the increase in oocyte size over time, suggesting that the movements seem to reflect the state in vivo.

2.2.2 Protein structure and phylogenetic analysis

The protein sequence of *wanderlust* was annotated using the "IMP annotator" (www.annotator.org). *Wanderlust* exhibits an inactive carboxylesterase domain, a transmembrane domain and an intracellular domain with no annotated function (figure 2.15) presumably required for signaling.

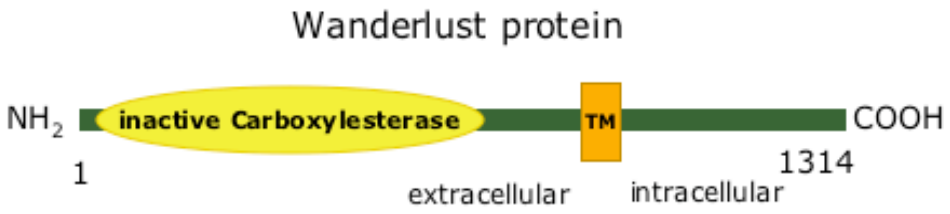

Figure 2.15: Protein model of *wanderlust*. Wanderlust protein consists of 1314 amino acids, an enzymatically inactive carboxylesterase domain, a transmembrane domain and and intracellular domain.

A phylogenetic protein sequence analysis of *wanderlust* revealed that it is conserved and that it belongs to the family of neuroligins. There are four *Drosophila* neuroligins which are orthologs to the mouse and human neuroligins. However, it is not possible from sequence analysis to conclude which of the *Drosophila* neuroligins corresponds to the human or mouse neuroligins (figure 2.16).

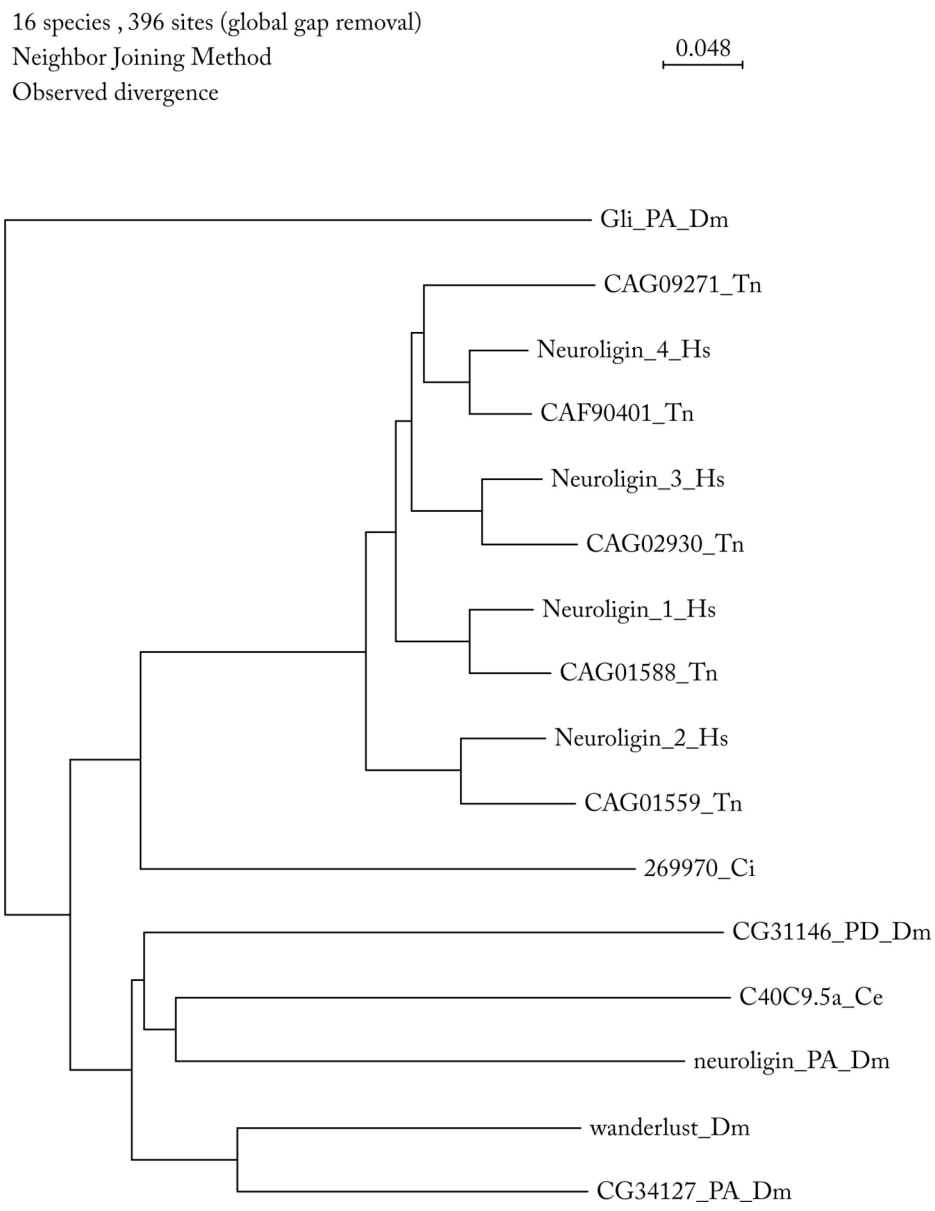

Figure 2.16: Phylogenetic analysis of vertebrate and *Drosophila* neuroligins. Protein sequences were subjected to neighbor joining and resampling using bootstrapping (bootstrap values not shown), *Drosophila* gliotactin was used as outgroup. Abbreviations: *Dm-Drosophila melanogaster, Tn-Tetraodon nigroviridis, Hs-Homo sapiens, Ci-Ciona intestinalis, Ce-Caenorhapditis elegans*

All four Drosophila putative neuroligins *CG34139*, *CG31146*, *neuroligin* and *CG34127* group with a *C.elegans* ortholog *C40C9.5a*. None of the *Drosophila* neuroligins were

studied so far, however Flybase designated *CG13772* as *neuroligin*, only on the basis of sequence comparison. Until recently, it was thought that *Drosophila gliotactin (Gli)* is the closest relative to mammalian neuroligins since gliotactin exhibits a carboxylesterase like domain (Gilbert, Smith et al. 2001), however from the phylogenetic analysis it became evident, that gliotactin does not cluster with neuroligins, on the contrary, it served as outgroup.

All neuroligins studied in mammals so far, were found to be involved in synapse maturation and function, and even related to brain disorders such as mental retardation or autism spectrum disorders. It is therefore interesting to find neuroligins outside their conventional habitat the nervous system, in the context of epithelial cells and migration.

2.2.3 Confirmation of the RNAi phenotype with a hypomorphic wanderlust allele

Classical genetic analyses depend on the investigation of mutants in order to study proposed gene functions. In *Drosophila*, random mutants can be generated by ionizing irradiation, chemicals or the insertion of transposon-based vectors into random gene loci. The site of a mutation can influence gene function in various ways ranging from a complete loss of function allele (null allele), gain of function allele (hypermorph), a hypomorph (reduced function) or no visible effect (silent mutation). Nowadays, considerable effort is being directed towards the generation of a mutant each gene present in the *Drosophila melanogaster* genome, in order to be able to annotate a function to each gene. In the case of genes without available mutants, the researcher has to generate specifically designed mutants using e.g. homologous recombination, which is similar to the Cre/Loxp mouse mutant generation technique.

Fortunate for the present project was the generation by the Hugo Bellen lab, in August 2007 of a fly stock exhibiting an insertion in the locus of *CG34139* (*Mi(ET1)CG34139*^{MB03367} abbreviated as *Mi-CG31439* or *Mi-wanderlust*). They use a so-called minos-element in combination with minos transposase for the generation of insertions, which is supposed to preferably insert into exons flanking the nucleotides AT (Metaxakis, Oehler et al. 2005). The fly stock *Mi-wanderlust* is homozygous viable, fertile and flies do not exhibit obvious visible body phenotypes.

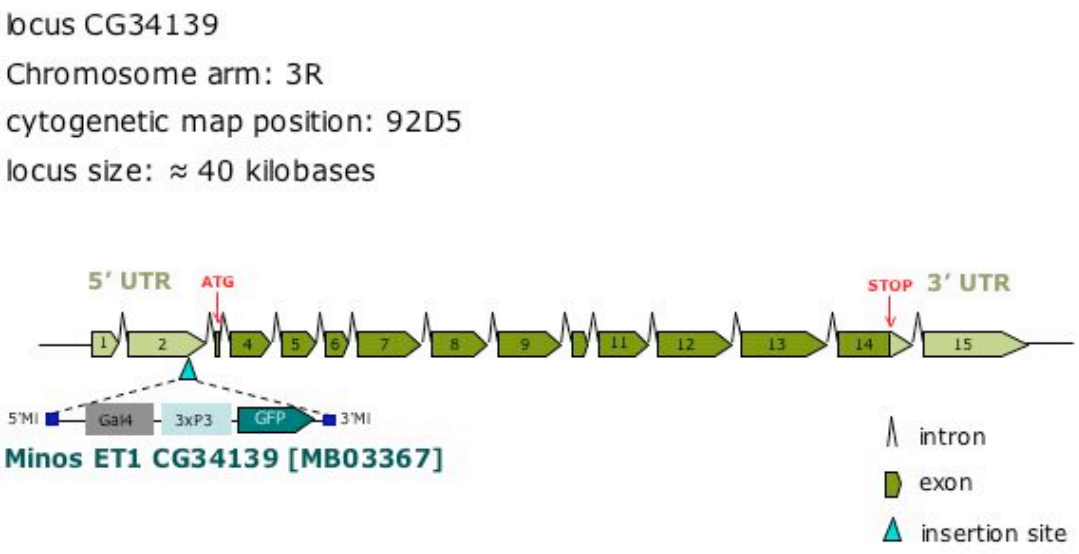

Figure 2.17: Genomic region of the *wanderlust* locus *CG34139* and insertion site of *Mi-wanderlust*. *wanderlust* mRNA is composed of 15 exons, the start codon is located in exon 3, the minos element insertion is located in exon 2. The entire locus spans about 40 kilobases-

The *wanderlust* locus is located on the third chromosome on the right arm (Chr 3R), the locus is very large, meaning it spans 40 kilobases. *wanderlust* mRNA consists of 15 exons, whereas exons 1, 2 and 15 belong to the 5' and 3' untranslated regions (UTR) (see figure 2.17). The minos element *Mi- wanderlust* inserted into the exon 2 of the 5' UTR.

About 25 % of stage 10 egg chambers homozygous for *Mi-wanderlust* show severe border cell migration defects, indicating that *wanderlust* influences border cell migration, thereby confirming the primary identification by RNAi. *Mi-wanderlust* could be either a loss of function allele or a hypomorph with some leftover protein activity. To test which type of allele *Mi-wanderlust* is, I crossed *Mi-wanderlust* to flies containing a large genetic deletion (designated as Deficiency6027, abbreviated Def6027), lacking the entire *CG34139* locus and about 40 more genes. Offspring of these parents exhibit only one mutated *wanderlust* allele instead of two in a healthy animal. If *Mi-wanderlust* would be a complete null allele, one would expect either dead flies if the gene is essential for genetic development, or a drastic increase of border cell migration defects. However, if *Mi-wanderlust* would be a hypermorph, only a slight increase in border cell migration defects is expected, if at all, since it can compensate lack of the second wild type copy in a transheterozygous *Mi-wanderlust*/Deficiency situation since one copy could drive expression as much as two copies.

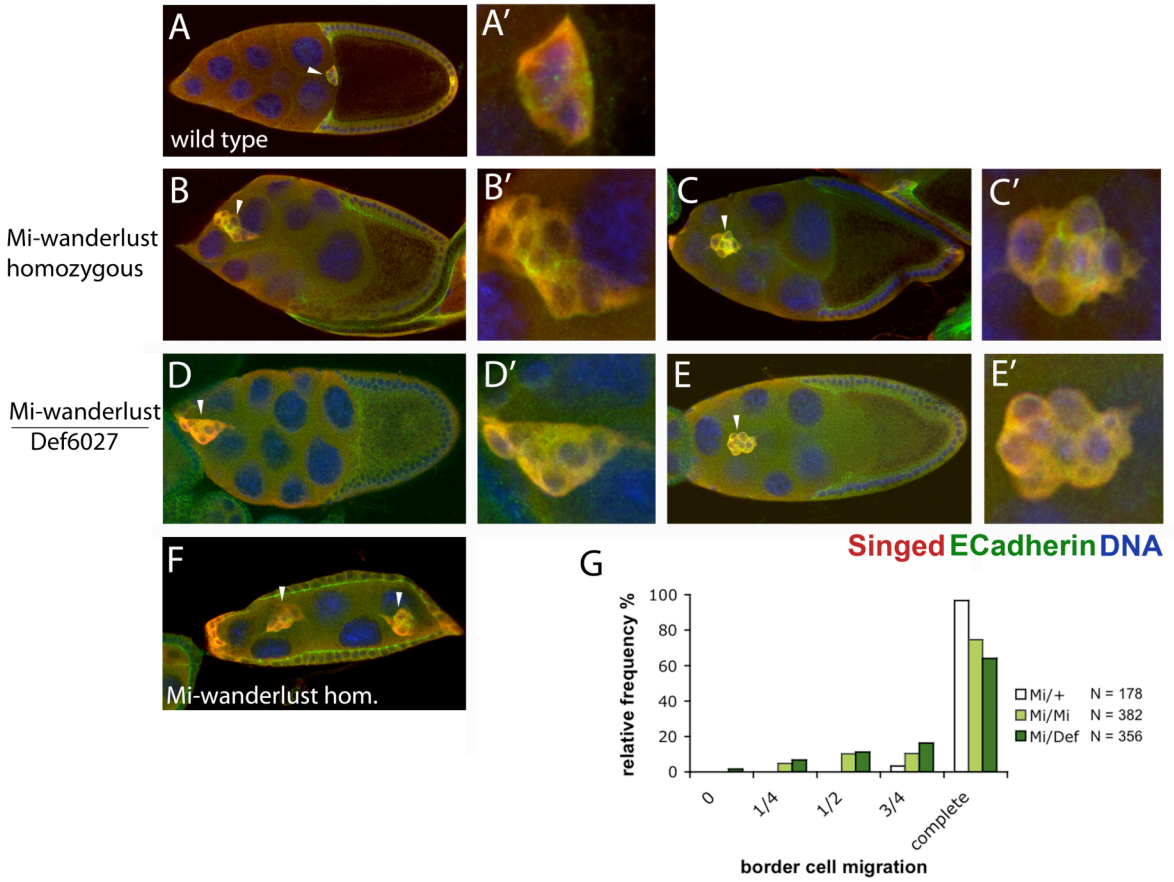

Figure 2.18: *Mi-wanderlust* is a hypomorph resulting in border cell migration defects. A - E): stage 10 egg chambers were stained for singed (red), ECadherin (green) and DNA (blue), **A-A')** wild type egg chamber, border cells. **B, B', C, C')** *Mi-wanderlust* homozygous egg chamber with aberrantly located or delayed border cells. **D, D', E, E')** transheterozygous *Mi-wanderlust* /Def6027 egg chamber, with arrested or delayed border cells. **F)** *Mi-wanderlust* homozygous egg chamber of undefined stage with premature border cell migration and a second, ectopic border cell cluster at the posterior side, migrating in the opposite direction to the anterior side. **G)** Border cell migration quantification of *Mi-wanderlust* genotypes: wild type (+/+), heterozygous (Mi/+), homozygous (Mi/Mi) and trans heterozygous (Mi/Def) stage 10 egg chambers.

Figure 2.18 shows the border cell migration defect phenotypes of wild type, homozygous *Mi-wanderlust* and transheterozygous *Mi-wanderlust/Def6027* with quantifications, respectively. In total, 25% of all homozygous *Mi-wanderlust* egg chambers show delayed or even no border cell migration (figure 2.18 B+C). In addition, egg chambers showing defective border cell migration frequently exhibit a smaller oocyte than expected. The size of the oocyte can be judged relative to the entire egg chamber or relative to the follicle cells. Follicle cells cover exactly the posterior half of the egg chamber at stage 10 and the oocyte is perfectly covered by follicle cells under wild type conditions. In homozygous *Mi-wanderlust* and transheterozygous *Mi-wanderlust* /Def6027, the oocyte is smaller than the area covered by follicle cells (Figure 2.18 B, C, E), indicating that the oocyte itself has growth defects or the nurse cells do not produce enough material to increase oocyte growth. Furthermore, some premature egg chambers exhibit border cell clusters on both the

anterior and posterior tip of the egg chamber (Figure 2.18 F), sometimes even migrating in opposite directions. Egg chambers with ectopic border cell clusters on the posterior side do not show the proper anterior-posterior body axis. Posterior fate of follicle cells is induced by EGFR signaling, promoted by production of Gurken by the oocyte (Gonzalez-Reyes, Elliott et al. 1995). Absent EGFR signaling inhibits posterior cell fate and thereby anterior cell fate on the posterior side of the egg chamber is maintained in EGFR mutants (see figure 1.8 for overview). Defective or misregulated EGFR signaling can be an explanation for the phenotype of anterioralized border follicle cells in *Mi-wanderlust* homozygous egg chamber. Figure 2.18F shows an egg chamber with no visible oocyte, thereby lacking the source of Gurken for posterior axis formation. A lack of the oocyte could induce posterior fate on the anterior side. However, I could observe as well egg chambers with oocytes and posterior fate follicle cells on the anterior side (not shown). The results of the hypomorph *Mi-wanderlust* egg chamber experiments suggests multiple roles of wanderlust in border cells during migration, in posterior fate of follicle cells and in growth and cell number of germline-derived cells.

2.2.4 Generation and characterization of a polyclonal antibody

I generated a peptide antibody against the extracellular domain of *wanderlust* and tested *wanderlust* expression in wild type (w-) embryo and ovary cell extracts. In addition, I performed a competition assay with the peptide antigen to test which bands are specifically recognized by the antibody.

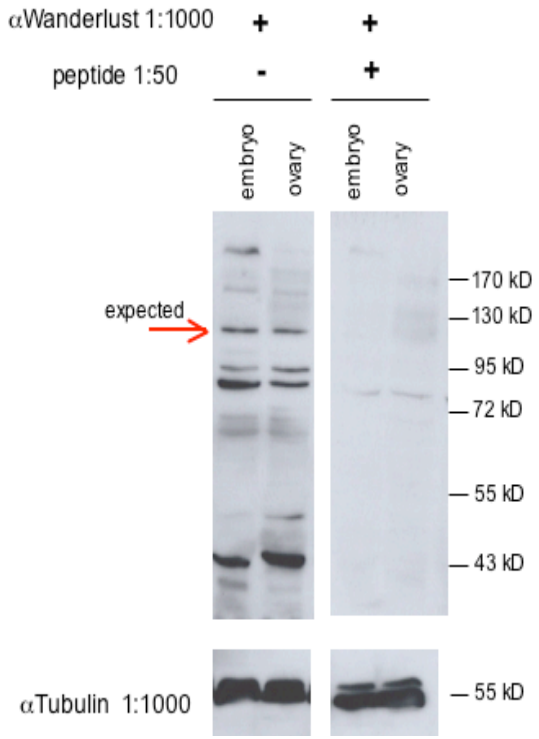

Figure 2.19: αWanderlust recognizes multiple bands in wild type embryo and ovary extracts

Figure 2.19 shows immuno detection of wanderlust protein using chemiluminuescence. The expected size of *wanderlust* is 130 kDa and indeed, a band of such size can be detected (red arrow). In addition, other bands of the sizes 90 – 95 kDa and about 40 kDa are visible. It is possible that *wanderlust* is cleaved into a 90 kDa and 40 kDa protein explaining these additional bands by protein cleavage. It remains to be addressed, if this cleavage is physiological or a result of lysis. Embryo extract and ovary extracts show overall the same band distribution, except that the embryo extract shows an extra high molecular weight band of unestimated size, which is not present in the ovary extract. All bands detected with αwanderlust can be specifically blocked by competition with the antigen peptide (1:50 dilution of 1 mg/mL stock) indicating that all bands are specific to wanderlust.

2.2.5 Subcellular localization

I tested the subcellular localization of *wanderlust* in egg chambers using the polyclonal antibody αwanderlust.

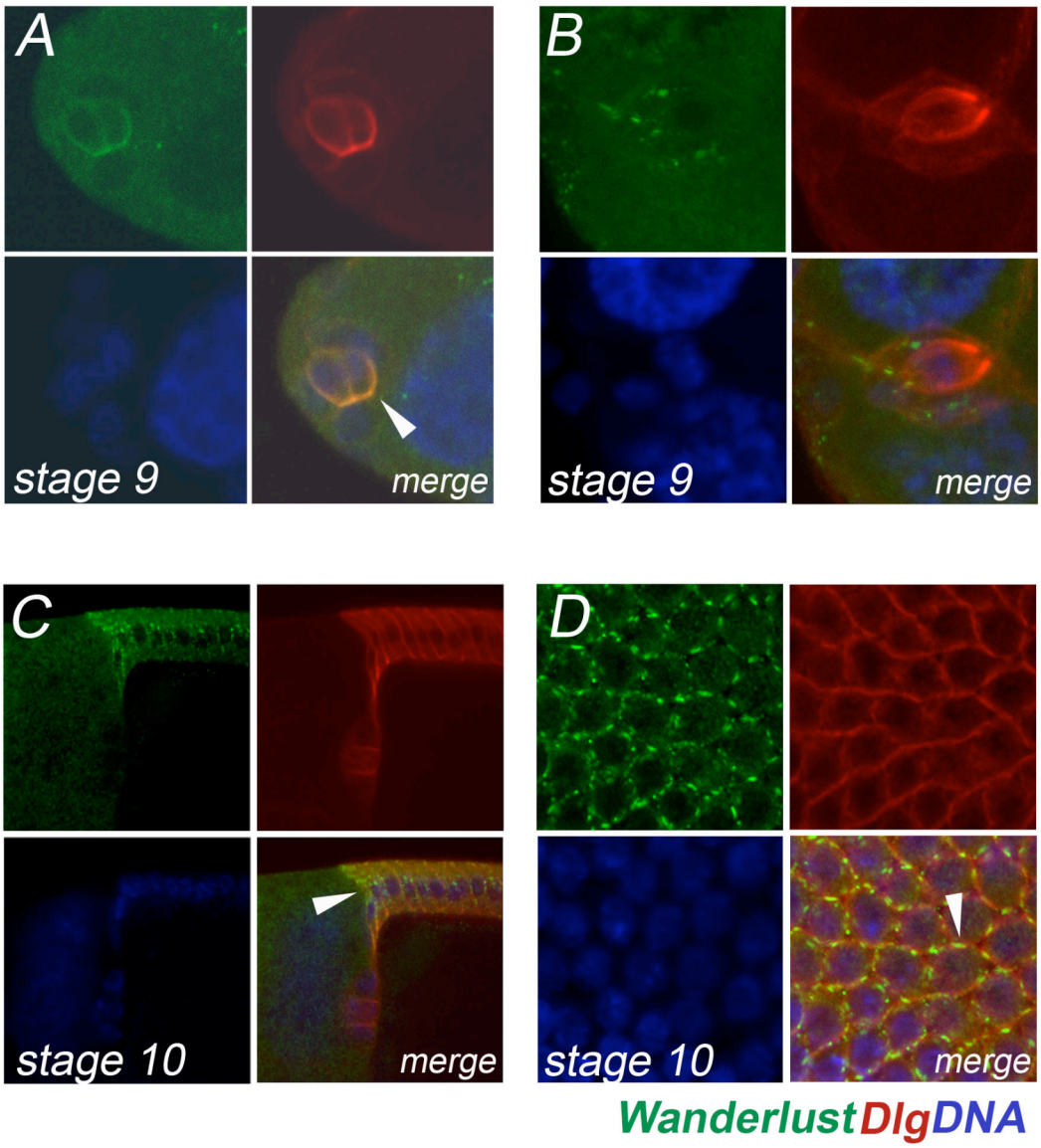

Figure 2.20: Subcellular wanderlust protein in the follicular epithelium. Immunostainings of egg chambers showing Dlg (red), wanderlust (green) and DNA (blue) localization. **A)** stage 9: *Wanderlust* localizes apically in polar cells, arrowhead marks the apical wanderlust localization. **B)** stage9: *wanderlust* is found in punctae on the cortex of the border cell cluster. **C)** stage 10: follicle and centripetal follicle cells showing lateral punctae of wanderlust. arrowhead indicates increased expressionof wanderlust in centripetal cells. **D)** top view of main body follicle cells, arrowhead marks a cell-cell adhesion site.

Figure 2.20 shows *wanderlust* antibody stainings of stages 9 and 10 wild type egg chambers. All follicle cells express *wanderlust*, showing localization at lateral cell-cell

contacts, indicating that *wanderlust* marks a type of cell junction (figure 2.20C). I tested the colocalization of *wanderlust* with E-cadherin, a marker for adherens junctions and did not find any overlap, ruling out adherens junctions as localization sites for *wanderlust*. The septate junction protein Dlg (septate junctions are the invertebrate equivalent to tight junctions) showed complete overlap in polar cells of stage 9 prior to migration (figure 2.20A). However, I could observe only partial overlap of Dlg protein with *wanderlust* in main body follicle cells indicating that *wanderlust* localizes to septate junctions (figure 2.20C+D), but exhibits a more restricted localization pattern than Dlg. In addition, *wanderlust* seems to be upregulated in centripetal follicle cells prior to invagination (figure 2.20D arrowhead). I can detect wanderlust staining in the border cells just before they delaminate in a cortical punctae pattern, however, as soon as the border cell cluster has delaminated I cannot detect wanderlust antibody signal. I think this does not reflect the expression of wanderlust, but is a technical issue of accessibility of the antibody.

In addition I observe expression of *wanderlust* in polar cells just before delamination (figure 2.20 A). As the border cell cluster forms, polar cells adopt a rounded cell shape and start to enrich Fas2, Lgl (lethal giant larvae) and Dlg to the apical side of polar cells. Neighboring follicle cells exhibit lateral localization of Dlg, whereas polar cells show apical polarization. Dlg is a tumor suppressor gene known to be a septate junction component. Follicle cells mutant for Dlg develop ectopic tumor-like tissue in the egg chamber. So far, it is not possible to make statements if wanderlust is expressed in migrating border cells or not. The staining pattern is extremely variable for reasons I cannot explain. Personally, I think wanderlust is expressed in border cells throughout migration, as it is in all other follicle cells, but it is a technical problem to visualize. The wanderlust antibody epitope is located extracellularily between the carboxylesterase domain and the transmembrane domain. It is possible that the epitope is not well accessible for recognition of the antibody and this is the reason why only restricted signal can be obtained. It is also known that neuroligins in general are glycosylated and it could be that this modification obscures as well the epitope. In order to better investigate endogenous wanderlust localization I plan to generate antibodies recognizing intracellular epitopes of wanderlust, hoping to improve statements about subcellular localization.

2.2.6 Overexpression of a GFP fusion protein

In a collaborative effort with Constance Richter of the Knoblich group (IMBA) we generated a wanderlust-GFP fusion protein, GFP was fused to the c-term of wanderlust. I tested the subcellular localization of overexpressed wanderlust-GFP in ovarian follicle cells using slbo-Gal4 and heatshock-Gal4 as inducer. The fusion protein localizes to the lateral cortex in a punctae pattern as already observed with the wanderlust antibody (figure 2.21). In addition, wanderlust-GFP is found highly enriched in the apical domain, probably the marginal zone of epithelial cells. The strong apical signal found in figure 2.21 A-B originates from dense wanderlust-GFP punctae on the apical side, visible if viewed from top of the epithelium (figure 2.21 C). Interestingly, heatshock-Gal4 drives expression in almost all epithelial cells, except for few single cells lacking wanderlust-GFP expression. Cell-cell contacts between a non-expressing and a wanderlust-GFP expressing cell do not exhibit lateral GFP punctae, indicating that wanderlust might act as homophilic adhesion interaction molecule. Border cells expressing wanderlust-GFP exhibit GFP punctae on the cortex between border cells (figure 2.21 A), however sometimes quite some cytosolic GFP signal is observed (figure 2.21 B). Overexpression of wanderlust-GFP in border cells using slbo-Gal4 does not interfere with border cell migration. Interestingly, if wanderlust-GFP is expressed using heatshock-Gal4, very small ovaries are obtained, containing very few stage 10 egg chambers, but a normal amount of stage 9 egg chambers. It seems as if overexpression of wanderlust-GFP interferes with egg chamber maturation. The reason for this observation is not known and remains to be investigated. Expression of wanderlust-GFP with other Gal4 drivers such as inscuteable-Gal4 (expresses in neuroblasts) or 855a-Gal4 (broad epithelial expression) results in dead flies at pupal or undefined stage.

Wanderlust-GFP shows a similar subcellular localization compared with the wanderlust antibody, however it is not clear yet if the strong apical enrichment is the result of the overexpression and a gain of function phenotype or if this reflects rather the normal localization of wanderlust in epithelial cells. As already discussed above, the current available wanderlust antibody is likely to have limitations in terms of accessibility of the epitope, therefore it is difficult to judge, if wanderlust-GFP reflects endogenous protein localization or an overexpression phenotype.

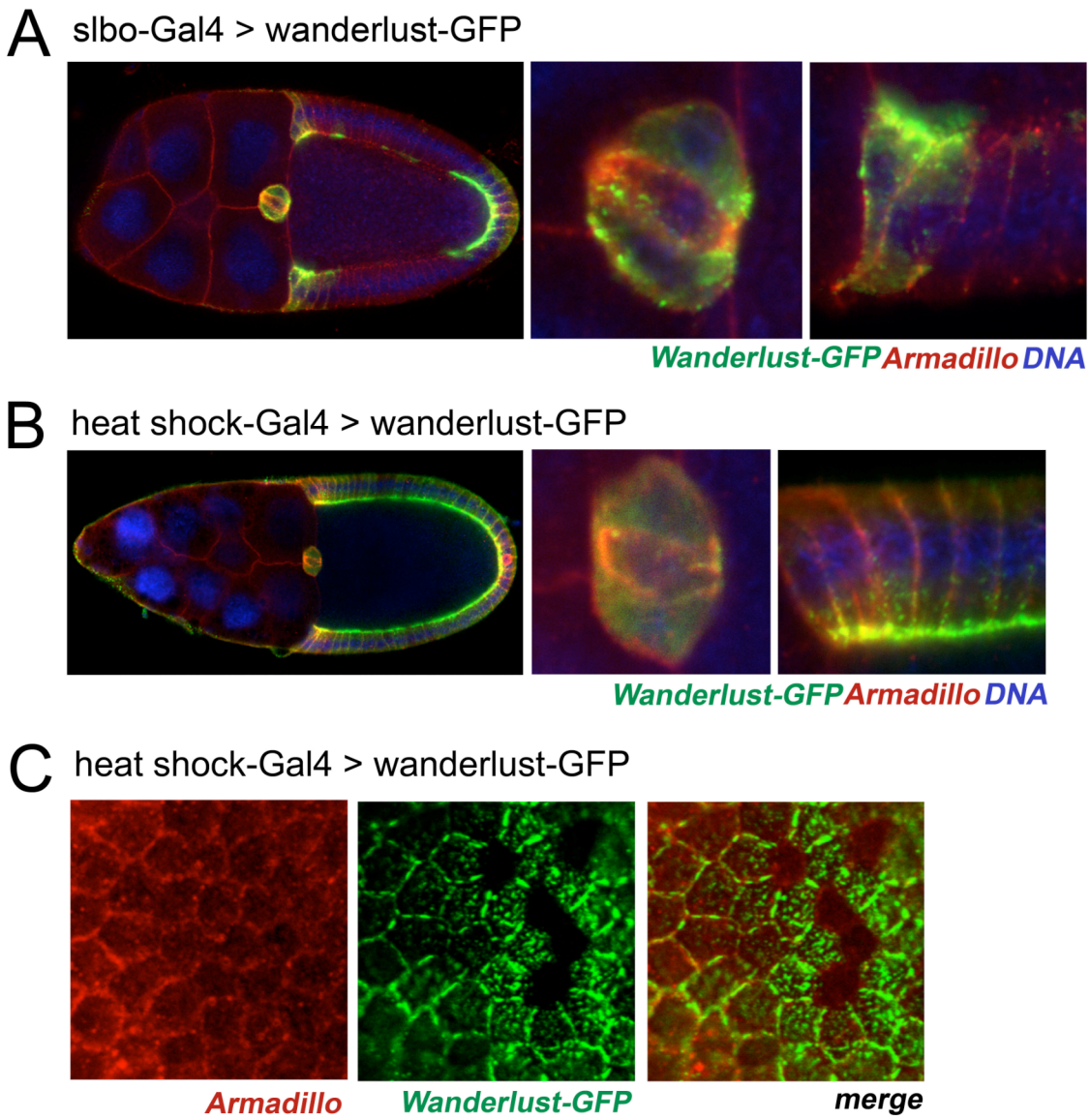

Figure 2.21: Overexpression of wanderlust-GFP in follicle cells of the ovarian epithelium. A) Stage 10 egg chamber expressing wanderlust-GFP under control of slbo-Gal4. Close ups of the border cell cluster and centripetal follicle cells. **B)** Stage 10 egg chamber expressing wanderlust-GFP under control of heatshock-Gal4. Close ups of the border cell cluster and centripetal follicle cells. **C)** Stage 10 follicular epithelium, view from top. Egg chambers are stained for armadillo (red) and DNA (blue).

The apical and lateral subcellular localization of wanderlust-GFP resembles staining patterns of aPKC in wild type egg chambers. In wild type egg chambers aPKC predominantly marks the apical side of epithelial cells, in addition faint punctae along lateral regions are visible (figure 2.22A+C). The similarity of wanderlust-GFP to aPKC is even more striking if Par6 is overexpressed using slbo-Gal4. Centripetal and posterior follicle cells expression ectopic Par6 exhibit increased aPKC staining in punctae at lateral regions (figure 2.22B+D) (Pinheiro and Montell 2004).

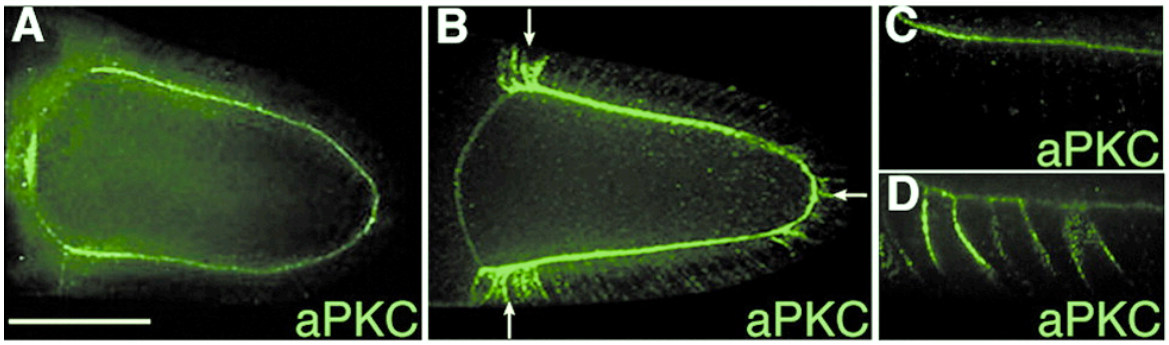

Figure 2.22: (Pinheiro and Montell 2004) Overexpression of Par6 induces enrichment of aPKC to lateral domains in ovarian follicle cells. **A+C)** wild type stage 10 egg chamber stained for aPKC (green). aPKC is found predominantly apically and in faint lateral punctae. **B+D)** Par6 overexpression with slbo-Gal4, a stage 10 egg chamber stained for aPKC shows enrichment of aPKC in lateral domains in a punctae pattern.

Par6 together with Par3 are required to restrict the area of the apical domain. Overexpression of Par6 leads to an expansion of the apical domain into lateral regions marked by localization of aPKC (figure 2.22 B+D). Both Par6 and Par3 are PDZ domain proteins, required for protein-protein interaction. It was shown that neuroligins interact with PSD95, a founding member of the PDZ domain protein class, via few amino acids on the c-term. This PDZ binding region is partially conserved in *Drosophila* neuroligins, implicating that wanderlust could interact with Par6 or Par3 with the c-terminus of the protein. With these findings in mind, it would be reasonable to speculate about an interaction of wanderlust with the Par-aPKC complex, thus regulating polarity in epithelial cells.

3 Discussion

3.1 Genome wide RNAi screen

3.1.1 Setup and conditions

The availability of the genome sequence of *Drosophila melanogaster* in 2003 triggered the systematic analysis of the genome structure and the establishment of tools to enable the attribution of genes with functions in the developing organism. Along this line of systematically dissecting gene function, the group of Barry Dickson at the IMP/IMBA generated a library of transgenic RNAi fruit flies, in which individual lines allow the silencing of one gene of the *Drosophila* genome (Dietzl, Chen et al. 2007). The library is now open to the research community and is distributed via the Vienna *Drosophila* RNAi Center (VDRC). I made use of this unique fly library as it was being generated in order to screen for genes involved in cell migration. I performed a systematic genome wide RNAi screen using border cell migration as a model system. Slbo-Gal4 was used as inducer line in order to express RNAi constructs and a GFP reporter gene specifically in border cells. I tested 21 111 lines represented by 12 000 genes and could identify 57 genes inducing defective border cell migration after knock down using RNAi. As positive controls we could knock down and phenocopy genes already known to be involved in border cell migration such as *shotgun, slbo, taiman, domeless* and *Mrtf/mal-d*. However, we could not phenocopy genes such as Par6 or Par3 genes which exhibit only minor phenotypes in null mutants or knock down with RNAi (Pinheiro and Montell 2004), suggesting that in an incomplete knock down situation, the phenotype to be observed is nonexistent or too subtle to be identified as a phenotype. In order to increase the knock down of proteins with long protein half-lives, the expression time of the RNAi construct must be increased. This can be achieved by choice of a different Gal4 driver, however none of the other border cell specific Gal4 drivers are appreciable longer active prior to border cell migration than slbo-Gal4. An alternative strategy would be to use a rather unspecific but inducible tissue driver like a heat shock-Gal4, whereby the Gal4 inducer protein is fused to a heat-shock promotor, The heat shock promoter is turned on after 1 hour heat-shock treatment at 37°C, and induces Gal4 directed expression of the long hairpin leading to gene silencing. However, a single heat shock is probably not enough to achieve a long-term expression of Gal4, therefore I would apply 1-2 heat shock rounds per day, depending how many days in advance knock down should be initiated. For

silencing genes in border cells to a greater extent I would heat shock for two days prior to dissection. However, this alternative strategy remains to be tested.

3.1.2 Analysis of border cell migration screening hits

Among border cell migration hits we obtained a surprising high number of transcription factors, indicating that with this screening set up, predominantly genes with a short protein half life are picked up. The reason for the enrichment of short-lived proteins is probably due as indicated above to the relatively short expression time window of the inducer line prior to border cell migration and the screening assay. An in silico prediction of on-targets and off-targets for all RNAi hits suggested a relatively high proportion of hits with a high off-target probability. It is known that genes with poly glutamine rich regions are prone to unspecific off-target effects. Indeed, I have picked up genes enriched for glutamine rich regions, coded by the nucleotide triplet CAN. For gene prioritization for further analysis I chose the off-target prediction in order to shortlist my hits. Short-listing according to off-target prediction does not implicate that genes with a high off-target prediction are not relevant, but they need to be re-evaluated individually. A particular interesting gene for me was *Dmel-CG34139*, a so far uncharacterized gene in *Drosophila* exhibiting vertebrate homologs, namely the protein family of neurolgins, which are already studied. The reasons for focusing on *CG34139* were phenotype, specificity of RNAi and the presence of homologs in vertebrates. RNAi mediated knock down of *CG34139* resulted in the robust and strong impairment of border cell migration visible at stage 10 of oogenesis. In silico gene target prediction suggested specific and exclusive knock down of *CG34139*. Mammalian homologs of *CG34139* are neuroligins, which are involved in neuronal synapse function. I chose to study the function of this gene family member in a completely different tissue environment.

For further characterization of the other screening hits I suggest to follow the ranking of the s19 score listing but relax the s19 cutoff to 0.5. I think s19 scores are useful but overestimate off-target effects. Future experiments of identified genes will show how accurate these predictions are in the end. Until then, they are guidelines. As a further criterion for gene prioritization I suggest to study border cell migration hit genes exhibiting orthologs in vertebrates.

3.1.3 Limitations of transgenic RNAi

From collected evidence in of different RNAi screens, it became evident that the site of transgene integration into the genome sometimes influences expression strength of the inverted repeat construct, or the insertion induces misexpression of nearby genes interfering with the RNAi assay. Site dependent expression variability is the reason why the VDRC keeps 1 - 2 independent transformants per construct in order to reduce this effect. Solutions to this problem can be overcome in various ways. Since the transgene is inserted using p-element technology (inducible transposon), the transgene can be mobilized and re-inserted at a different site by introduction of the enzyme transposase. However, the new site could exhibit the same, better or even worse expression properties, thereby not eliminating the problem. Recently, a technique for directing transgenes to a defined locus in the genome was developed, the so-called site-specific transformation (Bateman, Lee et al. 2006). A two-step insertion process is used for this. In the first step, a so-called landing site is created by p-element transformation using transposase. The landing site carries for recognition with the transgene to be inserted. In the second step the transgene is inserted with the enzyme phiC31 integrase. Using this technique, the landing site can be tested for expression properties and compared with other landing sites. Once an appropriate landing site is chosen, transgenes of all kinds including inverted repeat constructs can be used to be inserted into this locus, ensuring equal conditions and reproducibility.

As already discussed, another concern about the use of RNAi is unspecific silencing of non-target genes, called off-targeting, creating background defects and false positive hits. In silico predictions can indicate the likelihood of unspecific off-targets effects, but whether these predictions reflect real circumstances in the cell, remains open.

Long inverted repeat RNAi constructs have the advantage of multiple potent siRNA production, thereby increasing the likelihood of effective silencing. From in vitro siRNA silencing experiments it is known that a single highly potent siRNA is sufficient to effectively silence the target gene. Therefore, it would be interesting to know which siRNA for each gene is specific and efficient to mediate knock down. A recent publication (Haley, Hendrix et al.) introduced a novel technique to use transgenic RNAi in *Drosophila*, using only one siRNA sequence cloned into a micro RNA sequence. The exogenous siRNA is processed by the RNAi machinery as if it were the endogenous micro RNA, but instead of generation of the regulator miRNA, the siRNA induces degradation of a target gene. By using this technique, combined with a targeted site insertion of the transgene, off-target effects and unspecific expression effects can be reduced to a minimum.

3.2 Characterization of the neuroligin member "wanderlust"

3.2.1 Silencing of wanderlust blocks border cell migration

I identified *wanderlust* (*CG34139)* as a novel regulator of border cell migration in the course of a genome wide RNAi screen. *Wanderlust* is a member of the neuroligin family as judged by its protein structure. Neuroligins are transmembrane proteins known to interact with neurexins at neuronal synapses. RNAi knock down of *wanderlust* results in a block of border cell migration at the very beginning of delamination. I was faced with the interesting question as to how the down regulation of a protein apparently involved in adhesion inhibits migration of a cell cluster.

I generated a polyclonal peptide antibody against the extracellular region of wanderlust. In immunoblotting western experiments I observed a 130 kDa band in both ovary and embryo extracts, which is the expected size of wanderlust protein. In addition, other bands of about 90 – 95 kDa and about 40 kDa are detected, which could be cleavage products of the 130 kDa proteins. The two bands around 90 kDa could be phosphorylated and unphosphorylated cleavage products. Furthermore, the embryo extract exhibited a high molecular weight band, which could be the glycosylated form of wanderlust. In mammals, neuroligins were reported to be glycosylated.

α*wanderlust* localizes to lateral cell-cell contacts in main body follicle cells

Immunostaining experiment showed that wanderlust localizes to lateral areas of cell-cell contacts of main body follicle cells. However, during border cell cluster formation wanderlust switches localization from lateral to apical in border cells, a phenomenon known for proteins such as Dlg, Lgl and Fas2.

3.2.2 Border cells silenced for *wanderlust* retain highly dynamic activity

Following recent reports by three groups, I was able to visualize border cell migration live. (Prasad and Montell 2007) and (Bianco, Poukkula et al. 2007) used insulin as a key ingredient, whereas (Tekotte, Tollervey et al. 2007) imaged in halocarbon oil only, without

any additives. Whether or not insulin stabilizes this process rather than being absolutely required is an open question. More importantly, attention has to be paid to obtain isolated egg chambers. The isolation technique is demanding due to the need to remove the surrounding muscle sheath, which contracts periodically and makes imaging impossible. Egg chambers are very delicate and sensitive to contact with the dissection needles, even if no apparent damage of the egg chamber is visible. Under wild type conditions two factors during imaging are indicators for proper egg chamber development: border cell migration and oocyte growth. In vitro border cell migration can be observed in the absence of oocyte growth, but if the border cell cluster does not migrate, the oocyte hardly grows. The method works in general, but lacks robustness.

I established live border cell imaging according to (Bianco, Poukkula et al. 2007) with some modifications and I imaged *CG34139* RNAi egg chambers for their behavior. As already observed in fixed egg chambers, the majority of border cell clusters were stuck at the anterior tip of the egg chamber. Surprisingly, the immobile cluster exhibited activity of the individual cells. As in wild type clusters, *CG34139* RNAi border cells showed a dynamic behavior within the cluster and constantly changed position within the cluster, even cellular protrusions were visible, though the cluster did not move. Therefore I speculate that *CG34139* is required for minimal adhesion to the nurse cell environment. Another possibility discussed below, is that polarized movement of border cells is dependent on *wanderlust*.

3.2.3 Hypomorphic *wanderlust* partially impairs border cell migration

I obtained an insertion of a mobile element in the 5'UTR of the *CG34139* locus, which was homozygous viable. However, homozygous female flies exhibited reproducible border cell migration defects in about 25% of all stage 10 egg chambers, indicating that gene function or expression of *CG34139* is impaired due to the mobile element insertion. Upon combining the mobile element with a chromosome containing a large deletion including the *CG34139* locus, the border cell migration defect is increased, though the majority of egg chambers showed normal border cell migration. I conclude from these experiments that this insertion into *CG34139* acts as hypomorph.

3.2.4 Function of neuroligins

Neuroligins are transmembrane proteins characterized by their domain structure. Typically, neuroligins exhibit an enzymatically inactive extracellular carboxylesterase domain, a transmembrane domain and an intracellular domain required for interactions and signaling. The carboxylesterase domain lacks on of the residues in the catalytic triad in order to be enzymatically active, instead of catalyzing an enzyme reaction, this domain is used as interaction domain. Immunolabeling studies revealed that neuroligins are localized to the postsynaptic side of neuronal synapses, with the extracellular carboxylesterase domain facing the synaptic cleft. Synapses are formed between axons of neurons as asymmetric cell-cell junction that enables communication. Release of neurotransmitters into the so-called synaptic cleft and uptake of neurotransmitters is the basic mechanism of information flow. Synapses can be either excitatory or inhibitory. The balance of inhibitory and excitatory synapse action in the central nervous system is crucial for normal brain function. Imbalances of excitation and inhibition are likely to be the cause for brain disorders such as mental retardation or autism (Lisé and El-Husseini 2006).

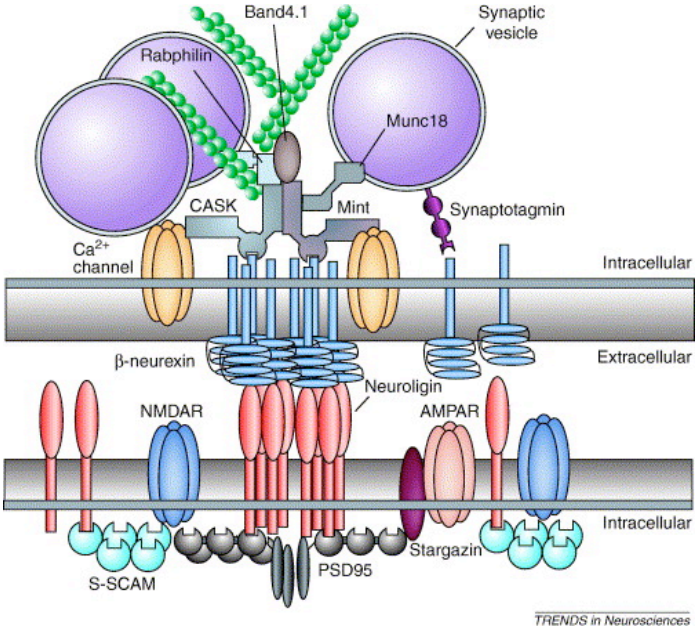

Figure 3. 1: Molecules at the synapse interacting with neuroligin/neurexin, schematic taken from (Dean and Dresbach 2006)

Neuroligins were shown to interact with neurexins through their extracellular carboxylesterase domain at the synapse, forming a so-called synaptic junction to promote adhesion between dendrites and axons and induce formation and maturation of the synapse. Neuroligins are found at the postsynaptic side, whereas neurexins are located at

the presynaptic side. Rodent and human euroligins are alternatively spliced in the extracellular region and exhibit posttranslational modifications such as glycosylation (Bolliger, Frei et al. 2001). It was shown that the last C-terminal amino acids of neuroligins bind PDZ (PSD95, Dlg, ZO-1) domains of scaffolding proteins such as PSD95 (post synaptic density protein 95), probably used for the assembly of large protein complexes(Irie, Hata et al. 1997). Neuroligins and neurexins were shown to induce synaptic protein recruitments after their mutual association across the synaptic cleft. The neuroligin/neurexin interaction seems to work as a bidirectional signaling system to induce synapse formation on either side of the synapse, shown by artificial clustering experiments (Dean, Scholl et al. 2003). Humans exhibit 5 neuroligins, whereas neuroligin 5 is located on the Y-chromosome. Other mammals exhibit 4 neuroligins. Recently, the crystal structure of neuroligin 1 was published as well as the heterotetrameric complex neuroligin 1 and neurexin β1 (Arac, Boucard et al. 2007; Fabrichny, Leone et al. 2007), comprising a homodimer of neuroligin1 with two neurexin β1 monomers. The neuroligin/neurexin interaction was shown to be Ca^{2+} dependent, two Ca^{2+} ions being located at the neuroligin/neurexin binding interface.

Rat neuroligins 1-3 were shown to be enriched in brain tissue (Ichtchenko, Hata et al. 1995; Ichtchenko, Nguyen et al. 1996). Human neuroligins exhibit a different expression profile: human neuroligin 1 is restricted to the central nervous system at excitatory postsynaptic sites. Human neuroligin 2 is located in inhibitory posynaptic sites and shows expression in pancreas or lung. Human neuroligin 3 exhibits broad expression in brain, heart, skeletal muscle, pancreas. Human neuroligin 4 expression levels were highest in heart, followed by liver, skeletal muscle and pancreas, brain tissue showed only little expression of neuroligin 4 (Bolliger, Frei et al. 2001; Lisé and El-Husseini 2006). In general, neuroligin expression is not restricted to neurons, suggesting additional non-neuronal functions, whereas the expression of human neurexins is restricted to the brain.

Human neuroligin 1 and 2 were implicated in synapse formation and maturation. The function of human neuroligin 3 and 4 are much less understood. Mutations or deletions in human neuroligin loci 3 and 4 result in various heterogeneous phenotypes ranging from autism spectrum disorders (ASD), Asperger disorders to Tourette syndrome, all these disorders underlie neurological defects of the central nervous system. A point mutation (R451C) in human neuroligin 3 present in some autism spectrum disorders was analyzed in knock in mice (Tabuchi, Blundell et al. 2007) resulting in mice with impaired social interactions but enhanced spatial learning capabilities. In addition the authors found that inhibitory synapse strength was increased in R451C knock in mice. In general, research about neuroligins revealed that deletion of neuroligins change synaptic strength rather than influence synapse numbers.

Human neuroligin 1 and 3 are generally found in excitatory synapses, whereas neuroligin 2 is present at inhibitory synapses in vivo indicating a role for maintaining a balance of excitation and inhibition. Triple knock out mice for neuroligin 1-3 died shortly after birth due to breathing problems, investigations of synapse showed that the number of synapses is normal, however vesicle marker expression was reduced indicating that neuroligin 1-3 do not influence synapse formation but maturation and function (Varoqueaux, Aramuni et al. 2006). Knock out mice for neuroligin 4 showed reduced interest in their environment and other animals, characteristics resembling autism spectrum disorders in humans (Jamain, Radyushkin et al. 2008).

3.2.5 Adhesion in border cell migration

Adhesion to the extracellular environment is required in order to move forward. However, from cancer studies it is known that decreased adhesion is a prerequisite of tumor metastasis and invasion. In *Drosophila* border cell migration, complete loss of shotgun (E-cadherin) blocks border cell migration. In this migration model, a certain level of adhesion is required for migration. (Melani, Simpson et al. 2008) identified the transcription factor hindsight (hnt) as a negative regulator of adhesion in border cells. Upon loss of hnt, cell adhesion molecules such as E-cadherin or armadillo (β-catenin) are significantly upregulated in border cells and thereby block border cell migration. Therefore, the level of adhesion towards the environment (nurse cells) and within the cluster (border cells-border cells) seems to be critical for proper migration and is tightly regulated.

In neurons, neuroligins were shown to be involved in adhesion at synaptic junctions. As I show, one member of the *Drosophila* neuroligin family *wanderlust* regulates the migration of the border cell cluster. Border cells are a completely different type of cells compared to neurons, they are epithelial cells undergoing morphological changes and migrate in a stereotyped process in normal oogenesis. My finding therefore highlights a subtle regulation in adhesion dynamics in border cells whose disturbances can lead to migration arrest.

3.2.6 Wanderlust localizes asymmetrically in dividing neuroblasts

Mammalian neuroligins are reported to be localized to synapses, however I observed expression of a *Drosophila* neuroligin *wanderlust* (*CG34139)* in follicular cells of the egg chamber in discrete spots in lateral regions of cell-cell contacts. In addition, by a lucky coincidence I observed together with C. Richter, that the antibody against *wanderlust* exhibits an asymmetrical basal staining pattern in dividing neuroblasts in 3rd instar larval brains (figure 3.12. Furthermore, we found similar asymmetrical localization of *wanderlust* in neuroblasts of the embryo. The findings that a neuroligin member exhibits asymmetrical localization are surprising and unexpected. Indeed, *wanderlust* seems to be the first transmembrane protein identified that localizes asymmetrically in neuroblasts, raising intriguing questions about the parallels in function of *wanderlust* in border cells and neuroblasts. Indeed, *wanderlust* evoked even more interest to study its function throught our chance finding of its asymmetric distribution in neuroblasts. We thus continue to investigate *wanderlust* in a collaborative effort in two systems, border cell migration and neuroblast asymmetric cell division. I will give a short introduction to asymmetric cell division in the next paragraph to highlight the importance of asymmetric cell division and the novelty of our discovery.

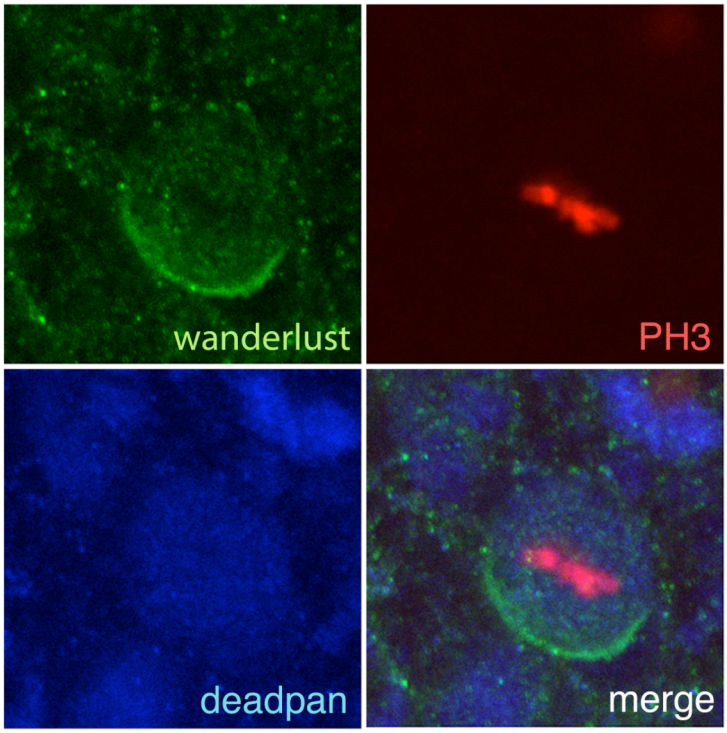

Figure 3. 2: Wanderlust localizes to the basal cortex in an asymmetrical manner, image taken by Constance Richter. Confocal image of L3 larval neuroblasts prior cell division as indicated by phosphohistone3 staining (PH3, red), deadpan is a marker for neuroblasts (blue), *wanderlust* (green)

Asymmetric cell division enables a multi-cellular organism to create diversity and specificity. A cell undergoing a symmetric division, gives rise to two identical daughter cells, however if a cell divides in an asymmetric manner, the resulting daughter cells are different in terms of their content of so-called cell fate determinants. Cell fate determinants in *Drosophila* neuroblasts are Prospero (Pros), Brain tumor (Brat), Numb (Nb), Partner of Numb (Pon) and Miranda (Mira), all these proteins localize to the basal cell cortex prior division and are segregated into one daughter cell, the ganglion mother cell. In addition to polarization of the neuroblast, the mitotic spindle has to form orthogonal to the apical basal axis, otherwise the division would result in two identical daughter cells. Asymmetric neuroblasts division produces a neuroblast with self-renewal ability and a smaller ganglion mother cell capable of one more division and differentiation into two neurons or glia, contributing to central nervous system development.

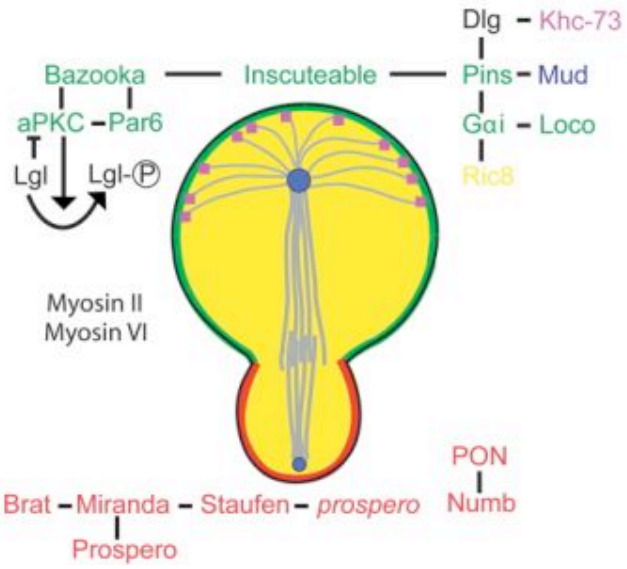

Figure 3. 3: Localization and action of key molecules in asymmetric cell division in larval neuroblast, drawing taken from (Chia, Somers et al. 2008)

Larval brain tissue mutant for cell fate determinants including Miranda, Pros, Brat, Numb, or proteins involved in the polarity establishment such as the tumor suppressor lethal giant larvae (Lgl), Partner of Inscuteable (Pins) produce massive, eventually lethal overgrowth after transplantation into the abdomen of wild type hosts. Transplanted brain tissue appears to be immortal even after multiple rounds of transplantations and shows similarities to malignant growth such as metastasis formation. Therefore, larval neuroblast division serves as model for tumorigenesis in *Drosophila*. Failure or a complete loss of asymmetric cell

division leads to incorrect fate specification and in consequence to overproliferation of neuroblasts.and tumorigenesis (Chia, Somers et al. 2008).

What do border cells and neuroblasts have in common? It is known that par proteins are involved in both processes. Is *wanderlust* required as an adhesion molecule to tether the ganglion mother cell to the neuroblast, until cytokinesis is completed or even longer after cell division? If *wanderlust* is required to link neuroblast cell and ganglion mother cells, I would expect a loss of the grape like architecture of daughter cells. Instead, daughter cells could be scattered around the ganglion mother cell. Is *wanderlust* a cell fate determinant? If so, I would expect upon complete loss of function, that neuroblasts divide in an uncontrolled manner giving rise to gigantic brains full of undifferentiated neuroblasts as described for Prospero for example (Chia, Somers et al. 2008). Experiments are now underway to analyze the effects of wanderlust depletion in neuroblasts by generation of a null allele of *wanderlust*.

Neuroligins were shown to interact with PSD-95, a PDZ domain protein, via the extreme amino acids of the c-term of neuroligin (Irie, Hata et al. 1997; Bolliger, Frei et al. 2001). The consensus PDZ interaction motif is S/T- Xaa - V. The alignment of human and *Drosophila* neuroligins reaveals (figure 3.4), that in the case for wanderlust, the last 2 amino acids are conserved compared to human neuroligins, suggesting a conserved function for the c-term of wanderlust.

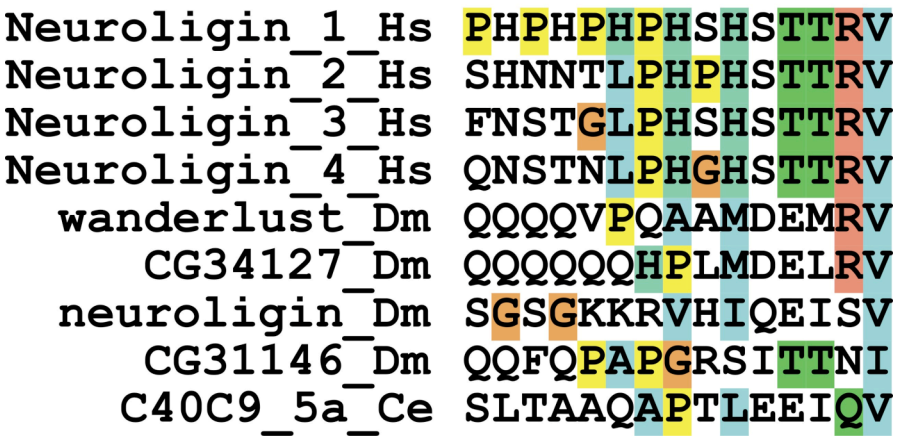

Figure 3. 4:: C-term alignment of neuroligin family members, *Hs- Homo sapiens, Dm-Drosophila melanogaster, Ce-Caenorhabditis elegans.*

3.3 Future experiments, outlook

Null mutant generation and mosaic analysis of wanderlust

It is now absolutely necessary, to prove *wanderlust* function in border cell migration and asymmetric cell division by the generation and testing of a mutant. I showed with the hypomorph experiments that border cell migration is partially impaired but the crucial experiment will be to investigate null mutant cells. Preparations for these experiments are ongoing.

Generation of antibodies towards the intracellular region of wanderlust

The first antibody generated for wanderlust gave insights on where wanderlust is expressed, though we think due the nature of the extracellular epitope, we observe only fractions of endogenous wanderlust protein in epithelial cells or the border cell cluster. In addition, we want to know if wanderlust is cleaved as a consequence of signaling. Therefore, we would be interested in the localization of the intracellular part of wanderlust and we would like to know if and which part of wanderlust is cleaved. We designed 2 peptides located in the intracellular region of wanderlust in order to generate polyclonal antibodies. This time we intend to generate the antibodies in guinea pigs to allow multi labeling with other mouse and rabbit derived available antibodies.

Ultrastructural analysis of wanderlust localization

We would like to know the precise localization of wanderlust in the lateral domain of epithelial cells. Based on the antibody studies and GFP overexpression experiments it is very tempting to speculate that wanderlust localizes to junctions. It would be interesting to know to what type of junctions wanderlust localizes, pleated/smooth septate junctions or gap junctions. These analyses will be carried out using electron microscopy techniques with the overexpression of wanderlust-GFP in the follicular epithelium.

Dynamics of wanderlust-GFP

The overall signal intensity of wanderlust-GFP is very strong, therefore it would be possible to perform live cell imaging with this construct. It would be interesting to know the dynamics of the lateral punctae of wanderlust-GFP during migration and the resting epithelium, which will be part of future experiments.

Functional correlation of human and *Drosophila* neuroligin family members

It would be of great interest to me to know if the other *Drosophila* neuroligins exhibit similar properties or if there is no functional redundancy. Neuroligins were implicated in autism spectrum disorders. Indeed it was shown that neuroligin 4 knock out mice exhibited a lack of interest in their environment, resembling autism behavior. It would be interesting if such a environment related interest behavior is present in *Drosophila*. If such an assay could be set up, the functions of the *Dmel*-neuroligin mutants could be tested for requirements in this behavior, speculating that fruit flies could serve as possible model organism for autism disorders.

4 Material and methods

4.1 Drosophila methods

4.1.1 Breeding

Drosophila melanogaster stocks were kept on carbohydrate and protein enriched agar medium consisting of corn flour, molasses extract, sugar beet molasses, dry yeast, soy flour and agar (made by the IMP/IMBA fly food kitchen). Flies were kept at 25°C for standard breeding and crosses, at 18°C for maintaining stocks and at 27°C for RNAi experiments.
Drosophila males exhibit a lack of meiotic recombination during spermatogenesis. Chromosomes inherited from the parents are handed down unchanged to the offspring. It is not known why there is no rearrangement of chromosomes and what could be the benefits. Clearly it is a benefit for *Drosophila* genetics, since any genotype in a male is maintained and for one generation, no balancer chromosomes are needed.

4.1.2 Flystocks

Slbo-Gal4/CyO was obtained by Pernille Rorth (Rorth, Szabo et al. 1998). Slbo-Gal4 contains a 2.4 kb fragment of the *slbo* promotor fused to Gal4, for reporting the expression pattern of the transcription factor slbo. I recombined slbo-Gal4 to a UAS-CD8GFP reporter construct, for detection of the border cell cluster; slbo-Gal4 expression is excluded from polar cells. For large scale generation of virgins, I generated a stock with a hs-hid gene on the Y chromosome, which , when is activated after a 1 hour heat shock, kills all male progeny due to massive induction of apoptosis, leaving females are unaffected. The gentype of the inducer line for large-scale screening was:
Yhs-hid; slbo-Gal4, UAS-CD8-GFP/CyO.

RNAi lines were generously provided by the VDRC. In detail, 3 males per genotype were separated and the corresponding tube was provided with a barcode including information about e.g. RNAi construct, date, which screen it was assigned to, and persons involved. This procedure ensured both efficient process management and blind and objective screening judgement.
The minos-element insertion in the *wanderlust* locus was generated by the Hugo Bellen lab and maintained at the Bloomington stock center, Mi(ET1)*CG34139*^{MB03367} (abbreviated as

Mi-*CG34139*). Mi-*CG34139* is located in the 5'UTR, exon number 2 and is homozygous viable.

The deficiency Df(3R)ED6027 (abbreviated as Def6027) was generated and obtained from the DrosDel project (Ryder, Ashburner et al. 2007), maintained in the Szeged stock center and lacks 473 kilobases (covering 54 genes including locus *CG34139*).

4.2 RNAi screen

4.2.1 Optimization of screening procedure steps

In this section I describe in overview which steps during the screening process I optimized along the way in order to save time. I have to mention that in times of absolute despair and lack of time, the best ideas arose in terms of simplicity and efficiency.

Design and constructing of a large-scale ovary washing tool: For the large-scale fixation and washing of ovaries, I designed together with the workshop, devices for collection and processing of ovaries for large scale handling. Two prototypes preceeded the screening device shown (figure 4.1A). The prototypes were made from empty tixo rolls or soft plastic caps, the bottom was covered with a mesh from nylon tights, two plastic pipettes were attached to the wells with tape to provide stability. However, the final screening device is a block of plastic with holes and a mesh glued to the bottom, called screening rack. Every well contains a small canal in order to allow air inside and outside of the well, after the barcode is attached as cover. Without these canals, washing or fixation liquid cannot enter or exit the well because a tight chamber is created.

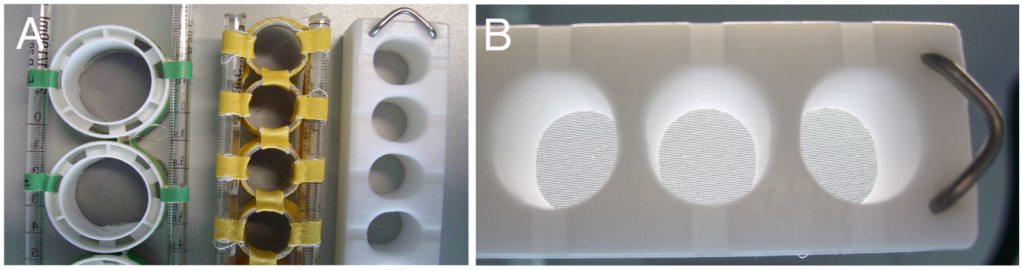

Figure 4. 1: Evolution of ovary washing tool. A) from left to right: prototype 1 made from empty tixo rolls with a mesh from nylon tights. Prototype 2 made from small soft plastic caps, mesh from nylon tights. Screening rack made by workshop. **B)** close up screening rack with air canals and metal handle.

Ovariole separation: Sample preparation depends on proper separation of ovarioles which is done for single samples using needles and performing knife and fork moves. Unfortunately this is very tedious and time consuming, therefore I switched to a smashing method using the coverslip and the mounting medium. The coverslip is gently moved over the ovaries in order to create shear forces in the liquid and thereby separating the ovarioles. After 3-4 shearing streaks, ovarioles are nicely separated.

Use of different objectives: In the beginning, I used for the visual screening a magnification of 100x (10x objective, 10x eyepiece) in order to judge individual egg chambers in a very detailed but time consuming manner. Soon, I reduced the magnification to 50x magnification (5x objective, 10x eyepiece) where I could get a better overview on many egg chambers at the same time and could save time by moving over the sample area faster.

Barcode assisted documentation: As everyone is used to view one sample per slide, I mounted one genotype including the bulky barcode label on a slide, resulting in a lot of handling necessary due to constantly changing of the slides for viewing. The problem was not to mount more genotypes on a slide but more the documentation of which sample belonged to which barcode. I wanted to keep sample and barcode always together and not rely on an additional coding scheme. Simply sticking barcodes on top of each other is possible, but the reverse process of separating them is time consuming if not impossible if they are torn. Instead, I turned a small piece of barcode and let it stick to itself, thereby creating a non-sticky flap. With this flap on each barcode, I could stick barcodes as a stack and also I could remove them easily one by one without damage (see materials and methods figure 4.1).

4.2.2 Large scale preparation of ovary samples

Solutions required:

Dissection buffer (= storage buffer and wash buffer): 0.1% Tween20, 1x PBS

Fixative: 3.7% formaldehyde, 0.1% Tween20, 1x PBS (formaldehyde was freshly added as 37 % formaldehyde)

Mounting medium (mowiol): 590 mM K_2HPO_4, 33% (w/v) polyvinylalcohol 488 (Fluka), 33% (w/v) glycerol 87%.

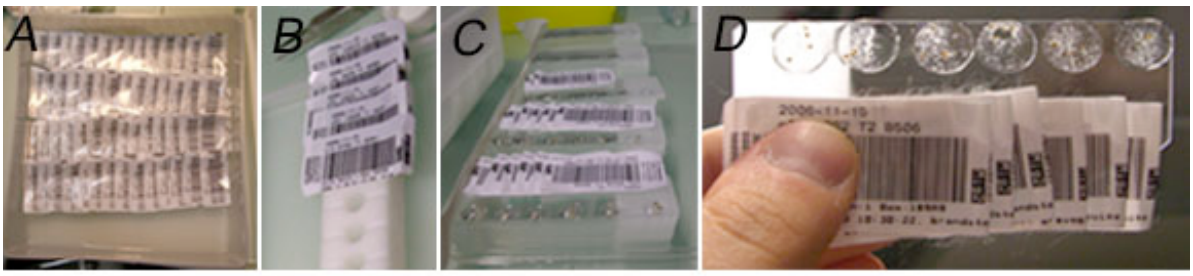

Figure 4. 2: large scale preparation of ovary samples. A) ovaries after fixation in a collection box, **B+C)** ovaries are transferred from the well to glass slides, **D)** 6 genotypes and corresponding barcodes mounted on a glass slide ready to be screened.

Ovary dissection: 3 fattened females were dissected per genotype and collected in a well, the bottom covered with storage buffer. After all three females were dissected the well was closed with the corresponding barcode, avoiding addition of ovaries of the following genotype into the previous well (figure 4.2A+B).

Ovary fixation: The self made well – block (figure 5.1B) contained 14 wells, after all were occupied by ovaries, the entire block was transferred from the storage buffer into fixative and bathed for 10 minutes without shaking. The well-block was washed 2 times 10 minutes each in wash buffer by transferring and bathing the entire block without shaking. Fixed and washed samples were collected in boxes with storage buffer (Fig…A) until mounted.

Mounting of egg chambers: ovaries were transferred from the wells into a drop of Mowiol on a glass slide using forceps. Per slide, 5–6 different genotypes could be arranged (depending on the glass slide type), including corresponding barcodes, stacked over each other. For separation into ovarioles, ovaries were squashed by applying 3 -4 shearing strokes with a small coverslip, bubble generation was avoided as much as possible. Slides were dried overnight and screened on the next day or later (well mounted samples without air inclusions could be screened up to 2 months after mounting) under the fluorescence microscope.

Screening for defective border cell clusters: mounted ovaries were screened under a Leica fluorescence microscope using a 5x objective. The position of the border cell cluster relative to egg chamber and oocyte was used as criterion to judge for border cell migration defects.

4.2.3 RNAi data collection and analysis

Genotypes of transgenic RNAi flystocks and screening data were organized and collected using barcode assisted databases. Raw data was exported into MS Access and evaluated for reproducibility of hits, screening progress, lethality rate and hit rate. Putative hits were subjected to bioinformatics analysis and database searches such as Flybase, IMP annotator, Flight, SMART, PFAM, HomoloGene for information on protein domains, available mutants and published genetic tools.

4.2.4 Live imaging of border cell migration

Solutions required:

Dissection and imaging medium: Grace insect medium, pH was adjusted to 6.8 with NaOH.

Live imaging of border cell migration was performed as described by (Prasad and Montell 2007) with slight modifications. In brief, fattened females were dissected in Grace medium with pH adjusted to 6.8, containing 200 μg insulin. It was claimed, that insulin is the essential ingredient to maintain border cell migration in vitro, however I never tried imaging without. Insulin was added freshly prior dissection, the medium was prewarmed to room temperature just before use.

Ovaries were dissected with a lot of care to avoid touching and damaging egg chamber surfaces with forceps. In the next step, single stage 9 egg chambers were isolated from ovarioles using a pair of self made steel needles, again avoiding any contact of egg chambers with the dissection tools. Egg chambers are covered with a muscle sheet, making the egg chambers contract and move, which is not wanted under imaging conditions. Therefore this muscle sheet must be gently removed by pulling away with forceps. Stage 9 egg chambers were identified roughly by total size, shape and oocyte size. Isolated egg chambers were transferred into an imaging chamber already filled with imaging medium. Dissection time was limited to 30 minutes. The chamber was closed with a coverslip, ready for imaging.

For imaging a Zeiss 510 confocal laser scanning microscope with an automated stage was used. Per imaging experiment, 5 individual egg chambers were imaged, one stack per minute was acquired. The efficiency of successful border cell migration in vitro is very variable and dependent on several factors, e.g. age of insulin or damage of egg chambers. Resulting stacks were processed with the Metamorph software.

4.3 Immunohistochemistry

4.3.1 Immunostainings of ovaries

Females were fattened with additional yeast for 1 day in order to increase egg production and reduce the proportion of old eggs within the ovary. Ovaries were dissected in 1x PBS, 0.1% Tween20. Fixation was carried out in 4% PFA, 0.1% TritonX-100, 1x PBS for 20 minutes under gentle agitation followed by 3 rounds of 10 minute washes in 0.1 % Triton, 1x PBS. Ovaries were blocked for 1 hour in 1% DHS (donor horse serum), 0.1% Triton (freshly added) in 1x PBS (= blocking solution). Primary antibodies were diluted in blocking solution and incubated for 1 – 3 hours, depending on the antibody.

DHSB supernatants: αSinged (clone SN7C, mouse 1:300), αDCad2 (rat 1:100), αDlg (mouse 1:50),

α*Wanderlust* 1:100

Ovaries were washed 3 times for 10 minutes in 0.1 % Triton, 1x PBS. Secondary antibodies coupled to Alexa-fluorophores were diluted in blocking solution (1:400) and incubated with the ovaries for 1 hour, followed by 3 washes for 10 minutes in 0.1 % Triton, 1x PBS each. PBS/Triton buffer was exchanged to PBS and ovaries were mounted in Vectashield for imaging. For confocal image acquisition a Zeiss LSM510 DUO confocal microscope was used. Images were taken using a 25x oil objective, a scan resolution of 1024x1024 pixels and a scan speed of 12.8 μs.

4.3.2 Western blot of *Drosophila* protein extracts

Embryo and ovary protein extracts

Lysis buffer: 50 mM Tris HCl pH 7.4, 2 mM EDTA, 75 mM NaCl, 0.05 mM DTT, 1% Triton X-100, 10% glycerol, protease inhibitor cocktail (complete, Roche)

Embryo protein extract: *Drosophila* embryos were collected on apple agar juice plates with extra yeast and staged for 1 day. Embryos were dechorionated by adding 50% household bleach (brand Danklor, diluted with distilled water) to each agar plate for 2 minutes. Embryos were washed with distilled water until the bleach smell was gone, excess water was removed and embryos were transferred into an Eppendorf tube. An equal volume of lysis buffer was added and tissue was ground with a battery driven motor pestle for about 30 seconds.

Ovary protein extract: *Drosophila* females were fattened with additional yeast for 1 day in order to increase egg production and reduce the proportion of old eggs within the ovary.

Ovaries were dissected and stored in 1x PBS, 0.1% Tween20 on ice. PBS Tween buffer was removed and replaced by an equal amount of lysis buffer containing protease inhibitors (complete Roche). Ovaries were ground by a motor pestle for about 30 seconds and incubated on ice for 30 minutes, followed by 15 minutes centrifugation at top speed in a table top centrifuge at 4°C. The supernatant was removed and stored at -20°C.

Western blot

30 – 50 μg of protein lysate were loaded per slot on 10% SDS PAGE gels, blotted on PVDF membrane using semi-dry blotting. Successful blotting was confirmed by reversible staining with PonceauS solution. Membranes were then incubated in 5% milk powder, 0.1% Tween20, 1x PBS for blocking for 1 hour. Primary antibodies were diluted in 1% milk powder, 0.1% Tween20, 1x PBS. α*Wanderlust* (rabbit 1:1000), αTubulin (mouse 1:2000)

4.3.3 Generation of a polyclonal peptide antibody

A peptide of 20 amino acids within the extracellular carboxylesterase domain (AA 659 – 678, sequence NPNEHHRQDSSLPVSKERNR) was selected using the program DNAstar. The parameters for potential antigenicity and hydrophobicity were used to find an appropriate sequence within the entire *wanderlust* protein. In addition, the peptide sequence must not contain the amino acid cysteine, since an additional cysteine is used for the conjugation to the immunogenic high molecular weight protein KLH (keyhole limpet hemo-cyanin,from a sea snail) to the peptide for a better immune response. The peptide was generated, linked to KLH and injected into rabbits for generation of a polyclonal antibody (Protein facility and Gramsch Laboratories). Rabbit sera were affinity purified using the original peptide, eluted in a high salt and low pH step and furthermore dialysed using vivaspin columns.

4.4 Phylogenetic and protein structure analysis

Protein sequences were sampled using fragment libraries. Full length protein sequences were then subjected to neighbor joining, a method to calculate how different protein sequences are to each other in terms of how many mutations probably occurred during evolution. In addition a resampling step was performed in order to confirm nodes. Alex Schleiffer conducted the phylogenetic analysis.

For analysis of the protein structure, I used the IMP annotator (www.annotator.org).

Project contributions

This project would not have been possible without the help and contribution of other people. In short, I want to summarize my contribution to this project followed by all contributions.

Pre-screen tests, conduction of the majority of the RNAi screen (with help see below), analysis of RNAi hits, live border cell imaging, description of the wanderlust RNAi phenotype in border cells, description of the *wanderlust* hypomorph allele, design and characterization of the *wanderlust* peptide antibody in ovaries and western blot, characterization of wanderlust-GFP in the follicular epithelium.

Screen helpers: Thorsten Boroviak, Anna Azarjana, Bernadette Bosse

Colleagues:
Steffi Benesch: joint effort establishing live border cell imaging
Zhengrui Xi: electron microscopy of border cells, ongoing

Collaborators:
Constance Richter: cloning of wanderlust-GFP, description of wanderlust localization in neuroblasts
Ralph Neumüller: generation of *wanderlust* mutant, ongoing), finding the name wanderlust
Alex Schleiffer: Phylogenetic analysis and alignment of neuroligins

Principle investigators:
Vic Small
Barry Dickson
Barry and Vic, or Vic and Barry (I do not know) initiated the project and came up with the idea to study border cell migration in a systematic fashion.

5 Appendix

5.1 List of lethal genes

Transcription	CG number	Gene name
mRNA cleavage	CG2097	CG2097
mRNA cleavage	CG7698	CG7698
mRNA processing	CG6413	Dis3
mRNA processing	CG3931	Rrp4
mRNA processing	CG4043	Rrp46
mRNA processing	CG8395	Rrp42
mRNA splicing	CG6143	Protein on ecdysone puffs
nuclear mRNA splicing	CG8427	Small ribonucleoprotein Sm D3
nuclear mRNA splicing	CG11985	CG11985
nuclear mRNA splicing	CG7757	CG7757
nuclear mRNA splicing	CG3058	Dim1
nuclear mRNA splicing	CG10418	CG10418
nuclear mRNA splicing	CG13277	CG13277
nuclear mRNA splicing	CG3605	CG3605
nuclear mRNA splicing	CG1405	lethal (1) G0007
nuclear mRNA splicing	CG10689	lethal (2) 37Cb
nuclear mRNA splicing	CG10333	CG10333
nuclear mRNA splicing	CG6227	CG6227
nuclear mRNA splicing	CG2807	CG2807
nuclear mRNA splicing	CG3193	crooked neck
nuclear mRNA splicing	CG6197	CG6197
nuclear mRNA splicing	CG13900	CG13900
nuclear mRNA splicing	CG3542	CG3542
nuclear mRNA splicing	CG10582	Sex-lethal interactor
nuclear mRNA splicing	CG2925	noisette
RNA elongation	CG12225	Spt6
RNA polymerase constituent	CG13628	Rpb10
RNA polymerase constituent	CG6840	Rpb11
RNA polymerase constituent	CG3180	RNA polymerase II 140kD subunit
RNA polymerase constituent	CG31155	Rpb7
RNA polymerase constituent	CG3284	RNA polymerase II 15kD subunit
RNA polymerase constituent	CG8344	RNA polymerase III 128kD subunit
RNA polymerase constituent	CG13418	RpI12
RNA polymerase constituent	CG7339	CG7339
RNA polymerase constituent	CG17209	CG17209
RNA polymerase constituent	CG4033	RNA polymerase I 135kD subunit
RNA polymerase constituent	CG10685	lethal (2) 37Cg
RNA polymerase constituent	CG12267	CG12267
RNA polymerase constituent	CG10122	RNA polymerase I subunit
RNA polymerase constituent	CG7885	RNA polymerase II 33kD subunit
RNA polymerase constituent	CG5380	CG5380
transcription	CG6189	lethal (1) 1Bi
transcription	CG5147	CG5147
transcription	CG1965	CG1965
transcription	CG5264	buttonless
transcription	CG2252	female sterile (1) homeotic
transcription	CG13773	CG13773
transcription	CG31237	Rpb4
transcription	CG16938	Tif-IA
transcription	CG1064	Snf5-related 1
transcription	CG6884	Mediator complex subunit 11

transcription	CG7957	Mediator complex subunit 17
transcription	CG12254	Mediator complex subunit 25
transcription coactivator	CG32045	furry
transcription coactivator	CG4303	Brahma associated protein 60kD
transcription coactivator	CG15319	nejire
transcription factor	CG4881	spalt-related
transcription factor	CG3644	bicaudal
transcription factor	CG5575	ken and barbie
transcription factor	CG6604	H15
transcription factor	CG11617	CG11617
transcription factor	CG5832	H6-like-homeobox
transcription factor	CG8669	cryptocephal
transcription factor	CG6667	dorsal
transcription factor	CG15696	CG15696
transcription factor	CG32778	CG32778
transcription factor	CG7839	CG7839
transcription factor	CG5799	defective proventriculus
transcription factor	CG18389	Eip93F
transcription factor	CG8367	combgap
transcription factor	CG5838	DNA replication-related element factor
transcription factor	CG31256	Brf
transcription factor	CG2905	Nipped-A
transcription factor	CG8426	lethal (2) NC136
transcription factor coactivator	CG13109	taiman
transcription factor complex	CG10281	Transcription factor IIFalpha
transcription factor complex	CG11115	Ssl1
transcription factor complex	CG7764	Tfb2
transcription factor complex	CG17603	TBP-associated factor 1
transcription factor complex	CG6711	TBP-associated factor 2
transcription factor complex	CG7704	TBP-associated factor 5
transcription factor complex	CG32211	TBP-associated factor 6
transcription repressor	CG9984	TH1
Translation		
elongation translation	CG11901	Ef1gamma
elongation translation	CG4849	CG4849
elongation translation	CG6050	Elongation factor Tu mitochondrial
elongation translation	CG8280	Elongation factor 1alpha48D
elongation translation	CG1873	Elongation factor 1alpha100E
ribosome	CG30481	mitochondrial ribosomal protein L53
ribosome	CG6090	Ribosomal protein L34a
ribosome	CG3661	Ribosomal protein L23
ribosome	CG5271	Ribosomal protein S27A
ribosome	CG12740	Ribosomal protein L28
ribosome	CG1821	-
ribosome	CG2033	-
ribosome	CG3195	-
ribosome	CG11522	Ribosomal protein L6
ribosome	CG18676	tipE homolog 3
ribosome	CG13096	CG13096
ribosome	CG2986	overgrown hematopoietic organs at 23B
ribosome	CG8849	mitochondrial ribosomal protein L24
ribosome	CG7808	Ribosomal protein S8
ribosome	CG8857	Ribosomal protein S11
ribosome	CG1263	Ribosomal protein L8
ribosome	CG17489	Ribosomal protein L5
ribosome	CG5219	mitochondrial ribosomal protein L15
ribosome	CG12261	mitochondrial ribosomal protein S22
ribosome	CG14048	mitochondrial ribosomal protein L14
ribosome	CG7038	mitochondrial ribosomal protein L30

ribosome	CG15871	mitochondrial ribosomal protein L38
ribosome	CG14413	mitochondrial ribosomal protein S25
ribosome	CG5242	mitochondrial ribosomal protein L40
ribosome	CG9353	mitochondrial ribosomal protein L54
ribosome	CG6547	mitochondrial ribosomal protein L37
ribosome	CG1524	Ribosomal protein S14a
ribosome	CG4866	CG4866
ribosome	CG4046	Ribosomal protein S16
ribosome	CG7014	Ribosomal protein S5b
ribosome	CG5827	Ribosomal protein L37A
ribosome	CG9354	Ribosomal protein L34b
ribosome	CG7424	Ribosomal protein L36A
ribosome	CG8332	Ribosomal protein S15
ribosome	CG6684	Ribosomal protein S25
ribosome	CG2998	Ribosomal protein S28b
ribosome	CG8495	Ribosomal protein S29
ribosome	CG1883	Ribosomal protein S7
ribosome	CG17521	Qm
ribosome	CG9730	mitochondrial ribosomal protein L21
ribosome	CG1475	Ribosomal protein L13A
ribosome	CG4759	Ribosomal protein L27
ribosome	CG3997	Ribosomal protein L39
ribosome	CG14792	stubarista
ribosome	CG12275	Ribosomal protein S10a
ribosome	CG5920	string of pearls
ribosome	CG15697	Ribosomal protein S30
ribosome	CG4247	mitochondrial ribosomal protein S10
ribosome	CG2099	Ribosomal protein L35A
ribosome	CG12324	Ribosomal protein S15Ab
ribosome	CG4897	Ribosomal protein L7
ribosome	CG14206	Ribosomal protein S10b
ribosome	CG8615	Ribosomal protein L18
ribosome	CG6846	Ribosomal protein L26
ribosome	CG6141	Ribosomal protein L9
ribosome	CG4087	Ribosomal protein LP1
ribosome	CG3203	Ribosomal protein L17
ribosome	CG7726	Ribosomal protein L11
ribosome	CG3782	mitochondrial ribosomal protein L28
ribosome	CG7622	Ribosomal protein L36
ribosome	CG4111	Ribosomal protein L35
ribosome	CG8039	mitochondrial ribosomal protein L19
ribosome	CG5502	Ribosomal protein L4
ribosome	CG7283	Ribosomal protein L10Ab
ribosome	CG3843	Ribosomal protein L10Aa
ribosome	CG10305	Ribosomal protein S26
ribosome	CG4207	bonsai
ribosome	CG8415	Ribosomal protein S23
ribosome	CG3751	Ribosomal protein S24
ribosome	CG15442	mitochondrial ribosomal protein L27
ribosome	CG13922	mitochondrial ribosomal protein L46
ribosome	CG8470	mitochondrial ribosomal protein S30
ribosome	CG13410	mitochondrial ribosomal protein L35
ribosome	CG18767	mitochondrial ribosomal protein L36
ribosome	CG10757	mitochondrial ribosomal protein S18B
ribosome	CG15693	Ribosomal protein S20
ribosome	CG8922	Ribosomal protein S5a
ribosome	CG4863	Ribosomal protein L3
ribosome	CG3314	Ribosomal protein L7A
ribosome	CG6253	Ribosomal protein L14
ribosome	CG2168	Ribosomal protein S3A

ribosome	CG11276	Ribosomal protein S4
ribosome biogenesis and assembly	CG7728	CG7728
ribosome biogenesis and assembly	CG7338	CG7338
ribosome biogenesis and assembly	CG2173	Rs1
ribosome biogenesis and assembly	CG8070	Mystery 45A
ribosome biogenesis and assembly	CG7490	Ribosomal protein LP0
ribosome biogenesis and assembly	CG32253	CG11583
translation initiation	CG17737	CG17737
translation initiation	CG9124	Eukaryotic initiation factor 3 p40 subunit
translation initiation	CG4954	eIF3-S8
translation initiation	CG2677	eIF2B-beta
translation initiation	CG10315	eIF2B-delta
translation initiation	CG9805	eIF3-S10
translation initiation	CG8882	Trip1
translation initiation	CG10840	eIF5B
translation initiation	CG7883	eIF2B-alpha
translation initiation	CG4153	Eukaryotic initiation factor 2beta
translation initiation	CG8190	eIF2B-gamma
translation initiation	CG10811	eukaryotic translation initiation factor 4G
translation initiation	CG8053	Eukaryotic initiation factor 1A
translation initiation	CG9677	Int6 homologue
translation initiation	CG9946	eIF-2alpha
translation initiation	CG4035	Eukaryotic initiation factor 4E
translation initiation	CG10192	off-schedule
translation initiation	CG3186	eIF-5A
translation initiation	CG4878	eIF3-S9
translation initiation	CG10881	CG10881
translation initiation	CG8636	CG8636
translation termination	CG6094	CG6094
translation termination	CG5605	eukaryotic release factor 1
RNA modifying		
mRNA binding	CG8759	Nascent polypeptide associated complex
mRNA cleavage	CG1957	CG1957
mRNA polyadenylation	CG2163	Pabp2
mRNA splicing	CG12085	poly U binding factor 68kD
mRNA splicing	CG9998	U2 small nuclear riboprotein auxiliary factor 50
mRNA splicing	CG5454	snRNP-U1
RNA binding	CG5064	Srp68
RNA binding	CG16941	CG16941
RNA binding	CG7006	CG7006
RNA binding	CG6249	-
RNA binding	CG4258	dribble
RNA cap binding	CG12357	cap binding protein 20
RNA Helicase	CG1666	Helicase
RNA Helicase	CG6375	pitchoune
RNA Helicase	CG4152	lethal (2) 35Df
RNA Helicase	CG5589	CG5589
RNA Helicase	CG9630	CG9630
RNA Helicase	CG9680	Dead box protein 73D
RNA Helicase	CG4916	maternal expression at 31B
RNA helicase	CG11107	CG11107
RNA helicase	CG9075	Eukaryotic initiation factor 4a
RNA helicase	CG7269	Helicase at 25E
RNA metabolism	CG13124	CG13124
RNA processing	CG7246	CG7246
RNA processing	CG7292	Rrp6
RNA processing	CG8025	Mtr3
RNA processing	CG15481	Ski6
RNA processing	CG9004	CG9004

RNA splicing	CG6322	CG6322
RNA splicing	CG10754	CG10754
RNA splicing	CG6015	CG6015
RNA splicing	CG6905	CG6905
RNA splicing	CG6876	CG6876
RNA splicing	CG6841	CG6841
RNA splicing	CG8877	prp8
RNA splicing	CG5352	Small ribonucleoprotein particle protein B
RNA splicing	CG10753	small nuclear ribonucleoprotein at 69D
RNA splicing	CG1249	snRNP2
RNA splicing	CG18591	CG18591
RNA splicing	CG9742	Small ribonucleoprotein G
RNA splicing	CG3780	Spliceosomal protein on the X
RNA splicing	CG8749	small nuclear ribonucleoprotein 70K
RNA splicing	CG13849	Nop56
RNAi	CG10883	CG10883
RNAi	CG10279	Rm62
rRNA modification	CG7009	CG7009
rRNA processing	CG12301	CG12301
rRNA processing	CG4202	Sas10
rRNA processing	CG11030	CG11030
rRNA processing	CG8064	CG8064
rRNA processing	CG9799	CG9799
rRNA processing	CG13097	CG13097
rRNA processing	CG1671	CG1671
rRNA processing	CG12396	Nnp-1
rRNA processing	CG8545	CG8545
rRNA processing	CG10206	nop5
rRNA processing	CG3527	CG3527
rRNA processing	CG1789	CG1789
rRNA processing	CG1542	CG1542
rRNA processing	CG33505	CG33505
rRNA processing	CG5728	CG5728
Cell cycle		
anaphase promoting complex	CG9198	shattered
anaphase promoting complex	CG11419	CG11419
anaphase promoting complex	CG6759	cdc16
cell cycle	CG10800	Regulator of cyclin A1
cell cycle	CG5363	cdc2
cell cycle	CG7597	CG7597
cell cycle	CG6191	CG6191
cell cycle	CycK	Cyclin K
cell cycle	CG16903	CG16903
cell cycle	CG5940	Cyclin A
cell cycle	CG7752	putzig
cell cycle	CG4274	fizzy
cell cycle	CG4364	CG4364
cytokinesis	CG2092	scraps
kinetochore	CG1558	kinetochore Mis12-Ndc80 network 1
kinetochore	CG9938	Ndc80
kinetochore	CG8902	Nuf2
kinetochore	CG7242	Spc25
kinetochore	CG18156	Mis12
kinetochore	CG13329	centromere identifier
mitosis	CG10726	barren
mitosis	CG1911	CAP-D2 condensin subunit
mitosis	CG2948	rev7
mitosis	CG8610	Cdc27
mitosis	CG12019	Cdc37

mitosis	CG2707	female sterile (1) Young arrest
mitosis	CG10583	Separase
mitotic chromosome condensation	CG17054	-
mitotic chromosome condensation	CG11397	gluon
mitotic sister chromatid cohesion	CG12352	separation anxiety
mitotic spindle	CG10648	RNA-binding motif protein 13
mitotic spindle	CG5148	chromosome alignment defect 1
mitotic spindle	CG2843	Cwc25
mitotic spindle	CG11451	Spc105-related
mitotic spindle organization	CG5525	CG5525
mitotic spindle organization + biogenesis	CG5785	three rows
mitotic spindle organization + biogenesis	CG31258	Cenp-C
mitotic spindle organization + biogenesis	CG13298	CG13298
sister chromatid cohesion	CG17509	pds5
sister chromatid cohesion	CG10212	SMC2
sister chromatid cohesion	CG11265	CG11265
Chromatin		
chromatin architecture	CG10712	Chromator
chromatin architecture	CG6990	HP1c
chromatin architecture	CG10223	Topoisomerase 2
chromatin architecture	CG31618	His2A:CG31618
chromatin assembly	CG4817	Structure specific recognition protein
chromatin modification	CG5109	Polycomblike
chromatin modification	CG18414	polyhomeotic proximal
chromatin modification	CG18412	polyhomeotic proximal
chromatin silencing	CG5595	Sex combs extra
chromatin silencing	CG9750	reptin
chromatin silencing	CG8409	Suppressor of variegation 205
chromatin silencing	CG6476	Suppressor of variegation 3-9
chromosome condensation	CG10480	Bj1 protein
chromosome condensation	CG4082	Minichromosome maintenance 5
chromosome condensation	CG4206	Minichromosome maintenance 3
chromosome condensation	CG4039	Minichromosome maintenance 6
nucleosome assembly	CG31613	His3:CG31613
nucleosome assembly	CG4236	Chromatin assembly factor 1 subunit
nucleosome assembly	CG4634	Nucleosome remodeling factor - 38kD
DNA modifying		
DNA elongation	CG6349	DNA polymerase alpha 180kD
DNA fragmentation during apoptosis	CG9414	Rep4
DNA recombination	CG5602	CG5602
DNA repair	CG2028	Casein kinase Ialpha
DNA repair	CG7769	DDB1
DNA repair	CG6779	Ribosomal protein S3
DNA replication	CG15220	CG15220
DNA replication	CG5313	RfC3
DNA replication	CG8142	CG8142
DNA replication	CG9273	Replication protein A2
DNA replication	CG8171	double parked
DNA replication	CG3041	Origin recognition complex subunit 2
DNA replication	CG1616	disc proliferation abnormal
DNA replication	CG14999	Replication-factor-C 40kD subunit
DNA replication	CG9193	mutagen-sensitive 209
DNA replication	CG7108	DNA polymerase alpha 50kD
DNA replication	CG5553	DNA polymerase alpha 60kD
DNA replication	CG9633	Replication Protein A 70
dsDNA binding	CG15367	Dorsal interacting protein 1
heterochromatin formation	CG12864	Su(var)2-HP2

Proteolysis		
proteasome	CG1341	Rpt1
proteasome	CG5289	Proteasome 26S subunit subunit 4 ATPase
proteasome	CG3455	Rpt4
proteasome	CG5378	Rpn7
proteasome	CG3416	Mov34
proteasome	CG4157	Rpn12
proteasome	CG18174	Rpn11
proteasome	CG7762	Rpn1
proteasome	CG10149	Proteasome p44.5 subunit
proteasome	CG10370	Tat-binding protein-1
proteasome	CG10484	Diphenol oxidase A2
proteasome	CG11981	Prosbeta3
proteasome	CG8392	lethal (2) 05070
proteasome	CG5266	Proteasome 25kD subunit
proteasome	CG4904	Proteasome 35kD subunit
proteasome	CG12000	Prosbeta4
proteasome	CG30382	CG30382
proteasome	CG17331	CG17331
proteasome	CG1489	Pros45
proteasome	CG4097	Proteasome 26kD subunit
proteasome	CG10938	Proteasome alpha subunit
proteasome	CG12323	Prosbeta5
proteasome	CG18495	Proteasome alpha6 subunit
proteasome	CG1519	Proteasome alpha7 subunit
proteasome	CG13779	CG13779
proteolysis	CG8571	smallminded
proteolysis	CG3228	kurz
proteolysis	CG10477	CG10477
proteolysis	CG7386	CG7386
proteolysis	CG15002	masquerade
proteolysis	CG1004	rhomboid
proteolysis	CG12785	CG12785
proteolysis	CG12386	etaTrypsin
proteolysis	CG18211	betaTrypsin
proteolysis	CG4933	CG4933
ubiquitination	CG16983	skpA
ubiquitination	CG11941	skpC
ubiquitination	CG10679	Nedd8
ubiquitination	CG5519	GTP-binding-protein
ubiquitination	CG7425	effete
ubiquitination	CG1877	lin-19-like
ubiquitination	CG1512	cul-2
ubiquitination	CG32479	CG32479
ubiquitination	CG7288	CG7288
ubiquitination	CG16982	Roc1a
ubiquitination	CG5087	CG5087
ubiquitination	CG8711	cul-4
Protein folding		
protein folding	CG8977	Cctgamma
protein folding	CG8439	T-complex Chaperonin 5
protein folding	CG8231	T-cp1zeta
protein folding	CG8258	CG8258
protein folding	CG8351	Tcp-1eta
protein folding	CG7033	CG7033
protein folding	CG7770	CG7770
protein folding	CG11267	CG11267
Metabolism		

amino acid biogenesis	CG13391	Alanyl-tRNA synthetase
amino acid biogenesis	CG9020	Arginyl-tRNA synthetase
amino acid biogenesis	CG10687	Asparaginyl-tRNA synthetase
amino acid biogenesis	CG5353	-
amino acid biogenesis	CG8431	Cysteinyl-tRNA synthetase
amino acid biogenesis	CG4062	Valyl-tRNA synthetase
amino acid biogenesis	CG5394	Glutamyl-prolyl-tRNA synthetase
amino acid biogenesis	CG10506	Glutaminyl-tRNA synthetase
amino acid biogenesis	CG6778	Glycyl-tRNA synthetase
amino acid biogenesis	CG15100	CG15100
amino acid biogenesis	CG4561	Tyrosyl-tRNA synthetase
amino acid biogenesis	CG5706	CG5706
amino acid biogenesis	CG2263	CG2263
amino acid catabolism	CG12781	nahoda
amino acid catabolism	CG10399	CG10399
amino acid metabolism	CG6661	CG6661
ATP-metabolism	CG3140	Adenylate kinase-2
ATP-metabolism	CG4307	Oligomycin sensitivity-conferring protein
ATP-metabolism	CG3612	bellwether
ATP-metabolism	CG3762	Vha68-2
ATP-metabolism	CG12403	Vha68-1
ATP-metabolism	CG1703	CG1703
ATP-synthase	CG7610	ATP synthase-gamma chain
ATP-synthase	CG8189	ATP synthase, subunit b
carbohydrate metabolism	CG10996	CG10996
carbohydrate metabolism	CG9466	CG9466
carbohydrate metabolism	CG17814	Peritrophin-15a
carbohydrate metabolism	CG3044	Cht11
carbohydrate metabolism	CG6201	CG6201
carbohydrate metabolism	CG3874	fringe connection
electron transport	CG1970	CG1970
electron transport	CG3683	CG3683
electron transport	CG6914	CG6914
electron transport	CG9160	mitochondrial acyl carrier protein 1
fatty acid metabolism	CG4501	bubblegum
fatty acid metabolism	CG5315	CG5315
ferritin complex	CG2216	Ferritin 1 heavy chain homologue
glucose metabolism	CG4797	CG4797
glucose metabolism	CG1152	Glucose dehydrogenase
metabolism	CG12068	CG12068
metabolism	CG7964	Menl-1
metabolism	CG8425	CG30095
mitochondrial electron transport	CG11015	CG11015
mitochondrial electron transport	CG3560	CG3560
mitochondrial respiratory chain	CG14235	CG14235
mitochondrion organization	CG3869	Mitochondrial assembly regulatory factor
mitochondrion organization	CG8728	CG8728
mitochondrion organization	CG3731	CG3731
phospholipid metabolism	CG15720	radish
respiratory chain	CG8885	CG8885
respiratory chain assembly	CG4510	Surfeit 6
transporter	CG6851	Mitochondrial carrier homolog 1
tricarboxylic acid cycle	CG10219	CG10219
Catalytic enzyme		
dephosphorylation	CG11440	lazaro
exonuclease	CG10354	CG10354
exonuclease	CG8368	CG8368
glutamate-cysteine ligase	CG4917	wolfram syndrome 1
guanylate cyclase	CG14877	CG14877

histone modification	CG13746	MrgBP
histone modification	CG6502	Enhancer of zeste
histone modification	CG12165	Inner centromere protein
hydrolase	CG3982	CG3982
kinase	CG11660	CG11660
kinase	CG11859	CG11859
kinase	CG15224	Casein kinase II beta subunit
myristoylation	CG7436	N-myristoyl transferase
phosphorylation	CG11486	CG11486
Rab GTPase	CG4552	CG4552
Rab GTPase	CG8155	CG8155
Rho family	CG8416	Rho1
ribonuclease	CG11606	RNaseP protein p30
ribonuclease	CG5651	pixie
ribonuclease	CG4129	lethal (1) G0045
ribonuclease	CG5033	CG5033
ribonuclease	CG5371	Ribonucleoside diphosphate reductase
RNA helicase	CG32344	CG32344
Ser/Thr kinase	CG12306	polo
Ser/Thr kinase	CG2829	Tousled-like kinase
Ser/Thr kinase	CG11245	Protein kinase C delta
Ser/Thr kinase	CG32019	bent
Ser/Thr kinase	CG18582	mushroom bodies tiny
Ser/Thr kinase	CG7109	microtubule star
sumoylation	CG12276	Aos1
sumoylation	CG3018	lesswright
transferase	CG6461	CG6461
transferase	CG2674	Minute (2) 21AB
transferase	CG17807	CG17807
transferase	CG8276	bicoid-interacting protein 3
transferase	CG9666	CG9666
transferase	CG31743	CG31743
transferase	CG18869	CG18869
transferase	CG1994	lethal (1) G0020
transferase	CG11989	Ard1
Tyr/Ser/Thr kinase	CG10371	PTEN-like phosphatase
Cytoskeleton		
cytoskeleton	CG10724	CG10724
cytoskeleton	CG6433	quail
cytoskeleton	CG1404	ran
cytoskeleton	CG10541	Tektin C
cytoskeleton	CG1258	pavarotti
cytoskeleton	CG8308	alpha-Tubulin at 67C
cytoskeleton	CG1913	alpha-Tubulin at 84B
cytoskeleton	CG3401	beta-Tubulin at 60D
cytoskeleton	CG5939	Paramyosin
cytoskeleton	CG9277	beta-Tubulin at 56D
cytoskeleton	CG13739	CG13739
cytoskeleton	CG32318	CG32318
cytoskeleton	CG9401	mago nashi
cytoskeleton	CG15792	zipper
cytoskeleton	CG8781	tsunagi
gap junction constituent	CG7537	inx5
molecular motor	CG9191	Kinesin-like protein at 61F
molecular motor	CG31302	CG31302
molecular motor	CG10859	CG10859
Adhesion		
adhesion	CG31970	CG15630

adhesion	CG16857	CG16857
adhesion	CG31004	CG31004
adhesion	CG10275	kon-tiki
adhesion	CG6445	Cad74A
adhesion	CG15354	CG33543
Receptor		
G-protein coupled receptor	CG3022	metabotropic GABA-B receptor subtype 3
G-protein coupled receptor	CG4875	CG4875
G-protein coupled receptor	CG10882	CG10882
taste receptor	CG13787	Gustatory receptor 28a
transmembrane receptor	CG18085	sevenless
Signaling		
cytokine signaling	CG2160	Suppressor of Cytokine Signaling at 44A
neuropeptide signaling	CG18105	Ecdysis triggering hormone
Notch signaling	CG2855	anterior pharynx defective 1
notch signaling	CG2863	Notchless
signaling	CG14873	pxb
signaling	CG5820	Gp150
wnt signaling	CG11990	hyrax
wnt signaling	CG7467	osa
Transport		
energy metabolism	CG16944	stress-sensitive B
nuclear pore	CG11092	CG11092
nuclear pore	CG6743	Nup107
nuclear pore	CG4579	Nup154
nuclear pore	CG4673	CG4673
phagocytosis	CG7275	CG7275
phagocytosis	CG5277	Intronic Protein 259
phagocytosis	CG10198	Nup98
phagocytosis	CG11132	DMAP1
phagocytosis	CG12750	nucampholin
protein import	CG13281	CAS/CSE1 segregation protein
protein transport	CG13387	embargoed
protein transport	CG11779	CG11779
protein transport	CG8330	tomboy40
protein transport	CG12157	Translocase of outer membrane 40
protein transport	CG7654	Translocase of outer membrane 20
protein transport	CG6819	members only
protein transport	CG2637	Female sterile (2) Ketel
protein transport	CG7398	Transportin
protein transport	CG1740	Nuclear transport factor-2
protein transport	CG10130	Sec61beta
protein transport	CG3460	Nonsense-mediated mRNA 3
transporter	CG18842	CG3191
transporter	CG9300	CG9300
transporter	CG32771	CG32771
vesicle transport	CG3071	CG3071
vesicle transport	CG3948	zetaCOP
vesicle transport	CG1528	gamma-coatomer protein
vesicle transport	CG6223	beta-coatomer protein
vesicle transport	CG4214	Syntaxin 5
vesicle transport	CG7073	sar1
vesicle transport	CG1250	sec23
vesicle transport	CG7961	alpha-coatomer protein
vesicle transport	CG6625	Soluble NSF attachment protein
vesicle transport	CG1967	p24-related-1

Other		
anti-apoptosis	CG12265	Deterin
anti-apoptosis	CG12284	thread
carbohydrate binding	CG7106	lectin-28C
chorion constituent	CG15349	Chorion protein a at 7F
chorion formation	CG3477	Peroxidase
cuticle biosynthesis	CG31725	dumpy
cuticle constituent	CG13222	Cuticular protein 47Ee
defense response	CG10284	CG10284
defense response	CG1676	cactin
defense response	CG6890	Tollo
Golgi organization and biogenesis	CG11176	Transport and Golgi organization 2
Golgi organization and biogenesis	CG11098	Transport and Golgi organization 1
Golgi organization and biogenesis	CG2331	TER94
growth factor activity	CG1221	miple
heat shock response	CG31366	Heat-shock-protein-70Aa
heat shock response	CG8542	Heat shock protein cognate 5
heat shock response	CG1242	Heat shock protein 83
heat shock response	CG5748	Heat shock factor
heat shock response	CG12101	Heat shock protein 60
membrane organization and biogenesis	CG9834	endophilin B
pheromone metabolic process	CG5714	ecdysoneless
planar polarity	CG17941	dachsous
potassium channel	CG10706	small conductance calcium-activated K-channel
potassium channel	CG13111	-
potassium channel	CG12215	KCNQ potassium channel
rRNA pseudouridine synthesis	CG5258	NHP2
rRNA pseudouridine synthesis	CG4038	CG4038
signal sequence binding	CG4659	Signal recognition particle protein 54k
telomere capping	CG6219	caravaggio
unknown function		
	CG1430	by S6
	CG9250	M-phase phosphoprotein 6
	CG7993	CG7993
	CG7989	lethal (2) k07824
	CG7686	CG7686
	CG3817	CG3817
	CG33270	CG33270
	CG32856	CG32856
	CG32132	CG32132
	CG32108	CG32108
	CG31847	CG31847
	CG30380	CG30380
	CG30176	within bgcn
	CG30126	CG30126
	CG1785	CG1785
	CG15055	CG42323
	CG12975	CG12975
	CG12136	-
	CR31616	His-Psi:CR31616
	CR31615	His-Psi:CR31615
	CG9667	CG9667
	CG9632	CG9632
	CG9573	CG9573
	CG9548	CG9548
	CG9246	CG9246
	CG8461	CG8461
	CG8435	CG8435
	CG8403	SP2353

	CG8326	CG8326
	CG8211	CG8211
	CG7845	CG7845
	CG7630	CG7630
	CG7516	CG7516
	CG6874	-
	CG6801	lethal (3) j2D3
	CG6724	CG6724
	CG6686	CG6686
	CG6156	-
	CG6030	-
	CG6026	CG6026
	CG5859	CG5859
	CG5778	CG5778
	CG5018	CG5018
	CG4741	CG4741
	CG4738	CG4738
	CG4669	CG4669
	CG3773	CG3773
	CG3735	CG3735
	CG3508	CG3508
	CG3363	CG3363
	CG33051	CG33051
	CG32791	CG32791
	CG32075	CG32075
	CG31990	Like Sm protein 4
	CG31551	CG31551
	CG31223	CG31223
	CG30349	CG30349
	CG30342	CG30342
	CG30161	CG30161
	CG30007	CG30007
	CG2875	CG2875
	CG2685	CG2685
	CG2260	CG2260
	CG2063	CG2063
	CG18844	CG18844
	CG18843	CG18843
	CG18275	CG18275
	CG18273	CG18273
	CG18166	CG18166
	CG17949	His2B:CG17949
	CG17742	CG17742
	CG17732	CG17732
	CG17437	will die slowly
	CG17290	CG17290
	CG1639	lethal (1) 10Bb
	CG15784	CG15784
	CG15730	CG15730
	CG15347	CG15347
	CG15322	CG15322
	CG15260	CG15260
	CG15240	CG15240
	CG15081	lethal (2) 03709
	CG15067	CG15067
	CG14805	CG14805
	CG14459	CG14459
	CG14210	CG14210
	CG14184	CG14184
	CG14180	CG14180

	CG14107	CG14107
	CG14084	CG14084
	CG13964	CG13964
	CG13814	CG13814
	CG13615	CG13615
	CG13372	CG18166
	CG13260	CG42389
	CG13235	CG13235
	CG13082	CG13082
	CG13023	CG13023
	CG13019	CG32791
	CG12885	CG12885
	CG12836	CG12836
	CG12784	CG12784
	CG12753	CG12753
	CG12601	dpr9
	CG12499	CG12499
	CG12420	CG12420
	CG12416	CG12416
	CG12325	CG12325
	CG12259	CG12259
	CG12050	CG12050
	CG11791	CG11791
	CG11786	CG11786
	CG11658	CG11658
	CG11555	CG11555
	CG11417	CG11417
	CG11395	CG11395
	CG11350	CG11350
	CG11100	-
	CG10483	CG10483
	CG1017	CG1017
	CG18130	CG18130
	CG12912	CG12912
	CG30441	CG30441
	CG10691	lethal (2) 37Cc
	CG31852	Two A-associated protein of 42kDa
	CG9748	-
	CG6815	belphegor
	CG13185	CG13185
	CG15765	CG15765
	CG4554	CG4554
	CG10805	lethal (2) k09022
	CG3173	CG3173
	CG16908	CG16908
	CG1575	CG1575
	CG1234	CG1234
	CG12113	lethal (1) G0095
	CG18586	CG18586
	CG1441	CG1441
	CG6613	CG6613
	CG10798	diminutive
	CG31151	winged eye
	CG14788	lethal (1) G0431
	CG3983	CG3983
	CG7639	CG7639
	CG11188	CG11188
	CG10265	CG10265
	CG5268	black pearl
	CG5786	peter pan

	CG4986	Male-specific RNA 57Dc
	CG9074	Male-specific RNA 57Da
	CG6937	CG6937
	CG6049	CG6049
	CG32062	CG32062
	CG14230	CG14230
	CG31761	bruno-2
	CG1884	Not1
	CG1874	Not1
	CG11180	CG11180
	CG10324	CG10324
	CG11263	CG11263
	CG3783	CG32809
	CG32708	CG32708
	CG7552	CG33967
	CG4192	kekkon-3
	CG8434	lambik
	CG8974	CG8974
	CG4325	CG4325
	CG11414	CG11414
	CG6834	CG6834
	CG12031	Mediator complex subunit 14
	CG4494	smt3
	CG3333	Nucleolar protein at 60B
	CG10977	CG33523
	CG3224	CG3224
	CG10267	CG10267
	CG4820	CG4820
	CG8108	CG8108
	CG13287	CG13287
	CG32830	CG32830
	CG4374	CG4374
	CG7317	-
	CG6831	
	CG4806	
	CG31168	
	CG17291	
	CG13673	
	CG11386	

6 References

Adams, M. D., S. E. Celniker, et al. (2000). "The Genome Sequence of Drosophila melanogaster." Science **287**(5461): 2185-2195.

Arac, D., A. A. Boucard, et al. (2007). "Structures of Neuroligin-1 and the Neuroligin-1/Neurexin-1[beta] Complex Reveal Specific Protein-Protein and Protein-Ca2+ Interactions." Neuron **56**(6): 992.

Bai, J., Y. Uehara, et al. (2000). "Regulation of Invasive Cell Behavior by Taiman, a Drosophila Protein Related to AIB1, a Steroid Receptor Coactivator Amplified in Breast Cancer." Cell **103**(7): 1047.

Bastock, R. and D. Strutt (2007). "The planar polarity pathway promotes coordinated cell migration during Drosophila oogenesis." Development **134**(17): 3055-3064.

Bateman, J. R., A. M. Lee, et al. (2006). "Site-Specific Transformation of Drosophila via phiC31 Integrase-Mediated Cassette Exchange." Genetics **173**(2): 769-777.

Bianco, A., M. Poukkula, et al. (2007). "Two distinct modes of guidance signalling during collective migration of border cells." Nature **448**(7151): 362.

Bolliger, M. F., K. Frei, et al. (2001). "Identification of a novel neuroligin in humans which binds to PSD-95 and has a widespread expression." Biochem. J. **356**(2): 581-588.

Borghese, L., G. Fletcher, et al. (2006). "Systematic Analysis of the Transcriptional Switch Inducing Migration of Border Cells." Developmental Cell **10**(4): 497.

Brand, A. H. and N. Perrimon (1993). "Targeted gene expression as a means of altering cell fates and generating dominant phenotypes." Development **118**(2): 401-415.

Cereijido, M., R. G. Contreras, et al. (2008). "Tight junction and polarity interaction in the transporting epithelial phenotype." Biochimica et Biophysica Acta (BBA) - Biomembranes **1778**(3): 770.

Chen, A., I. A. Muzzio, et al. (2003). "Inducible Enhancement of Memory Storage and Synaptic Plasticity in Transgenic Mice Expressing an Inhibitor of ATF4 (CREB-2) and C/EBP Proteins." Neuron **39**(4): 655.

Chia, W., W. G. Somers, et al. (2008). "Drosophila neuroblast asymmetric divisions: cell cycle regulators, asymmetric protein localization, and tumorigenesis." J. Cell Biol. **180**(2): 267-272.

De Lorenzo, C. c., B. M. Mechler, et al. (1999). "What is Drosophila Telling Us About Cancer?" Cancer and Metastasis Reviews **18**(2): 295.

Dean, C. and T. Dresbach (2006). "Neuroligins and neurexins: linking cell adhesion, synapse formation and cognitive function." Trends in Neurosciences **29**(1): 21.

Dean, C., F. G. Scholl, et al. (2003). "Neurexin mediates the assembly of presynaptic terminals." Nat Neurosci **6**(7): 708.

Dietzl, G., D. Chen, et al. (2007). "A genome-wide transgenic RNAi library for conditional gene inactivation in Drosophila." Nature **448**(7150): 151.

Duchek, P. and P. Rorth (2001). "Guidance of Cell Migration by EGF Receptor Signaling During Drosophila Oogenesis." Science **291**(5501): 131-133.

Duchek, P., K. l. n. Somogyi, et al. (2001). "Guidance of Cell Migration by the Drosophila PDGF/VEGF Receptor." Cell **107**(1): 17.

Ewald, A. J., A. Brenot, et al. (2008). "Collective Epithelial Migration and Cell Rearrangements Drive Mammary Branching Morphogenesis." Developmental Cell **14**(4): 570.

Fabrichny, I. P., P. Leone, et al. (2007). "Structural Analysis of the Synaptic Protein Neuroligin and Its beta-Neurexin Complex: Determinants for Folding and Cell Adhesion." Neuron **56**(6): 979.

Fire, A., S. Xu, et al. (1998). "Potent and specific genetic interference by double-stranded RNA in Caenorhabditis elegans." Nature **391**(6669): 806.

Fulga, T. A. and P. Rorth (2002). "Invasive cell migration is initiated by guided growth of long cellular extensions." Nat Cell Biol **4**(9): 715.

Geisbrecht, E. R. and D. J. Montell (2002). "Myosin VI is required for E-cadherin-mediated border cell migration." Nat Cell Biol **4**(8): 616.

Ghiglione, C., O. Devergne, et al. (2002). "The Drosophila cytokine receptor Domeless controls border cell migration and epithelial polarization during oogenesis." Development **129**(23): 5437-5447.

Gilbert, M., J. Smith, et al. (2001). "Neuroligin 3 is a vertebrate gliotactin expressed in the olfactory ensheathing glia, a growth-promoting class of macroglia." Wiley Liss **34**(3): 151-164.

Gonzalez-Reyes, A., H. Elliott, et al. (1995). "Polarization of both major body axes in Drosophila by gurken-torpedo signalling." Nature **375**(6533): 654.

Haley, B., D. Hendrix, et al. "A simplified miRNA-based gene silencing method for Drosophila melanogaster." Developmental Biology **In Press, Corrected Proof**.

Ichtchenko, K., Y. Hata, et al. (1995). "Neuroligin 1: A splice site-specific ligand for beta-neurexins." Cell **81**(3): 435.

Ichtchenko, K., T. Nguyen, et al. (1996). "Structures, Alternative Splicing, and Neurexin Binding of Multiple Neuroligins." J. Biol. Chem. **271**(5): 2676-2682.

Irie, M., Y. Hata, et al. (1997). "Binding of Neuroligins to PSD-95." Science **277**(5331): 1511-1515.

Jamain, S., K. Radyushkin, et al. (2008). "Reduced social interaction and ultrasonic communication in a mouse model of monogenic heritable autism." Proceedings of the National Academy of Sciences **105**(5): 1710-1715.

King, E. R. (1970). "Ovarian Development in Drosophila melanogaster."

Kulkarni, M. M., M. Booker, et al. (2006). "Evidence of off-target effects associated with long dsRNAs in Drosophila melanogaster cell-based assays." Nat Meth **3**(10): 833.

Landen, C. N., Jr., A. Chavez-Reyes, et al. (2005). "Therapeutic EphA2 Gene Targeting In vivo Using Neutral Liposomal Small Interfering RNA Delivery." Cancer Res **65**(15): 6910-6918.

Lisé, M. F. and A. El-Husseini (2006). "The neuroligin and neurexin families: from structure to function at the synapse." Cellular and Molecular Life Sciences (CMLS) **63**(16): 1833.

Liu, Y. and D. J. Montell (1999). "Identification of mutations that cause cell migration defects in mosaic clones." Development **126**(9): 1869-1878.

Liu, Y. and D. J. Montell (2001). "Jing: a downstream target of slbo required for developmental control of border cell migration." Development **128**(3): 321-330.

Mackay, D. J. G. and A. Hall (1998). "Rho GTPases." J. Biol. Chem. **273**(33): 20685-20688.

Martin, P. and W. Wood (2002). "Epithelial fusions in the embryo." Current Opinion in Cell Biology **14**(5): 569.

Mathieu, J., H.-H. Sung, et al. (2007). "A Sensitized PiggyBac-Based Screen for Regulators of Border Cell Migration in Drosophila." Genetics **176**(3): 1579-1590.

Melani, M., K. J. Simpson, et al. (2008). "Regulation of Cell Adhesion and Collective Cell Migration by Hindsight and Its Human Homolog RREB1." Current Biology **18**(7): 532.

Metaxakis, A., S. Oehler, et al. (2005). "Minos as a Genetic and Genomic Tool in Drosophila melanogaster." Genetics **171**(2): 571-581.

Montell, D. and D. Silver (2001). "Paracrine Signaling through the JAK/STAT Pathway Activates Invasive Behavior of Ovarian Epithelial Cells in Drosophila." Cell **107**: 831-841.

Montell, D. J. (2001). "Command and control: regulatory pathways controlling invasive behavior of the border cells." Mechanisms of Development **105**(1-2): 19.

Montell, D. J., P. Rorth, et al. (1992). "slow border cells, a locus required for a developmentally regulated cell migration during oogenesis, encodes Drosophila C/EBP." Cell **71**(1): 51.

Naora, H. and D. J. Montell (2005). "Ovarian Cancer Metastasis: Integrating insights from disparate model organisms." Nat Rev Cancer **5**(5): 355.

Napoli, C., C. Lemieux, et al. (1990). "Introduction of a Chimeric Chalcone Synthase Gene into Petunia Results in Reversible Co-Suppression of Homologous Genes in trans." Plant Cell **2**(4): 279-289.

Neeta Shrivastava, A. S. (2008). "RNA interference: An emerging generation of biologicals." Biotechnology Journal **3**(3): 339-353.

Nerlov, C. (2008). "C/EBPs: recipients of extracellular signals through proteome modulation." Current Opinion in Cell Biology **20**(2): 180.

Niewiadomska, P., D. Godt, et al. (1999). "DE-Cadherin Is Required for Intercellular Motility during Drosophila Oogenesis." J. Cell Biol. **144**(3): 533-547.

Oda, H., T. Uemura, et al. (1997). "Phenotypic analysis of null mutants for DE-cadherin and Armadillo in Drosophila ovaries reveals distinct aspects of their functions in cell adhesion and cytoskeletal organization." Genes to Cells **2**: 29.

Ong, A., S. Maines Bandiera, et al. (2000). "An ovarian adenocarcinoma line derived from SV40/E-cadherin-transfected normal human ovarian surface epithelium." International Journal of Cancer **85**(3): 430-437.

Pinheiro, E. M. and D. J. Montell (2004). "Requirement for Par-6 and Bazooka in Drosophila border cell migration." Development **131**(21): 5243-5251.

Prasad, M. and D. J. Montell (2007). "Cellular and Molecular Mechanisms of Border Cell Migration Analyzed Using Time-Lapse Live-Cell Imaging." Developmental Cell **12**(6): 997.

Riechmann, V. and A. Ephrussi (2001). "Axis formation during Drosophila oogenesis." Current Opinion in Genetics & Development **11**(4): 374.

Rogers, S. L., U. Wiedemann, et al. (2003). "Molecular requirements for actin-based lamella formation in Drosophila S2 cells." J. Cell Biol. %R **162**(6): 1079-1088.

Rorth, P., K. Szabo, et al. (1998). "Systematic gain-of-function genetics in Drosophila." Development **125**(6): 1049-1057.

Rottner, K., A. Hall, et al. (1999). "Interplay between Rac and Rho in the control of substrate contact dynamics." Current Biology **9**(12): 640.

Ryder, E., M. Ashburner, et al. (2007). "The DrosDel Deletion Collection: A Drosophila Genomewide Chromosomal Deficiency Resource." Genetics **177**(1): 615-629.

Sepp, K. J., P. Hong, et al. (2008). "Identification of Neural Outgrowth Genes using Genome-Wide RNAi." PLoS Genet **4**(7).
JF - PLoS Genetics

Somogyi, K. and P. Rorth (2004). "Evidence for Tension-Based Regulation of Drosophila MAL and SRF during Invasive Cell Migration." Developmental Cell **7**(1): 85.

Suzuki, A. and S. Ohno (2006). "The PAR-aPKC system: lessons in polarity." J Cell Sci **119**(6): 979-987.

Tabuchi, K., J. Blundell, et al. (2007). "A Neuroligin-3 Mutation Implicated in Autism Increases Inhibitory Synaptic Transmission in Mice." Science **318**(5847): 71-76.

Tekotte, H., D. Tollervey, et al. (2007). "Imaging the migrating border cell cluster in living Drosophila egg chambers." Developmental Dynamics **236**(10): 2818-2824.

Tepass, U., C. Theres, et al. (1990). "crumbs encodes an EGF-like protein expressed on apical membranes of Drosophila epithelial cells and required for organization of epithelia." Cell **61**(5): 787.

Valentin, G., P. Haas, et al. (2007). "The Chemokine SDF1a Coordinates Tissue Migration through the Spatially Restricted†Activation†of Cxcr7 and Cxcr4b." Current Biology **17**(12): 1026.

Varoqueaux, F., G. Aramuni, et al. (2006). "Neuroligins Determine Synapse Maturation and Function." Neuron **51**(6): 741.

Wang, X., J. Bo, et al. (2006). "Analysis of Cell Migration Using Whole-Genome Expression Profiling of Migratory Cells in the Drosophila Ovary." Developmental Cell **10**(4): 483.

Xi, R., J. R. McGregor, et al. (2003). "A Gradient of JAK Pathway Activity Patterns the Anterior-Posterior Axis of the Follicular Epithelium." Developmental Cell **4**(2): 167.